

Time-of-flight experiments on GaAs/Al_xGa_{1-x}As heterostructures

Citation for published version (APA):

Zwaal, E. A. E. (1991). *Time-of-flight experiments on GaAs/Al_xGa_{1-x}As heterostructures*. [Phd Thesis 1 (Research TU/e / Graduation TU/e), Applied Physics and Science Education]. Technische Universiteit Eindhoven. <https://doi.org/10.6100/IR361042>

DOI:

[10.6100/IR361042](https://doi.org/10.6100/IR361042)

Document status and date:

Published: 01/01/1991

Document Version:

Publisher's PDF, also known as Version of Record (includes final page, issue and volume numbers)

Please check the document version of this publication:

- A submitted manuscript is the version of the article upon submission and before peer-review. There can be important differences between the submitted version and the official published version of record. People interested in the research are advised to contact the author for the final version of the publication, or visit the DOI to the publisher's website.
- The final author version and the galley proof are versions of the publication after peer review.
- The final published version features the final layout of the paper including the volume, issue and page numbers.

[Link to publication](#)

General rights

Copyright and moral rights for the publications made accessible in the public portal are retained by the authors and/or other copyright owners and it is a condition of accessing publications that users recognise and abide by the legal requirements associated with these rights.

- Users may download and print one copy of any publication from the public portal for the purpose of private study or research.
- You may not further distribute the material or use it for any profit-making activity or commercial gain
- You may freely distribute the URL identifying the publication in the public portal.

If the publication is distributed under the terms of Article 25fa of the Dutch Copyright Act, indicated by the "Taverne" license above, please follow below link for the End User Agreement:

www.tue.nl/taverne

Take down policy

If you believe that this document breaches copyright please contact us at:

openaccess@tue.nl

providing details and we will investigate your claim.

**Time-of-flight experiments
on GaAs/Al_xGa_{1-x}As heterostructures**

E.A.E. Zwaal

Time-of-flight experiments on GaAs/ $\text{Al}_x\text{Ga}_{1-x}\text{As}$ heterostructures

PROEFSCHRIFT

ter verkrijging van de graad van doctor aan de Technische
Universiteit Eindhoven, op gezag van de Rector
Magnificus, prof.dr. J.H. van Lint, voor een commissie
aangewezen door het College van Dekanen in het
openbaar te verdedigen op vrijdag 15 november 1991 te
16.00 uur

door

Enneliena Aaffiena Elfriede Zwaal

geboren te Winterswijk

Dit proefschrift is goedgekeurd door de promotor
prof.dr. J.H. Wolter
en de copromotor
dr. J.E.M. Haverkort

The work described in this thesis was carried out at the Department of Physics of the Eindhoven University of Technology and was part of the research program of the Dutch Foundation for Fundamental Research on Matter (FOM), which is financially supported by the Dutch Organization for the Advancement of Research (NWO).

aan hen die achter mij stonden

Contents

Time-of-flight experiments on GaAs/Al_xGa_{1-x}As heterostructures

1. Scope of this thesis	7
References	15
2. High electric field effects in GaAs/Al_xGa_{1-x}As heterostructures	
2.1 Introduction	17
2.2 The modulation doped GaAs/Al _x Ga _{1-x} As heterostructure	21
2.3 Transport properties of the GaAs/Al _x Ga _{1-x} As heterostructure	26
2.4 High electric field effects in GaAs/Al _x Ga _{1-x} As heterostructures	31
2.5 Theoretical methods to calculate semiconductor transport	40
References	46
3. Time-of-flight experiments on GaAs/Al_xGa_{1-x}As heterostructures	
3.1 Introduction	51
3.2 The time-of-flight technique	54
3.3 Time-of-flight experiments on 2D semiconductor structures	59
3.4 Experiments	
3.4.1 Experimental set-up	63
3.4.2 Experimental results	68
3.5 Conclusions	79
References	80

4.	Current instabilities in GaAs/Al_xGa_{1-x}As heterostructures	
4.1	Introduction	83
4.2	Monte Carlo calculations	
4.2.1	The Monte Carlo program	86
4.2.2	High-field drift velocities in <i>n</i> -Al _x Ga _{1-x} As	91
4.2.3	Impact ionization in an <i>n</i> -Al _x Ga _{1-x} As layer	93
4.2.4	Electron drift velocities in a current filament	95
4.3	Impact ionization in a GaAs/Al _x Ga _{1-x} As heterostructure	
4.3.1	Time dependence of the injection and ionization process	96
4.3.2	Field dependence of the impact ionization	101
4.4	Experiments	
4.4.1	Experimental details	103
4.4.2	Room temperature experiments	105
4.4.3	Determination of the activation energy	110
4.4.4	Low temperature experiments	112
4.5	Conclusions	117
	References	119
5.	Imaging of current instabilities in GaAs/Al_xGa_{1-x}As heterostructures	
5.1	Introduction	121
5.2	The TROBIC technique	123
5.3	Experimental results	125
5.4	Conclusions	133
	References	134
6.	Time-of-flight experiments on two-dimensional semiconductors	135
	References	144
	Summary	145
	Samenvatting	147
	List of publications	149
	Curriculum Vitae	151

Chapter 1

Scope of this thesis

During the past decade, the research on semiconductors has shown an increasing interest in layered semiconductor structures. To a large extent, this is due to the commercial interest in electronic and electro-optic devices. Recent advances in epitaxial growth techniques like Molecular Beam Epitaxy¹ and Metal Organic Vapour Phase Epitaxy² have made it possible to grow semiconductor structures consisting of very thin layers of different materials with atomically abrupt interfaces. This enables one to tailor the effective band structure of the material. The most investigated semiconductor structures are those of the GaAs/Al_xGa_{1-x}As system, which can be grown relatively easy, since the lattice constants of GaAs and AlAs differ by less than one percent. The GaAs/Al_xGa_{1-x}As system, which nowadays serves as a kind of model system, is suitable to grow various types of two-dimensional structures, one of which is the modulation doped heterostructure^{3,4}.

In a modulation doped GaAs/Al_xGa_{1-x}As heterostructure the electrons are drifting in a two-dimensional channel at the GaAs/Al_xGa_{1-x}As interface, spatially separated from

their parent donors in the $\text{Al}_x\text{Ga}_{1-x}\text{As}$ layer. This spatial separation reduces the ionized impurity scattering, leading to very high electron mobilities at low temperatures⁵. Since this high mobility suggests a possibility for obtaining ultra-high speed devices⁶, a profound knowledge of the physical properties determining the performance of such devices is necessary. One of the principal questions is whether the high-field transport properties of two-dimensional systems are different from those of bulk semiconductors. Since the electron drift velocity is an important parameter in that context, measurements of the velocity-field characteristics of the two-dimensional electron gas (2DEG) are of central interest. Typical devices are operated at high electric fields. One therefore has to know how this high mobility varies with the electric field and how one can understand this variation. In other words: what scattering mechanisms determine the high-field mobility under device conditions and how does this high-field mobility correlate with the low-field mobility? The need to provide answers to these questions is one of the reasons for the current interest in the high-field transport properties of $\text{GaAs}/\text{Al}_x\text{Ga}_{1-x}\text{As}$ heterostructures. On the other hand, from a fundamental point of view the question arises how the carrier-phonon and carrier-carrier interactions in two-dimensional systems differ from the interactions in bulk semiconductors. Although several experiments have been performed in order to investigate these problems, the high-field transport properties of $\text{GaAs}/\text{Al}_x\text{Ga}_{1-x}\text{As}$ heterostructures are still only partly understood.

A number of current-voltage measurements have been performed on n -type modulation doped semiconductor structures^{7,8,9,10}. In these experiments, the carrier density and the mobility are not independently obtained. It is therefore difficult to determine the high-field mobility from current-voltage measurements, since the carrier concentration is not constant at high electric fields because of intervalley scattering and real space transfer of electrons to the $\text{Al}_x\text{Ga}_{1-x}\text{As}$ layer. To circumvent this problem, other techniques have been employed. K. Inoue *et al.*¹⁰, M. Inoue *et al.*^{11,12}, Shah¹³, Schubert *et al.*¹⁴, and Hirakawa and Sakaki¹⁵ have performed high-field Hall measurements to measure both the carrier concentration and the mobility. Masselink *et al.*¹⁶ have simultaneously measured the geometrical magneto-

resistance and the current-voltage characteristics, again to obtain the variation of the carrier density and mobility with the electric field.

In these experiments¹⁰⁻¹⁶, however, the high-field Hall mobility was determined, which is different from the drift mobility¹⁷. This difference is caused by several factors. Consider an n -type semiconductor containing electrons with a drift mobility μ_d , defined as

$$\mu_d = \frac{e \langle \tau \rangle}{m^*}, \quad (1.1)$$

where e is the electron charge, m^* is the effective mass, and $\langle \tau \rangle$ is the average momentum relaxation time, weighted with respect to the electron energy distribution¹⁷. The momentum relaxation time τ depends on the electron energy. Usually, the empirical relationship

$$\tau(\mathcal{E}) = \tau_0 \left(\frac{\mathcal{E}}{kT} \right)^\gamma \quad (1.2)$$

is used. Here, τ_0 is a proportionality constant, \mathcal{E} the electron energy, k the Boltzmann constant, and T the temperature. The exponent γ depends on the dominant scattering mechanism, and varies from $\gamma = -0.5$ for acoustic deformation potential scattering to $\gamma = +1.5$ for ionized impurity scattering. The Hall mobility μ_H is defined as

$$\mu_H = \sigma R_H. \quad (1.3)$$

Here, σ is the conductivity, given by $\sigma = n e \mu_d$, where n is the electron density. R_H is the Hall coefficient, defined as

$$R_H = \frac{1}{n e} \frac{\langle \tau^2 \rangle}{\langle \tau \rangle^2}. \quad (1.4)$$

From (1.3) and (1.4) follows that

$$\mu_H = \mu_d \frac{\langle \tau^2 \rangle}{\langle \tau \rangle^2}. \quad (1.5)$$

The factor $\langle \tau^2 \rangle / \langle \tau \rangle^2$ is called the Hall factor. To calculate the drift mobility from the Hall mobility, this Hall factor must be determined, and thus an assumption must be made for the value of γ in eq. (1.2). It is easily shown that, since γ varies from -0.5 to +1.5, the Hall factor varies from 1.18 to 1.93¹⁷. Thus the error introduced in the drift mobility by assuming a wrong value for γ can be about 60%. For this reason, high-field Hall measurements do not allow an accurate determination of the high-field drift velocity.

In the current-voltage experiments and the high-field Hall and geometrical magneto-resistance measurements mentioned above⁷⁻¹⁶, it was found that in GaAs/Al_xGa_{1-x}As heterostructures at low temperatures the electron mobility decreases rapidly with increasing electric fields, resulting in a saturation of the drift velocity. This is due to the scattering by optical phonon emission, which is expected to be different in the 2D case compared to the 3D case^{18,19}. According to Monte Carlo calculations, the velocity is predicted to decrease at a threshold field of 3 kV/cm due to intervalley scattering^{20,21}. An additional mechanism for a decreasing drift velocity is real space transfer, which is the transfer of electrons from the 2DEG into the Al_xGa_{1-x}As layer^{9,22,23}. Most of the experiments discussed above reveal values for peak velocities typically in the range of 1.0 to 1.8 x 10⁷ cm/s reached at an electric field of about 2 to 4 kV/cm^{8,13,14,16}. M. Inoue *et al.*^{11,12}, however, reported a saturation velocity of 3.8 x 10⁷ cm/s up to 2 kV/cm. Masselink *et al.*^{24,25} measured the velocity-field characteristics of a GaAs/Al_xGa_{1-x}As heterostructure using a microwave technique. They reported peak velocities of 2.3 to 2.8 x 10⁷ cm/s. At 3 kV/cm he observed a velocity decrease, which he ascribed to real space transfer. Hirakawa and Sakaki¹⁵ performed pulsed Hall experiments and measured a saturation of the drift velocity at 77 K and 4.2 K. No velocity decrease was observed up to electric fields of 6 kV/cm. The origin of the discrepancy between the experiments of Hirakawa and Sakaki and

the experiments mentioned above is not clear at present. Obviously, more experimental and theoretical work is needed to understand these results.

The most direct method of measuring carrier drift velocities in high electric fields is to excite locally in the semiconductor excess carriers using a short laser pulse, and to measure the time it takes for the carriers to arrive at the contact under the influence of an applied electric field. This time-of-flight technique has been applied quite successfully to bulk semiconductors²⁶. Here, the ambipolar drift velocity of optically excited excess carriers is equal to the drift velocity of the minority carriers. We decided to focus on this technique and to perform time-of-flight experiments on GaAs/Al_xGa_{1-x}As heterostructures. Of course, layered semiconductor structures are more complicated than bulk semiconductors and the question is to what extent the time-of-flight technique is suitable to study their high-field transport properties. Heterostructures exist of different materials with different high-field properties and there also is an interaction between the layers. Furthermore, what happens to the properties of the ohmic contacts, when high electric fields are applied? There is little known about the high-field behavior of the ohmic contacts. Ohmic contacts to a semiconductor heterostructure are fundamentally different from contacts to bulk material, as was explained by Hendriks *et al.*²⁷. They found that the transfer of electrons from the 2DEG to the Al_xGa_{1-x}As layer is not only possible via the mechanism of real space transfer in the sample, but also via the interconnection at the contacts. Therefore, in the case of time-of-flight experiments on a GaAs/Al_xGa_{1-x}As heterostructure one cannot separate the transport properties of the 2DEG in high electric fields, but one has to take into account also the high-field behavior of the Al_xGa_{1-x}As layer and the ohmic contacts.

Time-of-flight experiments on GaAs/Al_xGa_{1-x}As quantum wells were performed by Höpfel *et al.*^{28,29,30}. They measured the drift velocity of minority electrons in *p*-type modulation doped multiple quantum wells as a function of the applied electric field. They determined a low-field mobility of 1500 cm²/Vs at room temperature, which is much lower than the typical mobilities of majority electrons in *n*-type quantum wells

and heterostructures. This low mobility was attributed to the presence of the high-density hole plasma which causes strong electron-hole Coulomb scattering. Due to this low mobility a relatively low peak velocity of 1.1×10^7 cm/s was reached at a rather high field of 8 kV/cm. At higher electric fields the drift velocity showed a decrease, which was attributed to a loss of carriers from the quantum well by real space transfer. At low temperatures and electric fields below 0.3 kV/cm even negative mobilities of the minority carriers were observed due to carrier drag by the majority carriers^{31,32}. Time-of-flight experiments on a 350 nm thick *p*-type double heterostructure by Furuta *et al.*³³ showed an electron saturation velocity of 2.2×10^7 cm/s at room temperature and a velocity decrease also at 8 kV/cm. Shigekawa *et al.*³⁴ reported that the minority electron mobility in double heterostructures decreases with decreasing well widths from 200 to 20 nm, because of a larger overlap of the electron and hole wave functions.

All these results show that excess carriers in two-dimensional systems behave differently compared to excess carriers in bulk semiconductors. In bulk semiconductors, it is common practice to assume that the minority electron mobility in a *p*-type semiconductor is roughly the same as the majority electron mobility in the *n*-type semiconductor, since the mobility is mainly determined by impurity scattering³⁵. In a modulation doped semiconductor structure, however, the impurity scattering is reduced and the mobility is strongly dependent on carrier-carrier scattering. Therefore, the minority electrons show lower mobilities than two-dimensional majority electrons, leading to lower peak drift velocities, drag effects, and a different behavior with respect to transfer effects under hot electron conditions. This should be kept in mind all the time when interpreting time-of-flight experiments in two-dimensional systems.

Direct drift velocity measurements which can be related to current-voltage characteristics using the time-of-flight technique have not been reported for two-dimensional majority electrons. Majority carrier transport can be studied by high-field Hall measurements, but then the Hall mobility instead of the drift mobility is

determined. Time-of-flight experiments have been performed on p -type modulation doped heterostructures, but the minority electron mobility gives no information about the transport properties of two-dimensional majority electrons. One therefore has to think of a way to measure the mobility of the majority electrons via the time-of-flight technique. The only attempt to measure the drift velocity of majority electrons was reported by Höpfel *et al.*³⁶. They used a GaAs/ $\text{Al}_x\text{Ga}_{1-x}\text{As}$ heterojunction, grown on a heavily doped p -type GaAs layer, such that the two-dimensional well at the GaAs/ $\text{Al}_x\text{Ga}_{1-x}\text{As}$ interface lies just above the Fermi level. When this structure is locally illuminated, the electron-hole pairs created at the position of illumination are separated in the growth direction: the two-dimensional well is filled with electrons and the holes flow into the parallel p -doped GaAs layer. In this way two-dimensional "majority" electrons are created at the position of excitation. Here, the time-of-flight current due to the photo-excited carriers is determined by the drift velocity of the electrons in the two-dimensional well. In this structure, the electron-hole interaction is negligible due to the spatial separation of electrons and holes and an electron mobility of $8600 \text{ cm}^2/\text{Vs}$ at room temperature was determined. However, no low temperature experiments were reported and there still are a number of problems with this experiment. For example, the electrons investigated in this structure are not really majority electrons, since the two-dimensional electron gas in the well is only present at the position of excitation, so there is no lateral homogeneity and the height of the conduction band minimum changes drastically at the position of laser excitation. Furthermore, a larger time-of-flight current was measured for a laser excitation close to the negative contact, which cannot be understood within the time-of-flight theory.

The aim of the research described in this thesis was to investigate the transport properties of two-dimensional majority electrons in a GaAs/ $\text{Al}_x\text{Ga}_{1-x}\text{As}$ heterostructure at high electric fields and to study the possibilities and limitations of time-of-flight experiments on these structures. This thesis is organized as follows. Chapter 2 serves as an introduction, where the basic concepts of GaAs/ $\text{Al}_x\text{Ga}_{1-x}\text{As}$ heterostructures and their transport properties at high electric fields are discussed. In chapter 3 we present the results of our time-of-flight experiments on GaAs/ $\text{Al}_x\text{Ga}_{1-x}\text{As}$ heterostructures

leading to the determination of the high-field drift velocity of the minority carriers in this structure. At an electric field of about 1 kV/cm we measured an anomalous behavior of the time-of-flight current. In this regime also current instabilities in the bias current were observed. To investigate these current instabilities, we performed pulsed current-voltage measurements at high electric fields. These are discussed in chapter 4. A complicated time-dependent behavior of the current was measured, as well as hysteresis effects in the current-voltage characteristics, suggesting that at high electric fields the current is not distributed homogeneously in the sample. We therefore developed a technique to image the current distribution in the heterostructure under high electric field conditions. These imaging experiments, in which spatial current patterns are observed in the heterostructure, are presented in chapter 5. Using the results of time-resolved and spatially resolved experiments, we developed a phenomenological model describing the behavior of GaAs/ $\text{Al}_x\text{Ga}_{1-x}\text{As}$ heterostructures at high electric fields. This model describes the high-field current instabilities in terms of electron injection from the source contact into the $\text{Al}_x\text{Ga}_{1-x}\text{As}$ followed by avalanche processes in the $\text{Al}_x\text{Ga}_{1-x}\text{As}$ layer. This model was supported by the results of our Monte Carlo calculations, in which we calculated the velocities and energy distribution of the electrons in the $\text{Al}_x\text{Ga}_{1-x}\text{As}$ layer. From the experiments we conclude that the high-field properties of a modulation doped heterostructure cannot be described taking into account only the two-dimensional conducting channel. Instead, a full three-dimensional model of hot electron transport in these structures must be developed, including the high-field properties of the $\text{Al}_x\text{Ga}_{1-x}\text{As}$ layer and the contacts. Finally, in chapter 6 we summarize the main conclusions of this thesis and consider the possibilities and limitations of time-of-flight experiments on two-dimensional semiconductor structures.

References

1. K. Ploog, in *III-V Semiconductors* (Crystal Growth, Properties and Applications) (Springer Verlag, Berlin, Heidelberg, New York, 1980), Vol. 3, p. 73.
2. M.R. Leys, *Chemtronics* 2, 155 (1987).
3. R. Dingle, H.L. Störmer, A.C. Gossard, and W. Wiegmann, *Appl. Phys. Lett.* 33, 665 (1978).
4. H.L. Störmer, R. Dingle, A.C. Gossard, W. Wiegmann, and M.D. Sturge, *Solid State Commun.* 29, 705 (1979).
5. J.C.M. Hwang, A. Kastalsky, H.L. Störmer, and V.G. Keramidas, *Appl. Phys. Lett.* 44, 802 (1984).
6. T. Mimura, S. Hiamizu, T. Fuji, and K. Nanbu, *Jpn. J. Appl. Phys.* 19, L225 (1980).
7. T.J. Drummond, M. Keever, W. Kopp, H. Morkoç, K. Hess, B.G. Streetman, and A.Y. Cho, *Electron. Lett.* 17, 545 (1981).
8. M. Keever, W. Kopp, T.J. Drummond, H. Morkoç, and K. Hess, *Jpn. J. Appl. Phys.* 21, 1489 (1982).
9. M. Keever, H. Shichijo, K. Hess, S. Banerjee, L. Witkowski, H. Morkoç, and B.G. Streetman, *Appl. Phys. Lett.* 38, 36 (1981).
10. K. Inoue, H. Sakaki, and J. Yoshino, *Appl. Phys. Lett.* 47, 614 (1985).
11. M. Inoue, M. Inayama, S. Hiyamizu, and M. Inuishi, *Jpn. J. Appl. Phys.* 22, L213 (1983).
12. M. Inoue, *Superlat. Microstruct.* 1, 433 (1985).
13. J. Shah, A. Pinczuk, H.L. Störmer, A.C. Gossard, and W. Wiegmann, *Appl. Phys. Lett.* 44, 322 (1984).
14. E.F. Schubert, K. Ploog, H. Dämbkes, and K. Heime, *Appl. Phys. A* 33, 183 (1984).
15. K. Hirakawa and H. Sakaki, *J. Appl. Phys.* 63, 803 (1988).
16. W.T. Masselink, W. Kopp, T. Henderson, and H. Morkoç, *IEEE Trans. Electron Devices* ED-6, 539 (1985).

-
17. K. Seeger, *Semiconductor Physics* (Springer Verlag, Wien, New York, 1973), chapter 4.
 18. M. Al-Mudares and B.K. Ridley, *Physica* 134B, 526 (1985).
 19. M.A.E. Al-Mudares and B.K. Ridley, *J. Phys. C* 19, 3179, (1986).
 20. K. Yokoyama and K. Hess, *J. Appl. Phys.* 59, 3798 (1986).
 21. M. Artaki and K. Hess, *Phys. Rev. B* 37, 2933 (1988).
 22. K. Hess, H. Morkoç, H. Shichijo, and B.G. Streetman, *Appl. Phys. Lett.* 35, 469 (1979).
 23. M. Keever, K. Hess, and M. Ludowise, *IEEE Trans. Electron Device Lett.* EDL-3, 297 (1982).
 24. W.T. Masselink, N. Braslau, D. LaTulipe, W.I. Wang, and S.L. Wright, *Solid State Electron.* 31, 337 (1988).
 25. W.T. Masselink, N. Braslau, W.I. Wang, and S.L. Wright, *Appl. Phys. Lett.* 51, 1533 (1987).
 26. A. Neukermans and G.S. Kino, *Phys. Rev. B* 7, 2693 (1973).
 27. P. Hendriks, E.A.E. Zwaal, J.G.A. Dubois, F.A.P. Blom, and J.H. Wolter, *J. Appl. Phys.* 69, 302 (1991).
 28. R.A. Höpfel, J. Shah, A.C. Gossard, and W. Wiegmann, *Physica* 134B, 509, (1985).
 29. R.A. Höpfel, J. Shah, D. Block, and A.C. Gossard, *Appl. Phys. Lett.* 48, 148 (1986).
 30. R.A. Höpfel, J. Shah, and A.C. Gossard, *Phys. Rev. Lett.* 56, 765, (1986).
 31. R.A. Höpfel, J. Shah, P.A. Wolff, and A.C. Gossard, *Phys. Rev. Lett.* 56, 2736 (1986).
 32. R.A. Höpfel, J. Shah, P.A. Wolff, and A.C. Gossard, *Appl. Phys. Lett.* 49, 572 (1986).
 33. T. Furuta, N. Shigekawa, T. Mizutani, and A. Yoshii, *Appl. Phys. Lett.* 55, 2310 (1989).
 34. N. Shigekawa, T. Furuta, K. Maezawa, and T. Mizutani, *Appl. Phys. Lett.* 56, 1146 (1990).

-
35. W. Walukiewicz, J. Lagowski, L. Jastrzebski, and H.C. Gatos, *J. Appl. Phys.* 50, 5040 (1979).
 36. R.A. Höpfel, J. Shah, T.Y. Chang, and N.J. Sauer, *Appl. Phys. Lett.* 51, 1815 (1987).

Chapter 2

High electric field effects in GaAs/Al_xGa_{1-x}As heterostructures

2.1 Introduction

In this chapter we discuss the basic concepts of GaAs/Al_xGa_{1-x}As heterostructures, which have been used in the experiments described in chapters 3, 4, and 5. First, in section 2.2, we describe the GaAs/Al_xGa_{1-x}As heterostructure and the two-dimensional electron gas. The transport properties of the 2DEG are discussed in section 2.3. Here also the properties of the Al_xGa_{1-x}As layer are discussed shortly, since they give rise to some remarkable transport phenomena.

Since GaAs/Al_xGa_{1-x}As heterostructures are used to fabricate high electron mobility transistors (HEMTs), which operate at high electric fields, it is very important to know the high-field transport properties of GaAs/Al_xGa_{1-x}As heterostructures. These are discussed in section 2.4. Not only the high-field behavior of the 2DEG, like current saturation and real space transfer are considered, but also the properties of the Al_xGa_{1-x}As layer and the ohmic contacts, which may give rise to current instabilities at high electric fields.

In section 2.5 we describe two methods to calculate the transport properties of semiconductor heterostructures. First, we shortly discuss the relaxation time approximation of the Boltzmann transport equation. Next, we explain the principle of the Monte Carlo method, which is widely used to calculate the hot-electron transport properties of GaAs/ $\text{Al}_x\text{Ga}_{1-x}\text{As}$ heterostructures^{1,2}. We also review some Monte Carlo calculations on two-dimensional electron gases reported in the literature.

2.2 The modulation doped GaAs/Al_xGa_{1-x}As heterostructure

A modulation doped GaAs/Al_xGa_{1-x}As heterostructure consists of several epitaxial layers grown on a semi-insulating GaAs substrate. Usually a Si-doped Al_xGa_{1-x}As layer, with an aluminium fraction of about 0.3 and a donor concentration of typically $2 \times 10^{18} \text{ cm}^{-3}$, is grown on top of a GaAs layer, which is slightly *p*-doped due to background impurities, unintentionally built in during the growth. Because of the different bandgaps of GaAs and Al_xGa_{1-x}As the electrons, which are ionized from the Si-donors in the Al_xGa_{1-x}As, are transferred to the GaAs layer. The Coulomb interaction between electrons and ionized donors results in a confinement of the electron gas at the GaAs/Al_xGa_{1-x}As interface. The wave function of this so-called two-dimensional electron gas³ in the nearly triangular well can be solved quantum-mechanically. Due to the confining potential, quantized energy levels appear for the motion perpendicular to the interface, whereas the kinetic energy corresponding to the motion parallel to the interface is continuous.

Since the electrons in the 2DEG are separated from their parent donors, the ionized impurity scattering in the heterostructure is drastically reduced compared to the case of homogeneously doped bulk GaAs. Therefore, if the GaAs layer containing the 2DEG is free from background impurities, much higher mobilities can be achieved in a GaAs/Al_xGa_{1-x}As heterostructure than in bulk GaAs. Further enhancement of this high mobility is accomplished by growing an undoped Al_xGa_{1-x}As "spacer" layer between the GaAs layer and the Si-doped Al_xGa_{1-x}As layer, enlarging the distance between the electrons and their parent donors even more. Typical dimensions of the layered structure are depicted in Fig. 2.1(a). Between the substrate and the actual heterojunction, a GaAs buffer layer or a GaAs/AlAs superlattice is grown, which serves to getter impurities and to smear out during the growth irregularities of the substrate. The thin GaAs cap layer on top of the Al_xGa_{1-x}As layer is grown to protect the structure from oxidation.

Fig. 2.1(b) shows the bandstructure of the heterojunction. At the GaAs/ $\text{Al}_x\text{Ga}_{1-x}\text{As}$ interface the conduction and valence bands are bent due to the electric field between electrons and ionized donors. The band bending at the surface is a result of the surface states. Since GaAs is a covalent semiconductor, dangling bonds appear at the free surface. These dangling bonds create surface states in the bandgap of the semiconductor. Electrons from the Si-doped $\text{Al}_x\text{Ga}_{1-x}\text{As}$ layer are trapped in these surface states and a positively charged depletion layer is formed. The minimum of the $\text{Al}_x\text{Ga}_{1-x}\text{As}$ conduction band is located above the Fermi level, hence in equilibrium the $\text{Al}_x\text{Ga}_{1-x}\text{As}$ layer does not contain conduction electrons.

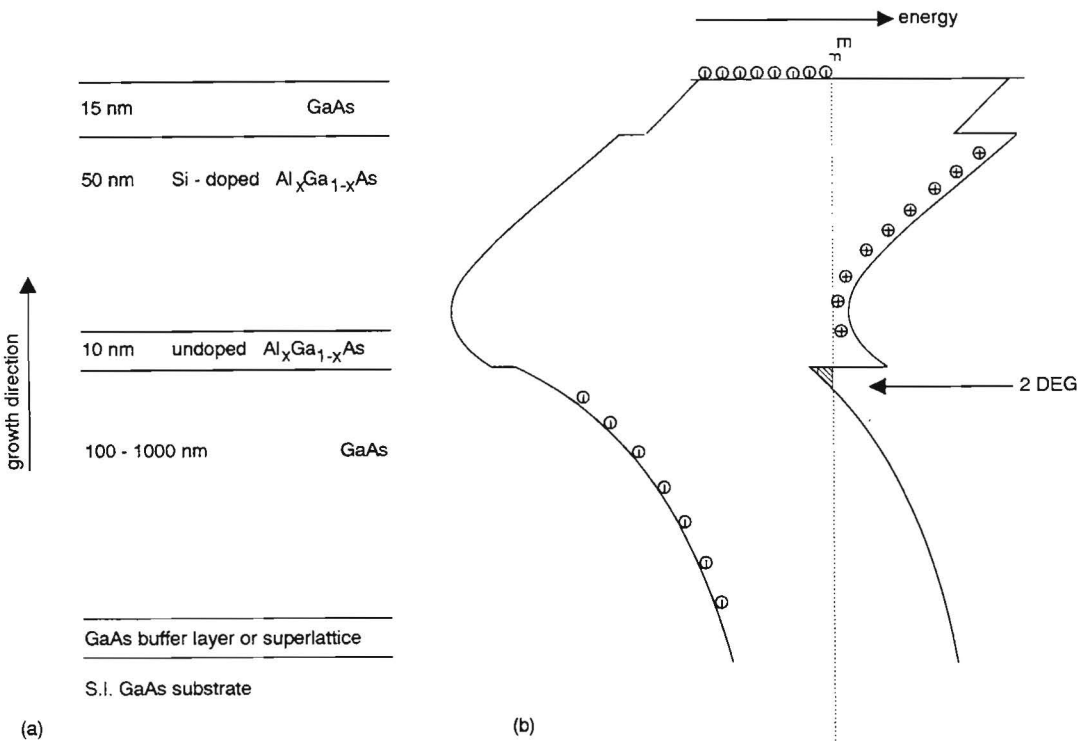


Fig. 2.1 (a) Typical dimensions of the layers of a GaAs/ $\text{Al}_x\text{Ga}_{1-x}\text{As}$ heterostructure and (b) the bandstructure of a GaAs/ $\text{Al}_x\text{Ga}_{1-x}\text{As}$ heterostructure.

In the remainder of this section, we discuss the processing and characterization of a GaAs/ $\text{Al}_x\text{Ga}_{1-x}\text{As}$ heterostructure. In the case of a GaAs/ $\text{Al}_x\text{Ga}_{1-x}\text{As}$ heterostructure used to fabricate a device, the wafer, after being grown, needs further processing. First, the geometry of the device must be defined. This is done photo-lithographically by mesa-etching the contour of the structure down to the buffer layer. Then, source and drain contacts are defined by evaporating AuGe/Ni using a lift-off technique. Subsequently the AuGe/Ni is alloyed through cap and $\text{Al}_x\text{Ga}_{1-x}\text{As}$ layer to make ohmic contact to the 2DEG. To be able to control the device, a gate electrode is defined to deplete the electron gas under the gate. For experiments in which it is not necessary to vary the electron density, the gate can be omitted.

After processing, the material and the contacts have to be characterized to determine their properties. The sample should be as homogeneous as possible and the contacts should show ohmic behavior and have a low resistance. Lateral homogeneity of the samples is very important, since inhomogeneities result in spatial variations of the optical and electrical properties of the device, making a reliable and reproducible behavior impossible. Inhomogeneities in a 2DEG can originate from the presence of microcracks or dislocations or from variations in the doping concentration and electron density^{4,5}. To investigate the homogeneity of the samples, several experimental methods can be used. The method used frequently in the work described here, is the optical beam induced current (OBIC) technique. In the experiments described in chapter 4, we use the OBIC technique to check whether the samples showing inhomogeneous properties at high electric fields are homogeneous at low electric fields. The OBIC technique is based on the lateral photo effect, which occurs when a heterostructure is illuminated locally and a lateral photo-voltage develops between the contacts^{4,6,7}. A schematical picture of the lateral photo effect is shown in Fig. 2.2(a). In the illuminated area, electron-hole pairs are created and separated in the growth direction, giving rise to a transverse photo voltage, $V_{\perp}(x)$. In the 2DEG, a constant electron diffusion current J_e flows away from the illuminated spot to the contacts. This diffusion current J_e gives rise to a potential distribution V_e in the 2DEG, according to

$$\frac{dV_e}{dx} = \rho_e J_e, \tag{2.1}$$

where ρ_e is the resistivity of the 2DEG and J_e the lateral electron diffusion current. When the sample is illuminated not exactly in the center between the two contacts, the result is a lateral photo voltage between the contacts, given by

$$\Delta V_e = \rho_e J_e (x_1 - x_2), \tag{2.2}$$

where x_1 and x_2 are the distances from the illuminated spot to the contacts C1 and C2, respectively. In a perfectly homogeneous sample, the lateral photo voltage depends

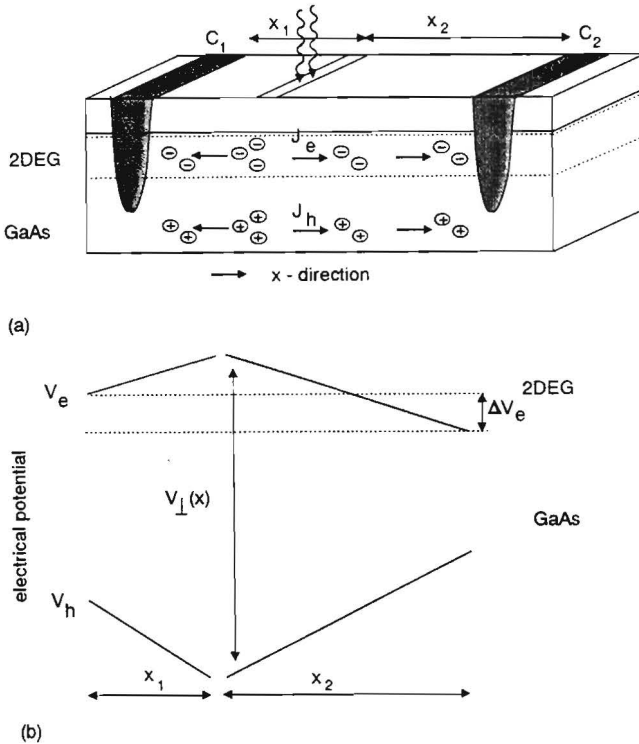


Fig. 2.2

(a) A schematic picture of the lateral photo effect. Visible are the creation of electron-hole pairs and the resulting diffusion currents J_e and J_h . C_1 and C_2 are the ohmic contacts (b) The potential distributions of V_e and V_h and the lateral photo voltage ΔV_e are schematically indicated.

linearly on the position of illumination. If there are any resistivity variations present in the 2DEG, they occur as deviations from linearity and are visualized in the OBIC image. In this derivation of the lateral photo voltage, recombination is neglected. A complete discussion of the lateral photo effect, taking into account recombination effects has been given by Fontein *et al.*^{4,8}.

When the sample and the contacts are homogeneous, the GaAs/Al_xGa_{1-x}As heterostructure is characterized with respect to its electrical properties. Usually Hall or van der Pauw experiments are performed to determine the carrier concentration and the Hall mobility as a function of temperature. These experiments are performed at low electric fields. The scattering mechanisms determining this low-field Hall mobility are discussed in section 2.3. From these experiments no information is obtained about the mobility in high electric fields. However, high electron mobility transistors normally are operated at high electric fields. It is therefore of great interest to understand the behavior of GaAs/Al_xGa_{1-x}As heterostructures at high electric fields and consequently high-field experiments are of great importance. These will be discussed in section 2.4.

2.3 Transport properties of the GaAs/Al_xGa_{1-x}As heterostructure

In this section we describe the transport properties of a GaAs/Al_xGa_{1-x}As heterostructure at low electric fields. First, we consider the properties of the two-dimensional electron gas and secondly we discuss two phenomena related to the properties of the Al_xGa_{1-x}As layer: the persistent photo conductivity (PPC) effect and parallel conduction.

The transport properties of the electrons in the 2DEG are determined by the scattering at irregular Coulomb potentials in the crystal. These irregularities originate from ionized impurities and from lattice vibrations (acoustic or optical phonons). Also roughness of the GaAs/Al_xGa_{1-x}As interface has to be taken into account. Several authors have calculated the scattering probabilities for these scattering mechanisms^{9,10,11,12,13}. The temperature dependence of the various scattering mechanisms and their contribution to the overall electron mobility is shown in Fig. 2.3¹². The mobilities are calculated for a GaAs/Al_xGa_{1-x}As heterostructure with a spacer of 20 nm and a carrier density of $5.3 \times 10^{11} \text{ cm}^{-2}$. The solid line (μ_{exp}) represents the experimental data by Hiyamizu *et al.*¹⁴. In this Figure we see that, with decreasing temperature, the predominant scattering mechanism shifts from optical phonon scattering, which is dominant for temperatures above 90 K, to acoustic phonons, for the range between 80 K and 10 K, and finally to ionized impurity scattering, which determines the mobility at low temperatures. In these calculations, the remote ionized impurity scattering was treated according to the conventional and to the revised theory by van Hall^{12,13}. This will be discussed below.

Let us first consider the scattering by ionized impurities. There are two types of ionized impurity scattering. First, the Coulomb interaction with the background impurities, which are mainly charged carbon acceptors, incorporated in the GaAs layer during the growth, and secondly, the interaction with the ionized silicon donors in the Al_xGa_{1-x}As layer. These are called remote ionized impurities. Except for samples with a very thick spacer or a very high background impurity concentration, the remote ionized impurities

contribute more to the scattering than the background impurities. In most calculations reported in the literature, the scattering probabilities of the ionized impurities are calculated from the total impurity distribution. However, van Hall^{12,13} has pointed out that in the remote impurity distribution only the fluctuations should be regarded as a scattering potential, since the average impurity distribution is already accounted for in the calculation of the electron wave function. This quantum mechanical "double counting" of the remote ionized impurity scattering results in an underestimation of the low-field mobility of the 2DEG.

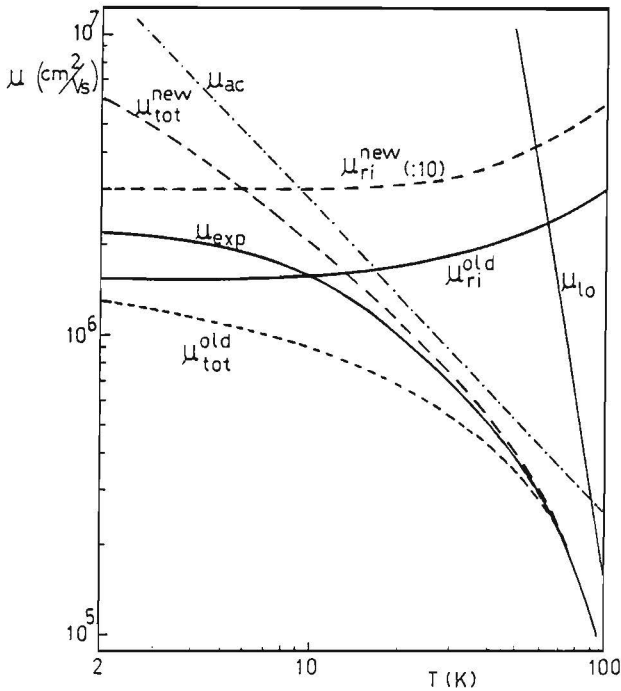


Fig. 2.3

Temperature dependence of the mobility in a GaAs/Al_xGa_{1-x}As heterostructure with a 20 nm spacer and a carrier density of $5.3 \times 10^{11} \text{ cm}^{-2}$. The scattering mechanisms are optical (lo) and acoustic (ac) phonon scattering and remote ionized impurity (ri) scattering. The remote ionized impurities are determined by the conventional (old) as well as by the revised (new) theory by van Hall. The overall electron mobility μ_{tot} is also shown, both according to the old and to the new theory. The line indicated by μ_{exp} represents the experimental data by Hiyamizu¹⁴.

We now turn to the scattering by acoustic and optical phonons. At low electric fields, where the energy of the electrons is lower than the threshold for optical phonon emission, the electrons can only be scattered by acoustic and optical phonons, already present in the lattice. The number of phonons present in the lattice strongly depends on the temperature. At intermediate temperatures ($15 \text{ K} < T < 80 \text{ K}$) the scattering process is dominated by acoustic phonon scattering via the deformation potential coupling and piezoelectric coupling¹⁰. In semiconductors, both scattering processes can be considered elastic. Scattering by optical phonons, which is dominant above 90 K, however, is highly inelastic, due to the large optical phonon energy of 36 meV in GaAs. Since the elasticity of GaAs and $\text{Al}_x\text{Ga}_{1-x}\text{As}$ are not too different, a three-dimensional approach to optical phonon scattering is commonly accepted for the 2DEG and the optical phonon limited mobility can be approximated by the mobility calculated for bulk GaAs^{10,15,16}. For this reason, also the experimentally determined mobility of the 2DEG is roughly the same as the electron mobility in bulk GaAs at these temperatures.

Finally, there is the scattering by the roughness of the GaAs/ $\text{Al}_x\text{Ga}_{1-x}\text{As}$ interface. This can be minimized by optimizing the growth conditions. Although the influence of interface roughness scattering on the mobility of the 2DEG is not well documented experimentally, it is supposed to be only important at high electron densities, since then the relative contribution of ionized impurity scattering is decreased due to screening effects^{10,17}.

Although usually the transport properties of GaAs/ $\text{Al}_x\text{Ga}_{1-x}\text{As}$ heterostructures are described in terms of the scattering mechanisms for the electrons in the 2DEG, it is very important to include the properties of the $\text{Al}_x\text{Ga}_{1-x}\text{As}$ layer as well. For example, it is well known that at temperatures below 110 K $\text{Al}_x\text{Ga}_{1-x}\text{As}$ shows a persistent photo conductivity (PPC) effect^{3,18}, which has a major influence on the transport properties of the heterostructure device. We therefore now describe the origin of this effect. In addition, we discuss parallel conduction in the $\text{Al}_x\text{Ga}_{1-x}\text{As}$ layer, which is a well known parasitic effect occurring in transport measurements.

The PPC effect is observed as an increased persistent conductivity of the 2DEG due to illumination at low temperatures. The origin of the PPC effect is the Si-donor in the $\text{Al}_x\text{Ga}_{1-x}\text{As}$ layer, which gives rise to two energy levels in the energy gap: a shallow and a deep donor level. The shallow donor lies about 5 meV below the Γ conduction band minimum and supplies its donor electrons to the conduction band. The energy of the deep level, which is called the DX center¹⁹, depends on the aluminium fraction and has been determined by several methods^{20,21}. Values between 120 and 200 meV below the L minimum have been reported. For an aluminium fraction of about 33% the energy of the DX center below the Γ minimum was determined theoretically and experimentally to be about 80 meV²². The occupation of both shallow and deep level and the free electron concentration in bulk Si- $\text{Al}_x\text{Ga}_{1-x}\text{As}$ have been calculated by Blom *et al.*²¹. The origin of the DX center is not exactly clear at present, but it is generally believed that it arises from a Si donor which has moved to an interstitial site¹⁹. When the minimum of the $\text{Al}_x\text{Ga}_{1-x}\text{As}$ conduction band lies above the Fermi level, the electrons, ionized from the DX centers by illumination, are transferred to the 2DEG. At temperatures below 110 K, when the illumination is switched off, the photo-ionized electrons in the 2DEG are not recaptured by the DX centers. To explain this, we have to consider two potential barriers: first, the potential barrier between the 2DEG and the $\text{Al}_x\text{Ga}_{1-x}\text{As}$ layer, and secondly the potential barrier between the ionized and bound state of the DX center itself. In bulk $\text{Al}_x\text{Ga}_{1-x}\text{As}$ the PPC effect has been observed in the same temperature range as in $\text{GaAs}/\text{Al}_x\text{Ga}_{1-x}\text{As}$ heterostructures²⁴. The observed similarity of the PPC effect in bulk $\text{Al}_x\text{Ga}_{1-x}\text{As}$ and in $\text{GaAs}/\text{Al}_x\text{Ga}_{1-x}\text{As}$ heterostructures leads to the conclusion that the potential barrier between ionized and bound state of the DX center in the $\text{Al}_x\text{Ga}_{1-x}\text{As}$ layer is responsible for the PPC effect²³. At temperatures of about 110 K there is only a very small fraction of the electrons in the 2DEG which have sufficient thermal energy to populate the $\text{Al}_x\text{Ga}_{1-x}\text{As}$ layer by crossing the potential barrier between the $\text{Al}_x\text{Ga}_{1-x}\text{As}$ and the 2DEG. Still, even for these electrons it is not possible to be captured by the DX center, since their thermal energy is too low to overcome the potential barrier between the ionized and bound state of the DX center, which is about 60-80 meV, dependent on the aluminium fraction^{22,24}. Therefore at low temperatures no thermal equilibrium exists between the

electrons in the 2DEG and the DX centers. The electrons remain in the 2DEG when the illumination is switched off, and the photoconductivity effect is persistent. The PPC effect can be eliminated by heating the sample to temperatures above 120 K. However, Rochette *et al.*²⁴ showed that the PPC effect can also be removed by applying a large source-drain voltage to a HEMT. In both cases, electrons gain enough energy to overcome the potential barrier and are captured in the deep donors. We also observe this effect in the high-field current-voltage experiments presented in chapter 4.

The effect of parallel conduction in $\text{GaAs}/\text{Al}_x\text{Ga}_{1-x}\text{As}$ heterostructures occurs when electron transport takes place in both the 2DEG and in the $\text{Al}_x\text{Ga}_{1-x}\text{As}$ layer²⁵. If we increase the electron density in the heterostructure in such a way that the Fermi level rises above the Γ minimum of the $\text{Al}_x\text{Ga}_{1-x}\text{As}$ conduction band, the electrons start to populate the $\text{Al}_x\text{Ga}_{1-x}\text{As}$ layer. Then, the heterostructure contains two conducting layers: one in the 2DEG, and one in the $\text{Al}_x\text{Ga}_{1-x}\text{As}$ layer. At low temperatures we can describe the heterostructure under these conditions by a system of two conducting layers, only interconnected at the contacts. At temperatures higher than about 110 K, however, the transfer of electrons across the $\text{GaAs}/\text{Al}_x\text{Ga}_{1-x}\text{As}$ interface is relatively easy and the heterostructure should be described as a system of two mutually interacting layers. Just like the PPC effect, which can be destroyed when high electric fields are applied, also parallel conduction in the $\text{Al}_x\text{Ga}_{1-x}\text{As}$ layer is affected by high electric fields. In a $\text{GaAs}/\text{Al}_x\text{Ga}_{1-x}\text{As}$ heterostructure showing purely two-dimensional behavior with no transport through the $\text{Al}_x\text{Ga}_{1-x}\text{As}$ layer at low electric fields, the $\text{Al}_x\text{Ga}_{1-x}\text{As}$ layer can be populated by electrons when high electric fields are applied. This phenomenon, which is called electric field induced parallel conduction (EFIPC) is one of the topics discussed in section 2.4.

2.4 High electric field effects in GaAs/Al_xGa_{1-x}As heterostructures

GaAs/Al_xGa_{1-x}As heterostructures are used to fabricate high electron mobility transistors (HEMTs)^{26,27,28}. A typical HEMT structure is shown in Fig. 2.4. It consists of a two-dimensional electron gas connecting the source and drain contact of the device. The device can be switched to the non-conducting state using a gate electrode to deplete the 2DEG under the gate. The switching time, which is equal to the time needed to deplete the 2DEG under the gate, is determined by the gate length, the carrier density, and the high-field drift velocity²⁹. Switching times of less than 10 ps have been reported for HEMT structures²⁹. HEMTs normally are operated with a source-drain voltage of several volts. Since the distance between source and drain is typically several microns, electric fields of several kV/cm easily are reached in a HEMT. In this section, we describe how the high electric field in the HEMT affects the electron drift velocity.

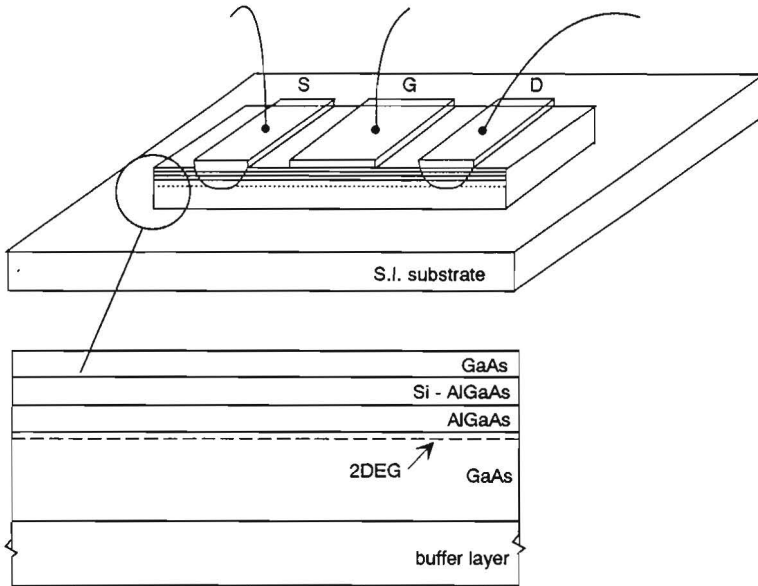


Fig. 2.4

Schematical picture of a high electron mobility transistor. Indicated are the 2DEG, the alloyed source (S) and drain (D) contact, and the gate electrode (G).

When an electric field is applied to a semiconductor, the electrons gain energy from the electric field and are accelerated. The electrons lose their energy to the lattice by scattering with phonons. This electron-phonon scattering leads to a continuous energy exchange between electrons and lattice. At low electric fields the energy acquired from the field is small compared to the average energy of the carriers in the absence of a field. The effective temperature of electrons and lattice is the same. Under these conditions, the Fermi-Dirac distribution function of the carriers exhibits a small shift in momentum space, which leads to the drift velocity. Since at low electric fields the deviations from equilibrium are small, the electron mobility remains independent of the applied electric field and Ohm's law is obeyed. At high electric fields, however, the energy the electrons gain from the electric field is no longer negligible compared to the equilibrium carrier energy, and the mean energy of the electrons is increased. In this regime the electron distribution function is significantly different from its equilibrium value, and can be characterized by an effective electron temperature, which is higher than the lattice temperature. Since at increasing electron energies additional scattering processes can occur, a lower electron mobility is observed at high electric fields^{30,31}. These, and other deviations from ohmic behavior are explained in this section. First, we consider the high-field behavior of the two-dimensional electron gas, and describe effects like current saturation and real space transfer. After that, we describe the high-field properties of the $\text{Al}_x\text{Ga}_{1-x}\text{As}$ layer and the ohmic contacts, leading to the occurrence of high-field current instabilities observed in HEMTs.

We now turn to the scattering mechanisms determining the high-field mobility of the two-dimensional electron gas. Hot-electron effects in two-dimensional systems are basically governed by the same phenomena as in bulk semiconductors, except that the carrier-phonon interactions are more complicated to evaluate because of the complex nature of the electron wave functions and the existence of several subbands. The problem of electron-phonon interaction in two-dimensional structures has been treated by a number of authors^{32,33,34,35,36,37}. They show that the scattering rate for optical phonon emission in two-dimensional semiconductor structures is

enhanced compared to the one in bulk semiconductors. At low temperatures and high electric fields, where the main scattering mechanism is optical phonon emission, this results in a saturation of the drift velocity.

Let us now derive the value for the saturation drift velocity for the case that the electron transport is completely dominated by optical phonon emission. The energy rate the electrons gain from the electric field, $(d\mathcal{E}/dt)_f$, is equal to

$$(d\mathcal{E}/dt)_f = F \cdot v = -eE (-\mu_d)E = eE\mu_d E = eE^2 \tau / m^*, \quad (2.3)$$

where \mathcal{E} is the electron energy, F is the force, v the electron velocity, e the electron charge, E the electric field, μ_d the electron drift mobility, τ the average momentum relaxation time, and m^* the effective mass³⁸. If the dominant scattering mechanism is optical phonon emission, the momentum relaxation time is equal to the electron scattering time for optical phonon emission, τ_{opt} , and the energy loss rate due to scattering, $(d\mathcal{E}/dt)_{sc}$, is equal to

$$(d\mathcal{E}/dt)_{sc} = \mathcal{E}_{opt} / \tau_{opt}, \quad (2.4)$$

where \mathcal{E}_{opt} is the optical phonon energy. In a steady state, the energy gain and energy loss rate are equal, leading to

$$\tau_{opt} = \frac{\sqrt{m^* \mathcal{E}_{opt}}}{eE}, \quad (2.5)$$

resulting in a saturation drift velocity of

$$v_{sat} = \mu_d E = \frac{E e \tau_{opt}}{m^*} = \sqrt{\frac{\mathcal{E}_{opt}}{m^*}}. \quad (2.6)$$

The optical phonon energy in GaAs is 36 meV and the effective mass is $0.067 m_0$,

where m_e is the free electron mass. This yields a theoretical saturation drift velocity of 3.1×10^7 cm/s. Note that since the saturation velocity only depends on the optical phonon energy and the effective mass, it is expected to be the same in two-dimensional structures and in bulk semiconductors. The experimentally observed saturation velocities in GaAs/Al_xGa_{1-x}As heterostructures range between 1.0 and 3.8×10^7 cm/s^{39,40,41,42,43,44,45}. The variation in these experimental data shows that the high-field transport in the 2DEG is not completely determined by optical phonon emission, but that also other effects play a role.

The electric field at which the saturation velocity is reached, depends on the low-field mobility μ_0 according to

$$E_{sat} = \frac{v_{sat}}{\mu_0} = \frac{\sqrt{m^* \mathcal{E}_{opt}}}{e \tau_0} . \quad (2.7)$$

Here, μ_0 is equal to $e \tau_0 / m^*$, where τ_0 is average momentum relaxation time at low electric fields. Since the low-field mobility in a GaAs/Al_xGa_{1-x}As heterostructure is much higher than in bulk GaAs, the saturation velocity is reached at relatively low electric fields. In Fig. 2.5 the velocity and mobility of a GaAs/Al_xGa_{1-x}As heterostructure are depicted as a function of the electric field at 4.2 K, 77 K, and 292 K, measured by Hirakawa and Sakaki, showing a saturation velocity of 2×10^7 cm/s⁴⁶.

If the high-field transport would be completely dominated by optical phonon emission, no electron energies higher than 36 meV could be reached in the two-dimensional electron gas. However, when the electric field is high enough, the amount of energy which the electrons gain from the electric field between two successive phonon emissions might become larger than the optical phonon energy. In that case, the energy the electrons gain from the electric field, $(d\mathcal{E}/dt)_f$, is larger than the energy loss rate by optical phonon emission, $(d\mathcal{E}/dt)_{opt}$, and energies higher than 36 meV can be reached.

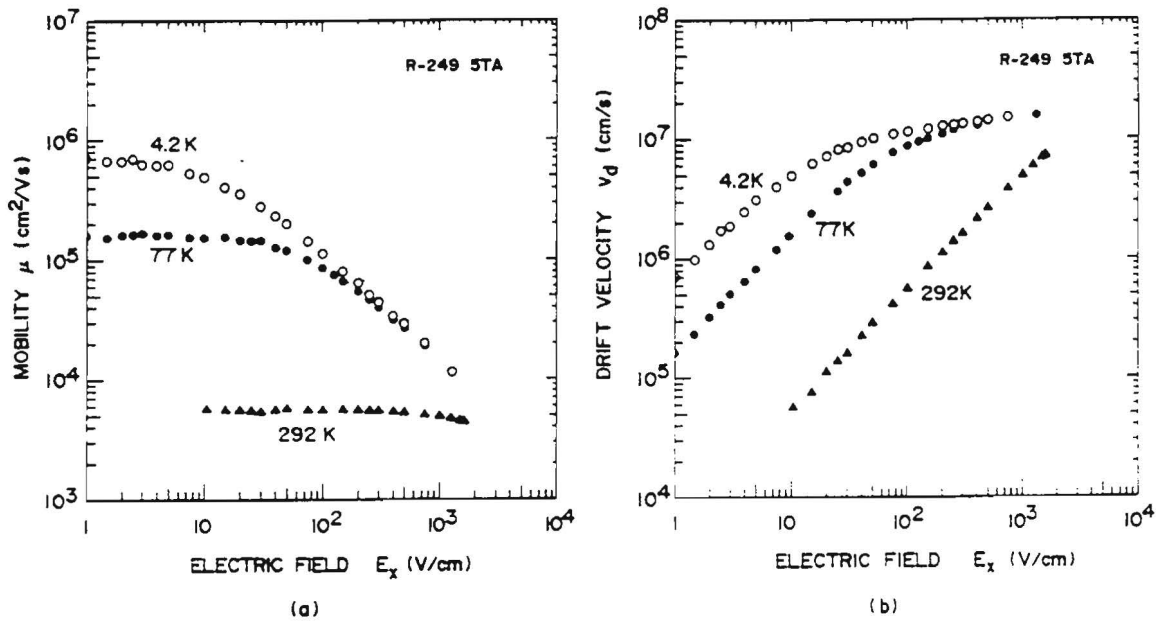


Fig. 2.5 (a) The Hall mobility and (b) the electron velocity in a GaAs/Al_xGa_{1-x}As heterostructure as a function of the electric field at 4.2 K, 77 K, and 292 K⁴⁶.

Another effect which can be responsible for electron heating above the threshold energy for optical phonon emission is a hot phonon distribution. When the lifetime of the emitted optical phonons is sufficiently long to build up a non-equilibrium hot phonon population, the energy loss rate of the electrons is reduced. Such hot-phonon effects have been considered theoretically⁴⁷, as well as observed experimentally^{48,49} in bulk semiconductors. Hot phonon effects in two-dimensional structures have been reported by Reinen *et al.*⁵⁰ and by Shah *et al.*⁵¹. They suggest that in high electric fields the emitted phonons can be re-absorbed by the electrons and energies of higher than 36 meV can be reached. The corresponding theory has been worked out by Price⁵². When the electrons are heated up above the optical phonon energy, additional scattering processes can occur. These are discussed below.

One of the scattering processes at higher energies is intervalley scattering from the Γ valley to the L and X valley. In GaAs the L valley lies about 300 meV above the Γ minimum and intervalley transfer occurs at electric fields of about 3 kV/cm⁵³. Since the effective mass in the L valley is larger, intervalley transfer leads to a decrease of the average drift velocity. According to Monte Carlo calculations, this velocity decrease due to intervalley scattering also occurs in GaAs/Al_xGa_{1-x}As heterostructures^{1,2}. A velocity-field characteristic calculated by the Monte Carlo method is shown in Fig. 2.6. Experimental evidence for the occurrence of intervalley transfer in GaAs/Al_xGa_{1-x}As heterostructures has not been reported until now. This might be due to the fact that at these high electric fields other processes take place in the heterostructure, which are not accounted for in the Monte Carlo calculations. Examples of these processes, such as real space transfer and parallel conduction in the Al_xGa_{1-x}As layer, are discussed below.

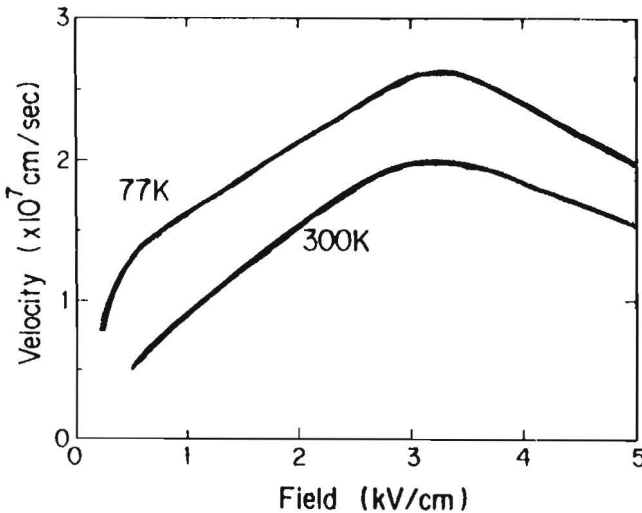


Fig. 2.6 Velocity-field characteristics¹ calculated by the Monte Carlo method for a GaAs/Al_xGa_{1-x}As heterostructure at 77 K and 300 K.

Real space transfer is the hot-electron thermionic emission of electrons from the 2DEG into the $\text{Al}_x\text{Ga}_{1-x}\text{As}$ layer^{54,55,56}. At high electric fields, the electrons in the 2DEG are heated to energies far above their thermal equilibrium value. As a result, the electrons in the 2DEG can be scattered to the $\text{Al}_x\text{Ga}_{1-x}\text{As}$ layer, across the energy barrier at the GaAs/ $\text{Al}_x\text{Ga}_{1-x}\text{As}$ interface. Since the mobility in the $\text{Al}_x\text{Ga}_{1-x}\text{As}$ layer is much lower than in the 2DEG, real space transfer leads to a decrease of the average electron drift velocity. At room temperature, a velocity decrease at 3.5 kV/cm ascribed to real space transfer was measured by Keever *et al.*⁵⁶ on a GaAs/ $\text{Al}_{0.17}\text{Ga}_{0.83}\text{As}$ heterostructure. Masselink *et al.* reported real space transfer in a GaAs/ $\text{Al}_{0.3}\text{Ga}_{0.7}\text{As}$ heterostructure, occurring at 4 kV/cm at room temperature and at 2 kV/cm at 77 K^{45,57}. In a GaAs/ $\text{Al}_{0.5}\text{Ga}_{0.5}\text{As}$ heterostructure, the $\text{Al}_x\text{Ga}_{1-x}\text{As}$ contains an indirect gap and the electrons are transferred from the 2DEG into the X minimum of the $\text{Al}_x\text{Ga}_{1-x}\text{As}$ conduction band. The threshold electric field for real space transfer in this case was measured by Masselink *et al.*^{57,58}. They reported a value of 3 kV/cm at 300 K and 2 kV/cm at 77 K. That the velocity decrease in these structures is caused by real space transfer and not by intervalley transfer in the GaAs layer was shown by Höpfel *et al.*⁵⁸. Luminescence experiments on a GaAs/ $\text{Al}_{0.48}\text{Ga}_{0.52}\text{As}$ quantum well structure showed that at the electric field where the velocity decrease is observed, the electron temperature is significantly lower than the electron temperature at which intervalley transfer is observed in GaAs.

The escape rates for electrons to scatter from the 2DEG to the three-dimensional states in the $\text{Al}_x\text{Ga}_{1-x}\text{As}$ layer were calculated by Lent *et al.*⁵⁹ They showed that the escape rates are relatively small compared to bulk scattering rates, even for electrons with energies larger than the band offset. Although these electrons have a large kinetic energy, their momentum is directed parallel to the interface. To escape from the 2DEG, the electrons need to shift their momentum such that they obtain a non-zero component in the direction perpendicular to the interface, for example by the emission or absorption of optical phonons.

Although real space transfer across the GaAs/ $\text{Al}_x\text{Ga}_{1-x}\text{As}$ interface is the most well known mechanism to transfer electrons from the 2DEG to the $\text{Al}_x\text{Ga}_{1-x}\text{As}$ layer, Hendriks *et al.*⁶⁰ showed that the injection of electrons into the $\text{Al}_x\text{Ga}_{1-x}\text{As}$ layer is also possible at the interconnection at the contacts, where the energy barrier between the 2DEG and the $\text{Al}_x\text{Ga}_{1-x}\text{As}$ layer is lower. Since we use this model to explain part of the experiments described in chapter 4 and 5, we now give a short description of this model. In a GaAs/ $\text{Al}_x\text{Ga}_{1-x}\text{As}$ heterostructure in equilibrium, electron transport only occurs through the 2DEG and not through the $\text{Al}_x\text{Ga}_{1-x}\text{As}$ layer, since the $\text{Al}_x\text{Ga}_{1-x}\text{As}$ conduction band lies above the Fermi level. This energy difference between the Fermi level and the $\text{Al}_x\text{Ga}_{1-x}\text{As}$ conduction band minimum is about 50 meV⁶¹. Therefore, at the ohmic contact there exists an energy barrier of only 50 meV between electrons at the Fermi level in the metal contact and the minimum in the $\text{Al}_x\text{Ga}_{1-x}\text{As}$ conduction band. Hendriks *et al.*⁶¹ showed that when a high electric field is applied, this barrier is decreased, and the electrons are injected from the source contact into the $\text{Al}_x\text{Ga}_{1-x}\text{As}$ layer. This process is called electric field induced parallel conduction (EFIPC).

The electron injection into the $\text{Al}_x\text{Ga}_{1-x}\text{As}$ layer gives rise to a time dependent behavior of the current in the heterostructure. Since the electron injection diminishes the positive charge density in the $\text{Al}_x\text{Ga}_{1-x}\text{As}$ layer and Poisson's equation and charge neutrality have to be obeyed, every extra electron injected into the $\text{Al}_x\text{Ga}_{1-x}\text{As}$ layer removes one electron from the 2DEG. Due to the fact that the mobility in the $\text{Al}_x\text{Ga}_{1-x}\text{As}$ is lower than in the 2DEG, the total current through the sample decreases in time^{60,61}. The decay time of the current depends on the properties of the $\text{Al}_x\text{Ga}_{1-x}\text{As}$ layer and the contact barrier. While the electron injection proceeds, the positive space charge in the $\text{Al}_x\text{Ga}_{1-x}\text{As}$ layer is diminished, thus the conduction band minimum rises with respect to the Fermi level. Electron injection into the $\text{Al}_x\text{Ga}_{1-x}\text{As}$ layer thus increases the injection barrier⁶¹. This increasing barrier height inhibits further carrier injection and the current reaches a steady state. After some time, the carriers leave the $\text{Al}_x\text{Ga}_{1-x}\text{As}$ at the drain contact and the 2D electron density returns to its original value. The depopulation time strongly depends on the properties of the $\text{Al}_x\text{Ga}_{1-x}\text{As}$ material, and on the occupation of deep and shallow traps. Depopulation times longer than several

microseconds were found, as we will observe in chapter 4, but also very short depopulation times were reported, leading to current oscillations during the pulse⁶⁶. This population-depopulation process in the $\text{Al}_x\text{Ga}_{1-x}\text{As}$ layer is a highly nonlinear process, which can give rise to steady state, oscillatory or chaotic behavior, dependent on the experimental conditions. Current instabilities in $\text{GaAs}/\text{Al}_x\text{Ga}_{1-x}\text{As}$ heterostructures had also been reported previously by other authors. Current collapse had been observed by Kastalsky and Kiehl⁶² and by Keever *et al.*⁶³ and current oscillations had been reported by Balkan and Ridley^{64,65} and by Hendriks *et al.*⁶⁶. However, at that time, none of them had given a satisfactory explanation for the observed phenomena.

The above discussion indicates that it is not possible to predict the performance of $\text{GaAs}/\text{Al}_x\text{Ga}_{1-x}\text{As}$ heterostructure devices at high electric fields based on extrapolations from zero field mobilities at low temperatures. For high electric fields velocity saturation effects and electric field induced parallel conduction often occur, thus limiting the performance improvements expected for modulation doped $\text{GaAs}/\text{Al}_x\text{Ga}_{1-x}\text{As}$ heterostructures.

2.5 Theoretical methods to calculate semiconductor transport

The transport properties of the electrons in a two-dimensional electron gas are determined by various scattering mechanisms. These scattering mechanisms, such as acoustic and optical phonon scattering^{34,35}, remote and background impurity scattering¹¹⁻¹³, interface roughness⁶⁷, and intervalley scattering⁶⁸ have been reviewed in the literature, and the scattering probabilities for these mechanisms have been calculated. When the scattering probabilities for all scattering mechanisms are known, the transport in a heterostructure can in principle be described and the electron mobility can be calculated. In this section we shortly describe two methods to calculate the electron transport properties of semiconductor heterostructures. First, we shortly discuss the relaxation time approximation of the Boltzmann transport equation and next we explain the principle of the Monte Carlo method. Finally, we discuss the results of some Monte Carlo calculations on two-dimensional electron gases, reported in the literature. In chapter 4 we will present the results of our Monte Carlo calculations on electrons in the $\text{Al}_x\text{Ga}_{1-x}\text{As}$ layer of a $\text{GaAs}/\text{Al}_x\text{Ga}_{1-x}\text{As}$ heterostructure.

To calculate the transport properties of a semiconductor we need the scattering rate for each scattering mechanism. The transition rate $W(k_i, k_f)$ for an electron to scatter from initial state k_i to final state k_f due to a scattering potential V_{sc} is given by

$$W(k_i, k_f) = \frac{2\pi}{\hbar} |V_{sc}(q)|^2 D(k_f), \quad (2.8)$$

where \hbar is Planck's constant, $q = k_i - k_f$, $D(k_f)$ is the density of states in the final state, and the squared matrix element $|V_{sc}(q)|^2$ is given by

$$|V_{sc}(q)|^2 = \langle \Psi_f | V_{sc}(q) | \Psi_i \rangle, \quad (2.9)$$

where Ψ_i and Ψ_f represent the initial and final wave function of the electron, respectively. Depending on whether we simulate transport in three or in two dimensions, we have to calculate the transition rates in equation (2.9) for a three or

a two-dimensional density of states and a 3D or 2D electron wave function. Since the scattering potentials are screened by the charges present, we have to divide the transition rates by a screening factor $S^2(q)$, where $S(q)$ is given by

$$S(q) = 1 + \frac{e^2 \Pi(q)}{\epsilon q^2}, \quad (2.10)$$

where $\Pi(q)$ is the polarizability and ϵ the dielectric constant of the material⁶⁹. In the case of a 2DEG, an additional form factor has to be included in eq. (2.10), to take into account the coupling of the various subbands⁷⁰.

When the Boltzmann transport equation is solved in the relaxation time approximation, the total scattering rate for each scattering mechanism is calculated by integrating the transition rates $W(k_j, k_f)$ over all possible scattering angles with a weight factor $(1 - \cos\theta)$ ⁷¹. This results in a momentum relaxation time, which defines a mobility for each mechanism. After that, the total mobility μ_{tot} is calculated by Matthiesen's rule

$$\frac{1}{\mu_{tot}} = \sum \frac{1}{\mu_j}, \quad (2.11)$$

where μ_j is the mobility for each scattering mechanism. The relaxation time approximation is only valid if, first, the electron distribution function deviates only slightly from equilibrium, and secondly, if the scattering processes are either randomizing or elastic. This means that in high electric fields the relaxation time approximation cannot be used because the deviations from equilibrium are considerably large.

A better and more realistic method to describe hot-electron transport in semiconductors is the widely used Monte Carlo method^{1,2,72}. The Monte Carlo method simulates the motion of an ensemble of electrons in an applied electric field. This motion consists of a series of subsequent free flights, each terminated by a scattering event. The duration of the free flight, the cause of the scattering, and the direction in which the next flight starts, are determined by choosing random numbers. To do this, a theoretical knowledge of the scattering probability distributions and the

band structure of the semiconductor is needed. If all features have been taken into account correctly, the particle velocities obtained by this method are distributed in the same way as in the real material and the material properties can be simulated rather accurately. An advantage of the Monte Carlo method is the fact that, contrary to the relaxation time approximation, the interdependence of the scattering mechanisms is taken into account. Furthermore, since an ensemble of electrons is considered one can readily account for the Pauli principle. When all scattering mechanisms are known the simulation gives exact solutions to the problems, be it with statistical errors. Another advantage is that the physics of the simulation is transparent and the modular structure of the simulation programs make them very flexible to be used in new problems or changed circumstances. Disadvantages are the fact that small errors easily remain unnoticed, the need for powerful computers, and a lot of computer time when high accuracy is required.

We now show some typical results of Monte Carlo calculations on GaAs/Al_xGa_{1-x}As heterostructures, reported in the literature. Typical velocity-field curves for a GaAs/Al_xGa_{1-x}As heterostructure at 300 K and at 77 K, calculated by Yokoyama and Hess¹ are shown in Fig. 2.7(a), and at 40 K and 10 K by Artaki and Hess² in Fig. 2.7(b). In Fig. 2.7(a) also the field dependence of the electron temperature is shown for 300 K and for 77 K. We see that at low temperatures the electrons are heated up more easily than at room temperature. Accordingly, the field at which intervalley transfer occurs shifts from 3.3 to 2.5 kV/cm with decreasing temperatures. Furthermore, the peak drift velocity increases with decreasing temperatures, which is due to the lower phonon scattering rates. The "shoulder" at about 0.5 kV/cm is attributed to the onset of optical phonon emission.

The velocity-field curves shown above are widely cited in the literature but still contain a number of irregularities which will be discussed below. In almost all Monte Carlo calculations reported, the scattering probabilities of the ionized impurities are calculated from the total impurity distribution. However, in section 2.3 we already

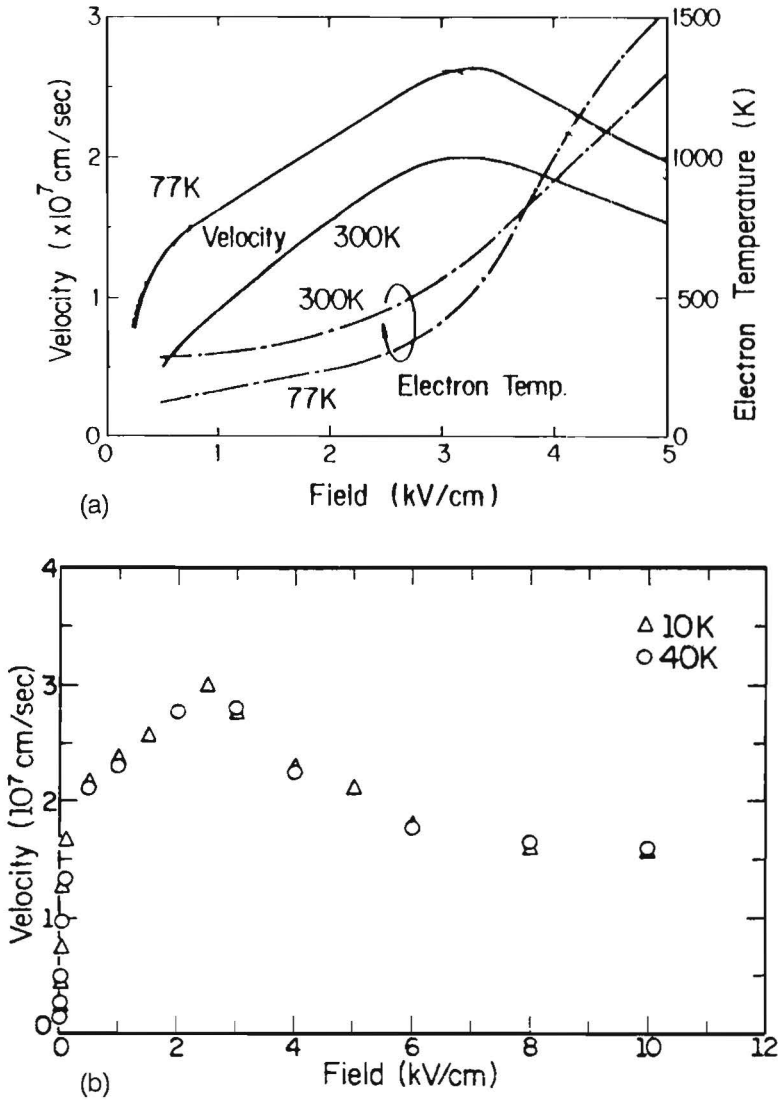


Fig. 2.7 (a) Drift velocity and electron temperature as a function of the electric field¹ for a GaAs/Al_xGa_{1-x}As heterostructure at 300 K and 77 K. (b) Velocity-field characteristics² for a GaAs/Al_xGa_{1-x}As heterostructure at 40 K and 10 K.

discussed that in the remote ionized impurity distribution only the fluctuations of the impurity distribution should be regarded as a scattering potential. However, since at high electric fields the ionized impurity scattering is not dominant, we expect this correction to be small at high electric fields. In Fig. 2.8 we show the mobility versus the electric field up to 1 kV/cm for a GaAs/ $\text{Al}_x\text{Ga}_{1-x}\text{As}$ heterostructure at 4.2 K, as calculated by van Hall *et al.*⁷³, taking into account the revised theory for the ionized impurity scattering.

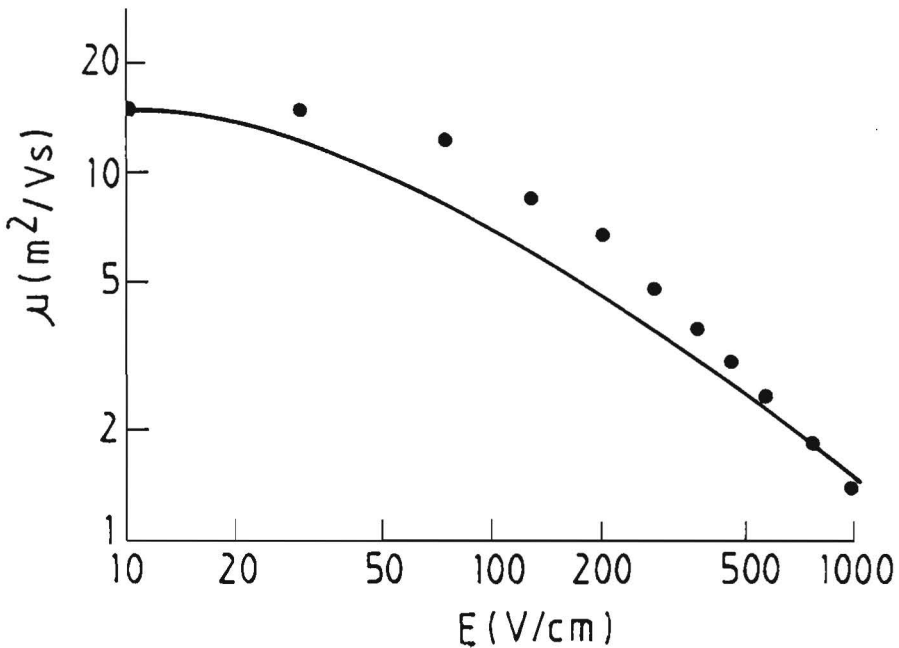


Fig. 2.8

Mobility as a function of the electric field for a GaAs/ $\text{Al}_x\text{Ga}_{1-x}\text{As}$ heterostructure with a spacer layer of 6 nm at a temperature of 4.2 K, as calculated by van Hall *et al.* The dots are experimental data by Hendriks⁵⁹.

Finally, there is another problem with the Monte Carlo calculations at high electric fields. As was discussed before, to describe a GaAs/ $\text{Al}_x\text{Ga}_{1-x}\text{As}$ heterostructure at high electric fields, not only the properties of the 2DEG should be included, but also processes like real space transfer into the $\text{Al}_x\text{Ga}_{1-x}\text{As}$ layer and electric field induced parallel conduction. Since these properties of the $\text{Al}_x\text{Ga}_{1-x}\text{As}$ layer are not included in the Monte Carlo calculations reported until now, care must be taken by using Monte Carlo calculations to predict the properties of novel devices. Obviously, more theoretical work is needed to extend this valuable technique to more realistic experimental circumstances.

References

1. K. Yokoyama and K. Hess, *J. Appl. Phys.* 59, 3798 (1986).
2. M. Artaki and K. Hess, *Phys. Rev. B* 37, 2933 (1988).
3. H.L. Störmer, R. Dingle, A.C. Gossard, W. Wiegmann, and M.D. Sturge, *Solid State Commun.* 29, 705 (1979).
4. P.F. Fontein, P. Hendriks, J. Wolter, R. Peat, D.E. Williams, and J.P. André, *J. Appl. Phys.* 64, 3085 (1988).
5. R. Woltjer, Ph.D. Thesis, University of Utrecht, the Netherlands (1988).
6. J.I. Pankove, *Optical Processes in Semiconductors* (Prentice Hall, Englewood Cliffs, New Jersey, 1971), p. 331.
7. G. Lucovsky, *J. Appl. Phys.* 31, 1088 (1960).
8. P.F. Fontein, A. Kucernak, R. Peat, J. Williams, *Proceedings SPIE* 1028, 197 (1988).
9. W. Walukiewicz, H.E. Ruda, J. Lagowski, and H.C. Gatos, *Phys. Rev. B* 29, 4814 (1984).
10. W. Walukiewicz, H.E. Ruda, J. Lagowski, and H.C. Gatos, *Phys. Rev. B* 30, 4571 (1984).
11. K. Hirakawa and H. Sakaki, *Phys. Rev. B* 33, 8291 (1986).
12. P.J. van Hall, T. Klaver, and J.H. Wolter, *Semicond. Sci. Technol.* 3, 120 (1988).
13. P.J. van Hall, *Superlat. Microstruct.* 6, 213 (1989).
14. S. Hiyamizu, J. Saito, K. Kondo, T. Yamamoto, T. Ishikawa, and S. Sasa, *J. Vac. Sci. Technol. B* 3, 585 (1985).
15. P.J. Price, *Surf. Sci.* 113, 199 (1982).
16. W. Walukiewicz, J. Lagowski, L. Jastrzebski, M. Lichtensteiger, and H.C. Gatos, *J. Appl. Phys.* 58, 899 (1979).
17. T. Ando, *J. Phys. Soc. Jap.* 51, 3900 (1982).
18. H.L. Störmer, A.C. Gossard, W. Wiegmann, and K. Baldwin, *Appl. Phys. Lett.* 39, 912 (1981).

-
19. P.M. Mooney, J. Appl. Phys. 67, R1 (1990).
 20. J.C.M. Henning and J.P.M. Ansems, Semicond. Sci. Technol. 2, 1 (1987).
 21. P.W.M. Blom, P.M. Koenraad, F.A.P. Blom, and J.H. Wolter, J. Appl. Phys. 66, 4269 (1989).
 22. N. Chand, T. Henderson, J. Klem, W.T. Masselink, R. Fischer, Y.C. Chang, and H. Morkoç, Phys. Rev. B 30, 4481 (1984).
 23. W. Timelthaler, W. Jantsch, and G. Weimann, Semicond. Sci. Technol. 5, 686 (1990).
 24. J.F. Rochette, P. Delescluse, M. Laviro, D. Delagebeaudeuf, J. Chevrier, and N.T. Linh, Inst. Phys. Conf. Ser. 65, chapter 5, 385 (1983).
 25. S. Luryi and A. Kastalsky, Appl. Phys. Lett. 45, 164 (1984).
 26. T. Mimura, Surface Science 113, 454 (1982).
 27. T. Mimura, S. Hiyamizu, T. Fuji, and K. Nanbu, Jpn. J. Appl. Phys. 19, L225 (1980).
 28. T.P. Pearsall, Surf. Sci. 142, 529 (1983).
 29. M. Feng, C.L. Lau, V. Eu, and C. Ito, Appl. Phys. Lett. 57, 1233 (1990).
 30. E.J. Ryder and W. Shockley, Phys. Rev. 81, 139 (1951).
 31. E.J. Ryder, Phys. Rev. 90, 776 (1953).
 32. B.K. Ridley, J. Phys. C 15, 5899 (1982).
 33. F.A. Riddoch and B.K. Ridley, J. Phys. C. 16, 6971 (1983).
 34. P.J. Price, Ann. Phys. 133, 217 (1981).
 35. K. Hess, Appl. Phys. Lett. 35, 484 (1979).
 36. M. Al-Mudares and B.K. Ridley, Physica 134B, 526 (1985).
 37. M.A.E. Al-Mudares and B.K. Ridley, J. Phys. C 19, 3179, (1986).
 38. S. Wang, *Solid State Electronics* (McGraw-Hill, New York, 1966), p. 232.
 39. E.F. Schubert, K. Ploog, H. Dämbkes, and K. Heime, Appl. Phys. A33, 183 (1984).
 40. M. Inoue, Superl. and Microstruct. 1, 433 (1985).

-
41. M. Inoue, M. Inayama, S. Hiyamizu, and M. Inuishi, *Jpn. J. Appl. Phys.* 22, L213 (1983).
 42. M. Keever, H. Shichijo, K. Hess, S. Banerjee, L. Witkowski, H. Morkoç, and K. Hess, *Jpn. J. Appl. Phys.* 21, 1489 (1982).
 43. K. Inoue, H. Sakaki, and J. Yoshino, *Appl. Phys. Lett.* 47, 614 (1985).
 44. W.T. Masselink, N. Braslau, D. LaTulipe, W.I. Wang, and S.L. Wright, *Solid State Electron.* 31, 337 (1988).
 45. M. Keever, W. Kopp, T.J. Drummond, H. Morkoç, and K. Hess, *Jpn. J. Appl. Phys.* 21, 1489 (1982).
 46. K. Hirakawa and H. Sakaki, *J. Appl. Phys.* 63, 803 (1988).
 47. W. Potz and P. Kocevar, *Phys. Rev. B* 28, 7040 (1983).
 48. J. Shah, R.C.C. Leite, and J.F. Scott, *Solid State Commun.* 8, 1089 (1970).
 49. J.A. Kash, J.C. Tsang, and J.M. Hvam, *Phys. Rev. Lett.* 54, 2151 (1985).
 50. H.J.A.M. Reinen, T.T.J.M. Berendschot, P.C.M. Christianen, H.J.A. Bluysen, K. Ploog, and M. Leys, *Solid State Electron.* 32, 1315 (1989).
 51. J. Shah, A. Pinczuk, A.C. Gossard, and W. Wiegmann, *Phys. Rev. Lett.* 54, 2045 (1985).
 52. P.J. Price, *Physica* 134B, 164 (1985).
 53. J.G. Ruch and W. Fawcett, *J. Appl. Phys.* 41, 3843 (1970).
 54. K. Hess, H. Morkoç, H. Shichijo, and B.G. Streetman, *Appl. Phys. Lett.* 35, 469 (1979).
 55. M. Keever, H. Shichijo, K. Hess, S. Banerjee, L. Witkowski, H. Morkoç, and B.G. Streetman, *Appl. Phys. Lett.* 38, 36 (1981).
 56. M. Keever, K. Hess, and M. Ludowise, *IEEE Trans. Electron Device Lett.* EDL-3, 297 (1982).
 57. W.T. Masselink, N. Braslau, W.I. Wang, and S.L. Wright, *Appl. Phys. Lett.* 51, 1533 (1987).
 58. R.A. Höpfel, J. Shah, D. Block, and A.C. Gossard, *Appl. Phys. Lett.* 48, 148 (1986).
 59. C.S. Lent, L. Liang, and W. Porod, *Appl. Phys. Lett.* 54, 2315 (1989).

-
60. P. Hendriks, E.A.E. Zwaal, J.G.A. Dubois, F.A.P. Blom, and J.H. Wolter, *J. Appl. Phys.* 69, 302 (1991).
 61. E.A.E. Zwaal, P. Hendriks, P.T.J. van Helmond, J.E.M. Haverkort, and J.H. Wolter, submitted to *J. Appl. Phys.* (1991).
 62. A. Kastalsky and R.A. Kiehl, *IEEE Trans. Electron Devices* ED-33, 414 (1986).
 63. M. Keever, T. Drummond, K. Hess, H. Morkoç, and B.G. Streetman, *Electron. Lett.* 17, 93 (1981).
 64. N. Balkan and B.K. Ridley, *Semicond. Sci. Technol.* 3, 507 (1988).
 65. N. Balkan, B.K. Ridley, and J.S. Roberts, *Superlat. Microstruct.* 5, 539 (1989).
 66. P. Hendriks, A.A.M. Staring, R.G. van Welzenis, J.H. Wolter, W. Prost, K. Heime, W. Schlapp, and G. Weimann, *Appl. Phys. Lett.* 54, 2668 (1989).
 67. H. Sakaki, *Appl. Phys. Lett.* 51, 1934 (1987).
 68. R. Mickevičius and A. Reklaitis, *Semicond. Sci. Technol.* 5, 805 (1990).
 69. G. Bastard, *Wave mechanics applied to semiconductor heterostructures* (les éditions de physique, Les Ulis, France, 1988), p. 233.
 70. E.D. Siggia and P.C. Kwok, *Phys. Rev. B* 2, 1024 (1970).
 71. C. Jacoboni and P. Lugli, *The Monte Carlo method for semiconductor device simulation* (Springer Verlag, Wien, New York, 1989), p. 64.
 72. C. Jacoboni and L. Reggiani, *Rev. Mod. Phys.* 55, 645 (1983).
 73. P.J. van Hall, R. de Rooy, and J.H. Wolter, *Superlat. Microstruct.* 8, 309 (1990).

Chapter 3

Time-of-flight experiments on GaAs/Al_xGa_{1-x}As heterostructures

3.1 Introduction

In this chapter we discuss time-of-flight experiments on GaAs/Al_xGa_{1-x}As heterostructures containing a two-dimensional electron gas. The time-of-flight technique is well-known from bulk semiconductor physics, where it is used to measure the drift velocity under high electric field conditions. Since the aim of this work is to investigate the transport properties of two-dimensional semiconductor structures at high electric fields, the question arises whether the time-of-flight technique is suitable to measure high-field drift velocities in these two-dimensional semiconductors as well. We therefore have to examine the differences between two-dimensional semiconductors and bulk semiconductors with respect to the time-of-flight technique. Furthermore, we have to establish the experimental criteria under which a time-of-flight experiment yields the relevant high-field transport properties of a two-dimensional semiconductor structure.

Let us first discuss the principle of the time-of-flight technique^{1,2}. The experimental configuration is shown in Fig. 3.1(a). In a time-of-flight experiment, excess carriers are created locally in the semiconductor by a short laser pulse. Under the influence of an applied electric field the excess carriers drift through the sample, thus giving rise to an excess current in the external circuit, as is indicated in Fig. 3.1(b). Since the duration Δt of this excess current pulse directly corresponds to the time the carriers need to reach the contact, the drift velocity v of the excess carriers can be directly determined from the width of the time-of-flight current according to

$$v = \frac{\Delta x}{\Delta t}, \quad (3.1)$$

where Δx is the distance between the position of illumination and the contact. The time-of-flight technique thus is a very direct method to measure carrier drift velocities in semiconductors at high electric fields.

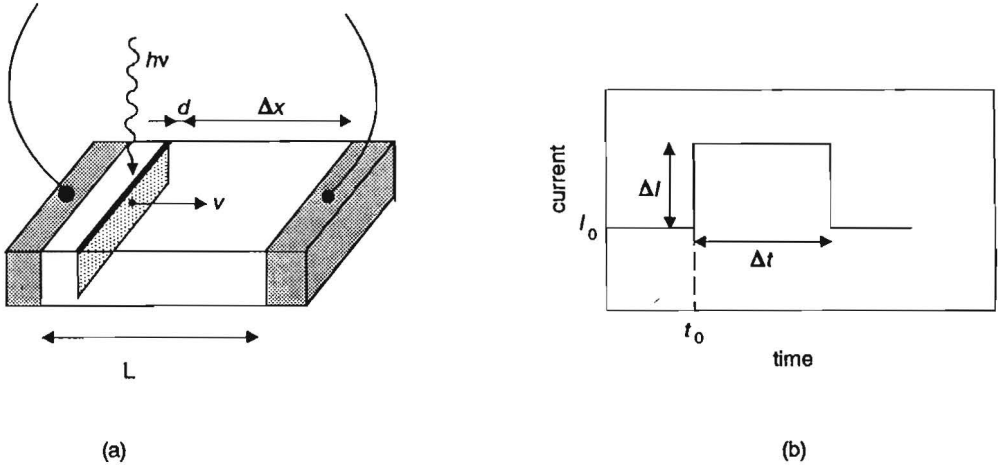


Fig. 3.1

(a) Experimental configuration of a time-of-flight experiment. Excess carriers excited by a laser pulse drift through the sample under the influence of the electric field. The grey areas are the ohmic contacts. (b) The excess carriers induce an increase of the current through the sample. I_0 is the bias current when no laser illumination is applied. At t_0 the laser pulse is given. The duration Δt of the excess current corresponds to the time-of-flight of the carriers.

The transport of the excess carriers in bulk semiconductors is described by the ambipolar transport equation^{2,3,4}, which will be discussed in section 3.2, where we review the time-of-flight technique as used in bulk semiconductors. In section 3.3 we discuss the conditions which must be satisfied for a time-of-flight experiment on a two-dimensional semiconductor structure. The results of our time-of-flight experiments on GaAs/Al_xGa_{1-x}As heterostructures are presented in section 3.4. Finally, in section 3.5, we summarize the results of this chapter.

3.2 The time-of-flight technique

In this section we take a closer look at the time-of-flight technique as used in bulk semiconductors. The time-of-flight technique as presented in section 3.1 was introduced in 1970 by Neukermans and Kino^{1,2}. It consists of a combination of two previously known techniques: the Haynes-Shockley experiment⁵, which was used to measure minority carrier drift velocities in extrinsic semiconductors, and the original time-of-flight technique to measure drift velocities in semi-insulating materials^{6,7,8,9,10}. The latter technique, introduced by Spear^{6,7}, uses a fully depleted back-biased *p-i-n* structure in which excess carriers are created by a pulsed electron beam. To obtain useful results, a highly uniform electric field is required in the intrinsic region. Since the internal field due to the space charges has to be much smaller than the high electric field applied, only very pure intrinsic materials can be used, which severely limits the applicability of this method.

In the classical Haynes-Shockley experiment⁵, an extrinsic semiconductor with ohmic contacts is used and an electric field is applied between these contacts. Minority carriers are injected by a voltage pulse on a separate emitting electrode at a time t_1 . The minority carriers move under the influence of the field, and at time t_2 their arrival is detected at a separate collector electrode. From the distance between the emitter and the collector and the time difference $t_2 - t_1$, the velocity of the minority carriers is obtained. The major drawback of this method are the pick-up problems at the collector caused by the pulsed voltage supply. To overcome these difficulties Neukermans and Kino modified the classical Haynes-Shockley experiment by using a pulsed electron beam to excite the excess electron-hole pairs and by measuring the transit time from the duration of the excess current. Later, the time-of-flight technique was performed using a pulsed laser beam instead of an electron beam^{11,12}.

We now examine the height of the excess current. Consider an *n*-type semiconductor with an electron density n_0 . When an electric field E is applied, the current density through the sample is given by $J_0 = n_0 e \mu_e E$. Here, e is the electron charge and μ_e

is the electron mobility. When excess electron-hole pairs are excited locally in the semiconductor, as was indicated in Fig. 3.1, the sample resistance is lowered instantaneously. At the time of the excitation the current density increases by

$$\Delta J = \frac{d}{L} \Delta n e (|\mu_e| + |\mu_h|) E, \quad (3.2)$$

where d is the width of the line shaped laser spot, Δn is the density of excited electron-hole pairs, L is the sample length, and μ_h is the mobility of the holes⁴.

Let us now consider the duration of the excess current. As was mentioned before, the duration of the excess current is determined by the so-called ambipolar drift velocity of the excess carriers^{2,3,4}. In order to examine the physical meaning of this ambipolar drift velocity we first discuss the dielectric relaxation time τ_D of the semiconductor, defined as $\tau_D = \epsilon \rho$. Here, ϵ is the dielectric constant and ρ is the resistivity of the semiconductor, equal to $1/n e \mu$. The dielectric relaxation time corresponds to the time it takes for the majority carriers to neutralize an uncompensated space charge in the semiconductor. In a semiconductor with a carrier density equal to 10^{14} cm^{-3} , a mobility of $10^3 \text{ cm}^2/\text{Vs}$, and a relative dielectric constant of 12, τ_D is about 60 ps, which means that on a time scale longer than 60 ps no space charges can exist in the semiconductor. For this reason, in an experiment taking place on a time scale longer than τ_D , excess electron-hole pairs cannot be separated by the electric field. The coupled motion of the excess electrons and holes is described by the ambipolar transport equation, which we derive below. If the electric field is applied in the x direction, the electron and hole current density in the x direction are given by

$$J_e = \sigma_e E_x + e D_e \frac{\partial n}{\partial x} \quad (3.3)$$

and

$$J_h = \sigma_h E_x - e D_h \frac{\partial p}{\partial x},$$

where σ_e and σ_h are the conductivities of the electrons and holes, given by $\sigma_e = n e \mu_e$ and $\sigma_h = p e \mu_h$, respectively. E_x is the electric field in the x direction, D_e and D_h are

the diffusion constants of the electrons and holes, and n and p are the electron and hole concentrations, respectively. Taking into account recombination, the complete continuity equations become

$$\frac{\partial n}{\partial t} = \frac{1}{e} \frac{\partial J_e}{\partial x} - \frac{\Delta n}{\tau_r} = \frac{\partial}{\partial x} (\mu_e n E_x) + D_e \frac{\partial^2 n}{\partial x^2} - \frac{\Delta n}{\tau_r}$$

and (3.4)

$$\frac{\partial p}{\partial t} = -\frac{1}{e} \frac{\partial J_h}{\partial x} - \frac{\Delta p}{\tau_r} = -\frac{\partial}{\partial x} (\mu_h p E_x) + D_h \frac{\partial^2 p}{\partial x^2} - \frac{\Delta p}{\tau_r},$$

where τ_r is the recombination lifetime, assumed to be equal for electrons and holes. If we assume that the material is homogeneous, only the excess carrier concentrations Δn and Δp are time dependent. We also assume that the mobilities μ_e and μ_h are independent of x . Due to local charge neutrality $\Delta n(x,t)$ is equal to $\Delta p(x,t)$. If we now multiply equations (3.4) by σ_h and σ_e , respectively, and take the sum of these equations, we get the ambipolar transport equation,

$$\frac{\partial \Delta p}{\partial t} = \frac{\partial \Delta n}{\partial t} = \mu_a E_x \frac{\partial \Delta n}{\partial x} + D_a \frac{\partial^2 \Delta n}{\partial x^2} - \frac{\Delta n}{\tau_r}. \quad (3.5)$$

In this equation, μ_a and D_a are the ambipolar mobility and the ambipolar diffusion constant, defined as

$$\mu_a = \frac{\sigma_h \mu_e - \sigma_e \mu_h}{\sigma}$$

and (3.6)

$$D_a = \frac{\sigma_h D_e + \sigma_e D_h}{\sigma},$$

where σ is equal to $\sigma_h + \sigma_e$. In a highly doped n -type semiconductor equation (3.6) turns into

$$\mu_a = \mu_h \quad \text{and} \quad D_a = D_h. \quad (3.7)$$

For a p -type semiconductor, the same derivation can be given. In that case, the ambipolar mobility and diffusion constant are given by $\mu_a = \mu_e$ and $D_a = D_e$ respectively. We thus arrive at the well-known result that in highly extrinsic semiconductors the ambipolar transport of excess electron-hole pairs is determined by the properties of the minority carriers. The ambipolar drift velocity of the excess carriers which determine the duration of the excess current in a time-of-flight experiment is thus equal to the drift velocity of the minority carriers. As the derivation of the ambipolar transport equation is based on a small signal theory, the excess carrier density in the time-of-flight experiment must be small compared to the equilibrium carrier density, which limits the maximum allowed excitation density in the experiment.

When diffusion and recombination effects are negligible, the time-of-flight current is constant during the transit time of the carriers resulting in a rectangular shape of the time-of-flight signal. In practice, however, deviations from this ideal case are observed. Diffusion of the excited carriers creates a spreading of the time-of-flight of the carriers and recombination causes a decrease of the time-of-flight current as a function of time. The effects of diffusion and recombination on the shape of the time-of-flight signal are illustrated in Fig. 3.2. Since the effects of recombination and diffusion on the time-of-flight current should be small, this also puts a constraint on the time-of-flight experiments.

After the introduction of the time-of-flight technique it was successfully applied to measure the drift velocity of minority carriers in various bulk semiconductors. The velocity-field characteristics of minority electrons at various temperatures were measured in InSb^{1,13}, Ge², Si^{11,12}, and InGaAs¹⁴. In p -GaAs the electron drift velocity up to 10 kV/cm was measured at 300 K for various majority hole concentrations¹⁵.

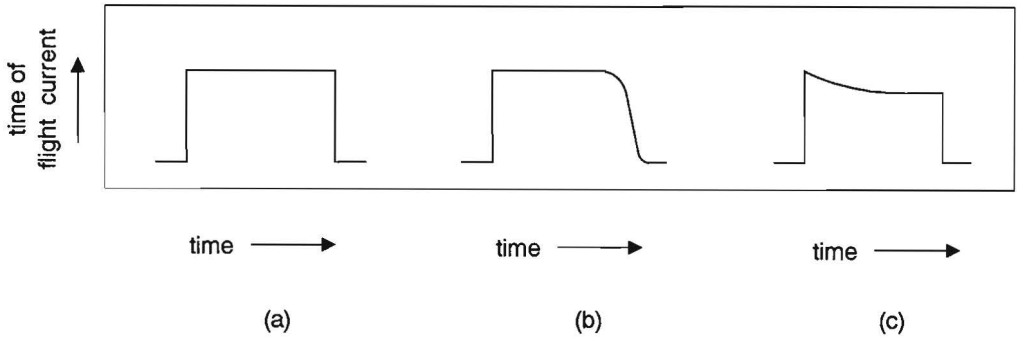


Fig. 3.2 Schematic drawing of the time-of-flight pulses under various experimental conditions. (a) drift, (b) drift and diffusion, and (c) drift and recombination.

With increasing hole concentrations, a decreasing drift velocity was measured, which was explained by an increased electron-hole scattering. Because of this increased carrier-carrier scattering the drift mobilities of minority carriers are always lower than the drift mobilities of majority carriers. Calculations have indicated that at equal doping densities the minority electron mobility in bulk p -GaAs is about 40% lower than the majority electron mobility in bulk n -GaAs^{16,17,18,19,20}. In bulk semiconductors these carrier-carrier interactions usually are neglected and it is common practice to assume that the minority electron mobility in a p -doped semiconductor is roughly equal to the majority electron mobility in the n -doped semiconductor^{21,22}. For that reason, the minority carrier drift velocities obtained by the time-of-flight technique are also used to estimate majority carrier drift velocities at high electric fields, which cannot be measured directly by any other experimental method. Unfortunately, this practice cannot be extended to two-dimensional semiconductor structures, as will be shown in the next section.

3.3 Time-of-flight experiments on 2D semiconductor structures

In order to examine to what extent the time-of-flight technique allows to measure high-field drift velocities in two-dimensional semiconductor structures, we now discuss the conditions for a correct determination of the ambipolar drift velocity. First, to study ambipolar transport we need an extrinsic semiconductor structure of low resistivity with ohmic contacts. Secondly, the recombination lifetime of the excited carriers has to be longer than the time-of-flight under all experimental conditions, since the time dependence of the excess current has to be determined by drift and not by recombination of the carriers. We consider two possible structures: the modulation doped quantum well and the modulation doped heterostructure. The difference between both structures is that in the quantum well the excited electron-hole pairs remain in the same layer, whereas in the heterostructure the electrons and holes are separated in the growth direction by the internal electric field. Due to the spatial separation of electrons and holes the low-temperature carrier lifetimes in a heterostructure are of the order of 10-100 ns²³, whereas in the quantum well typical values of about 1 ns are reported²⁴. Since a modulation doped heterostructure seems to be quite suitable for a time-of-flight experiment because of the enhanced carrier lifetime, we further examine the conditions for a time-of-flight experiment on a GaAs/Al_xGa_{1-x}As heterostructure.

Let us first consider the charge neutrality condition. Since a GaAs/Al_xGa_{1-x}As heterostructure consists of several different epitaxial layers, one has to consider charge neutrality both parallel and perpendicular to the layers. In the plane of the 2DEG the conductivity is high, corresponding to a very short (\ll 1 ps) dielectric relaxation time. Therefore, in the lateral direction of the heterostructure charge neutrality is maintained, corresponding to an equivalent situation as in an extrinsic bulk semiconductor. Hence, in the lateral direction separation of electron-hole pairs is not possible and the ambipolar transport equation can be applied.

In the direction perpendicular to the layers, however, the confinement of the electrons in the two-dimensional well makes conduction perpendicular to the layers impossible. For the perpendicular direction this leads to an infinitely long dielectric relaxation time, enabling space charge variations in the growth direction of the heterostructure. These space charge variations give rise to internal electric fields, inducing a bending of the conduction and valence bands, as for example the electric field between the ionized donors in the $\text{Al}_x\text{Ga}_{1-x}\text{As}$ layer and the electrons in the 2DEG. With respect to the time-of-flight experiment, it is important to realize how these internal electric fields affect the transport properties of the excess carriers. Consider, for example, an excess electron-hole pair in the GaAs layer of the heterostructure. Due to the internal electric field, this electron-hole pair is separated in the growth direction: the electron moves to the 2DEG, and the hole moves out of the depletion region in the GaAs layer.

From the arguments mentioned above we conclude that in a time-of-flight experiment on a $\text{GaAs}/\text{Al}_x\text{Ga}_{1-x}\text{As}$ heterostructure, with an electric field applied parallel to the layers, the ambipolar transport of electrons and holes in the GaAs layer is studied. These electron-hole pairs consist of a hole in the GaAs layer accompanied by an excess electron in the 2DEG in order to screen the space charge of the hole. During the ambipolar motion of the excess carriers in the GaAs layer an increased conductivity is measured due to the excess electrons in the 2DEG. The electron-hole pairs move in the direction of the negative contact with an ambipolar drift velocity, which is equal to the drift velocity of the minority holes. The duration of the time-of-flight current thus is determined by the drift velocity of the minority holes in the GaAs layer. These holes are not confined to a two-dimensional layer but show three dimensional behavior. A schematical picture of this ambipolar motion is given in Fig. 3.3.

Other conditions for a time-of-flight experiment on a $\text{GaAs}/\text{Al}_x\text{Ga}_{1-x}\text{As}$ heterostructure which have to be considered are related to the high electric field. In chapter 2 we already mentioned that the high-field properties of $\text{GaAs}/\text{Al}_x\text{Ga}_{1-x}\text{As}$ heterostructures are different from those of bulk semiconductors. We discussed the occurrence of

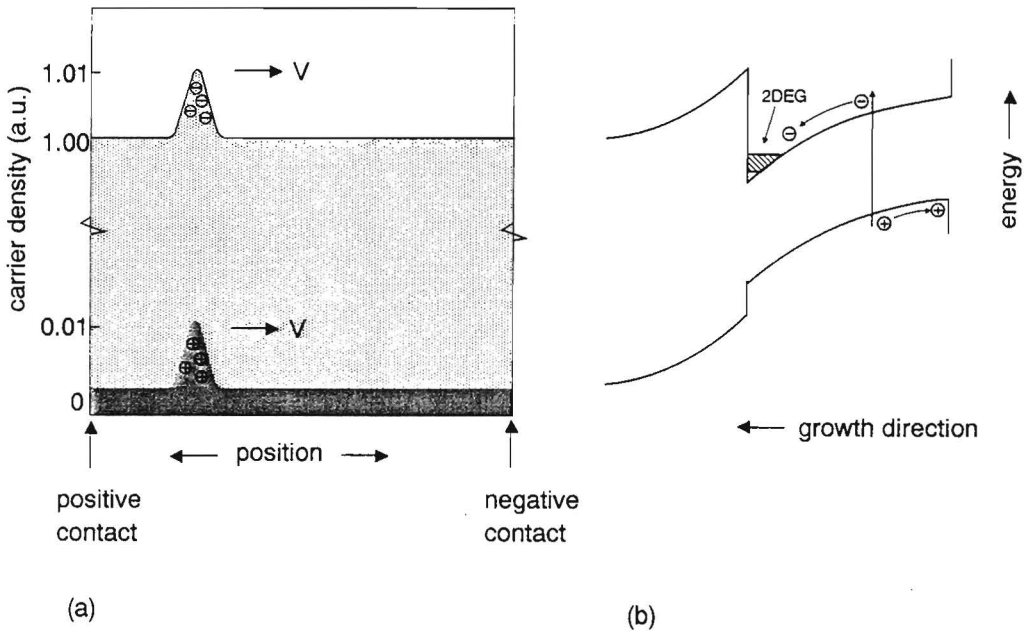


Fig. 3.3 Schematical representation of the ambipolar motion of locally excited excess carriers in a heterostructure. (a) The holes in the GaAs layer are drifting towards the negative contact. Their space charge is screened by a cloud of excess electrons in the 2DEG. (b) the electrons and holes are separated in the growth direction.

current instabilities caused by parallel conduction in the $\text{Al}_x\text{Ga}_{1-x}\text{As}$ layer at high electric fields. Since under these circumstances the current through the heterostructure shows a time-dependent behavior, a precise determination of the time-of-flight is not possible. We therefore have to be sure that the experimental conditions of the time-of-flight experiment are chosen in such a way that high-field current instabilities in the heterostructure are avoided. Another process which might occur at high electric fields is real space transfer of electrons from the 2DEG into the $\text{Al}_x\text{Ga}_{1-x}\text{As}$ layer. Since this real space transfer is measured as a conductivity decrease, it also obscures the time-of-flight experiment and should be avoided as well. These high-field effects limit the

applicability of the time-of-flight technique to a rather narrow window of the applied electric field. This is further discussed in chapter 6.

Finally, in a time-of-flight experiment on a GaAs/ $\text{Al}_x\text{Ga}_{1-x}\text{As}$ heterostructure, laser illumination can induce various excitations, such as electron-hole pair creation in the $\text{Al}_x\text{Ga}_{1-x}\text{As}$ and in the GaAs layer, and excitation of *DX* centers. The contributions of these different excitations to the time-of-flight signal are discussed in section 3.4.2.

3.4 Experiments

In this section we present the results of our time-of-flight experiments on GaAs/Al_xGa_{1-x}As heterostructures. In section 3.4.1 we discuss the experimental set-up and the samples used in the experiments. In section 3.4.2 we present the experimental results.

3.4.1 Experimental set-up

To enable a correct measurement of the ambipolar drift velocity, the experimental set-up for time-of-flight experiments has to obey the following requirements. Since high electric fields are applied, the power dissipation of the bias current is high, which leads to a heating or even a destruction of the sample. To avoid sample heating, pulsed experiments have to be performed in which the duty cycle of the electrical pulses is of the order of 10^{-3} . To avoid spurious reflections of the electrical pulses, a 50 Ω coaxial circuit is used. In our experiments, the electrical pulses are applied using a HP214A pulse generator at a repetition rate of 1 kHz and a pulse width of 3 μ s. The applied voltage and the photocurrent are measured by a LeCroy 9400 digital sampling oscilloscope, with a rise time of about 1 ns. A schematical picture of the electrical circuit used is given in Fig. 3.4. A second requirement for the experimental set-up is that the width of the line shaped laser spot exciting the excess carriers has to be much smaller than the sample dimensions. A diffraction limited laser spot has a size of the order of 1 to 2 μ m. This requirement limits the minimum sample dimensions to 10 to 100 μ m. Furthermore, the laser intensity has to be sufficiently low to create an excess carrier density which is low compared to the equilibrium carrier density in the sample. Otherwise, the disturbance from equilibrium is too large and the assumptions made in the derivation of the ambipolar mobility are not justified. Since the carrier density in the 2DEG typically is of the order of 10^{12} cm⁻², the excess carrier density has to be about 10^{11} cm⁻². This requirement is quite demanding with respect to the overall sensitivity of experimental set-up.

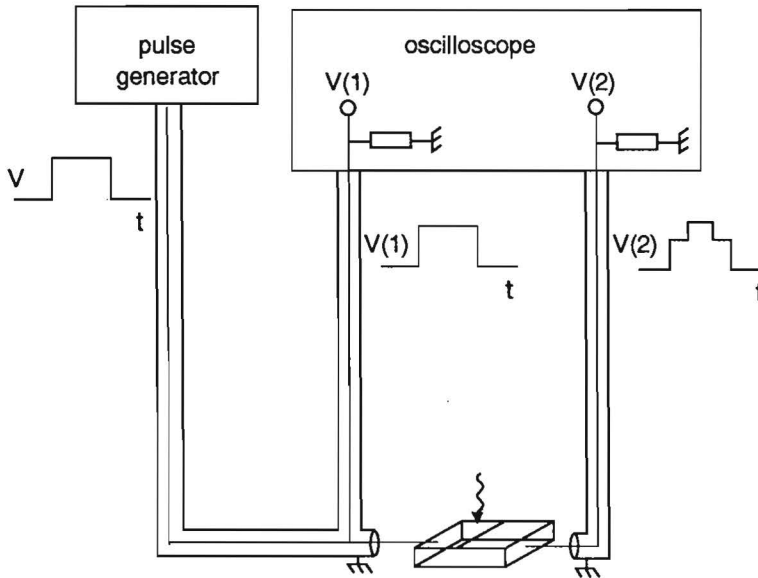


Fig. 3.4 Electrical circuit used in the time-of-flight experiments. The electrical pulses are applied by a pulse generator. The applied voltage and the photocurrent are measured by the $50\ \Omega$ input of the oscilloscope at V_1 and V_2 , respectively.

The optical part of the experimental set-up used for the time-of-flight experiments is schematically shown in Fig. 3.5. We use a Coherent series 700 cavity dumped picosecond dye laser which is synchronously pumped by a Quantronics mode-locked frequency doubled Nd:YAG laser, which is triggered synchronously with the pulse generator. The dye laser pulses have a width of less than 1 ps and a wavelength between 740 nm and 880 nm using a Styryl 9 dye. By means of a cylindrical lens and a Zeiss long working distance microscope objective a line shaped spot is created with a diffraction limited width of about $2\ \mu\text{m}$. In order to determine the focus and the

position of the laser spot on the sample, a simple microscope consisting of a halogen lamp and two lenses is integrated in the set up. Using this microscope, the reflection of the sample and the line shaped laser spot is imaged on a screen. A translation stage is used to focus the spot and to vary the position of the spot on the sample. The halogen lamp is also used to study the influence of a homogeneous background illumination with white light on the time-of-flight experiments. To allow measurements at low temperatures, the sample is mounted in a specially developed flow cryostat in which the sample is located only 8 mm from the outer window.

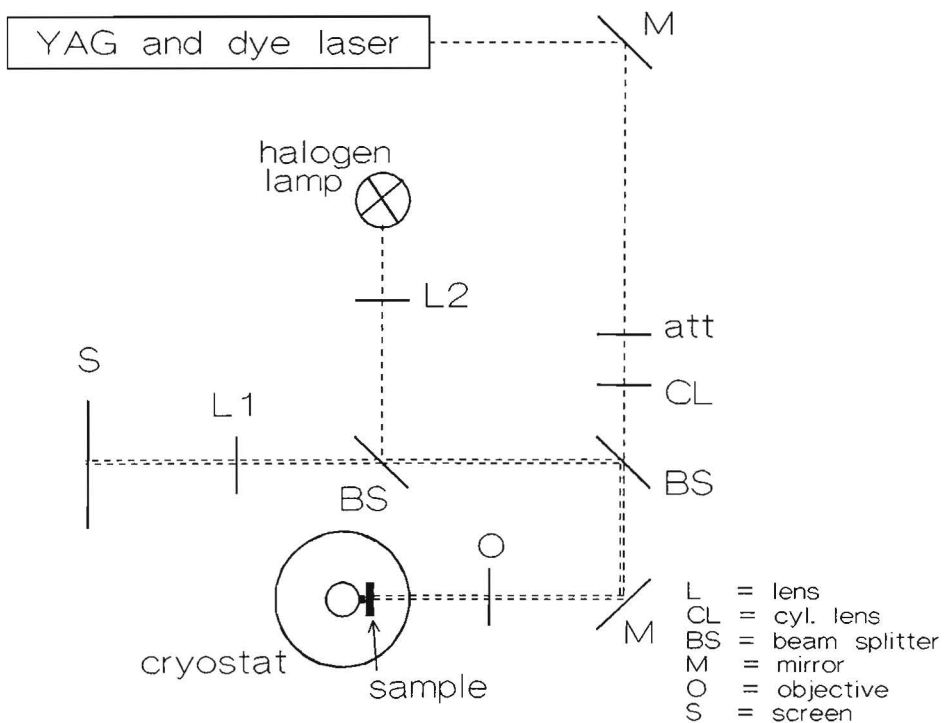


Fig. 3.5 Schematical picture of the optical part of the set-up used for the time-of-flight experiments. Using the halogen lamp, the microscope objective and lens L_1 , an image of the sample and the laser spot is created on the screen.

The photocurrents are measured by the LeCroy sampling oscilloscope, which is triggered by a fast photodiode in the laser beam. Since the excess carrier density has to be small compared to the equilibrium carrier density in the 2DEG and the excess carriers are excited only in a small area, the excess currents are only a few percent of the bias current. Typically, the measured time-of-flight currents are about $50 \mu\text{A}$, superimposed on a bias current of about 1 to 10 mA. Therefore the detection method has to be extremely sensitive. In our experiments the time-of-flight currents are measured differentially, using a broad band pulse transformer²⁵ to subtract the bias current, as is schematically shown in Fig. 3.6. In order to improve the signal to noise ratio, the time-of-flight currents are amplified by a HP 8447 amplifier. Subsequently they are averaged 50 times and a zero measurement is subtracted. In this way, the digitizing error of the sampling scope was reduced, resulting in an overall sensitivity of $5 \mu\text{A}$.

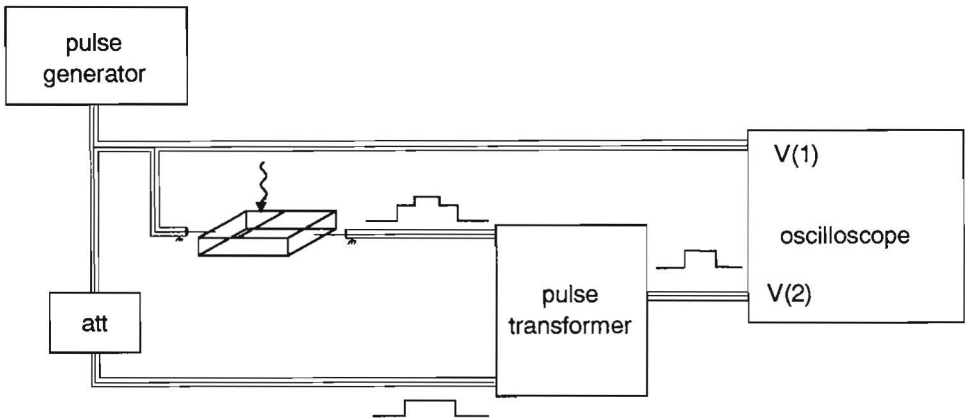


Fig. 3.6 Differential measurement of the time-of-flight current. A pulse transformer is used to subtract the bias current from the photocurrent.

In our experiments we used two different samples. Both samples are modulation doped GaAs/ $\text{Al}_x\text{Ga}_{1-x}\text{As}$ heterostructures, grown by Molecular Beam Epitaxy on top of a semi-insulating substrate. Sample I consists of a 40 nm Si-doped $\text{Al}_{0.33}\text{Ga}_{0.67}\text{As}$ layer, grown on top of a 20 nm undoped $\text{Al}_{0.33}\text{Ga}_{0.67}\text{As}$ spacer layer and a 4 μm GaAs buffer layer. As a cap layer an 18 nm undoped GaAs layer was grown. The electron density at 300 K is $7.1 \times 10^{11} \text{ cm}^{-2}$ with a mobility of $8.3 \times 10^3 \text{ cm}^2/\text{Vs}$. The layered structure of sample II is as follows. It consists of a 35 nm Si-doped $\text{Al}_{0.33}\text{Ga}_{0.67}\text{As}$ layer on top of a 10 nm undoped $\text{Al}_{0.33}\text{Ga}_{0.67}\text{As}$ spacer layer and a 55 nm GaAs layer, grown on a 25 period 5 nm/5 nm GaAs/AlAs superlattice. As a cap layer 17 nm undoped GaAs was grown. At 4 K, the electron density after illumination is $8 \times 10^{11} \text{ cm}^{-2}$ with a mobility of $4 \times 10^5 \text{ cm}^2/\text{Vs}$. At room temperature an electron density of $6 \times 10^{10} \text{ cm}^{-2}$ is measured in the dark with a mobility of $5 \times 10^3 \text{ cm}^2/\text{Vs}$.

To both samples ohmic contacts were made by evaporating and alloying AuGe/Ni. On sample I a rectangular structure was defined with a width of 100 μm and a contact spacing of 60 μm . The contact resistances at room temperature are about 0.3 Ωmm , and were determined using a transmission line geometry. Sample II contains a rectangular structure with a width of 200 μm and a contact spacing of 60 μm . Its contact resistances are about 0.6 Ωmm at 10 K and 10 Ωmm at room temperature.

3.4.2 Experimental results

Whereas in a bulk semiconductor illumination with an excitation wavelength corresponding to the bandgap creates one type of electron-hole pairs, in a GaAs/ $\text{Al}_x\text{Ga}_{1-x}\text{As}$ heterostructure various excitations are possible, as is schematically indicated in Fig. 3.7. We distinguish the excitation of electron-hole pairs in the $\text{Al}_x\text{Ga}_{1-x}\text{As}$ layer, in the GaAs layer, and ionization of DX centers. In this section we first investigate the contributions of these excitations to the time-of-flight current. After that, we discuss time-of-flight experiments on a GaAs/ $\text{Al}_x\text{Ga}_{1-x}\text{As}$ heterostructure and determine the ambipolar mobility.

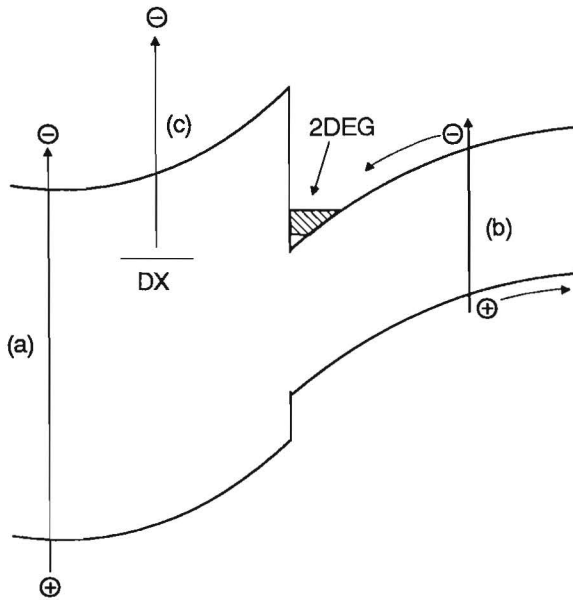


Fig. 3.7

Schematic indication of the various excitations in a GaAs/ $\text{Al}_x\text{Ga}_{1-x}\text{As}$ heterostructure (a) electron-hole pairs in the $\text{Al}_x\text{Ga}_{1-x}\text{As}$ layer, (b) electron-hole pairs in the GaAs layer, and (c) ionization of DX centers.

Excitation of electron-hole pairs in the GaAs layer, as was discussed before, gives rise to a time-of-flight current during the time the carriers are traversing the sample. The contribution of the excited DX centers to the time-of-flight current shows a completely different behavior. Excitation of a DX center creates a positive Si^+ ion and a free electron, which can be transferred to the 2DEG. These excess electrons in the 2DEG lower the resistance of the sample and give rise to a photocurrent in addition to the time-of-flight signal. The decay of this photocurrent current is determined by the capture time of the DX center, which varies from μs to hours, dependent on the temperature and the electric field. If we perform a time-of-flight experiment with an excitation wavelength corresponding to the band gap of GaAs, we expect two time constants in the current: a time-of-flight signal on a ns time scale due to the transport of electron-hole pairs in the GaAs layer, and a current contribution with a longer time constant due to the excitation of DX centers.

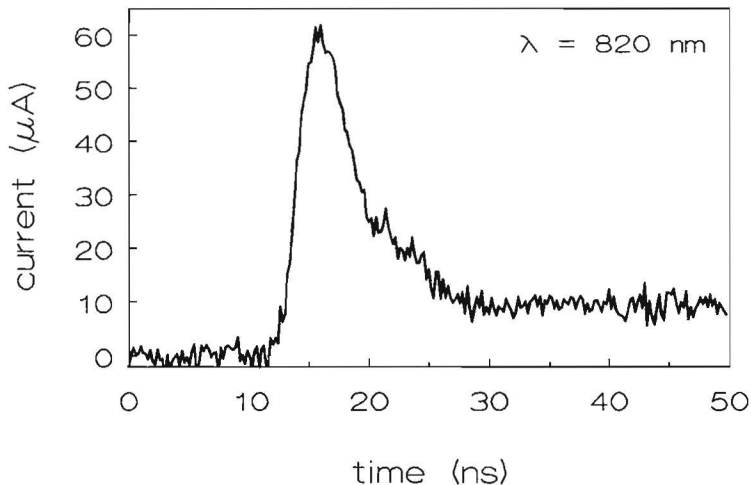


Fig. 3.8

A time-of-flight current of sample I at 77 K. The electric field is 1 kV/cm, the excitation wavelength 820 nm, and the excitation density is $2 \times 10^{11} \text{ cm}^{-2}$. At 77 K the bandgap of GaAs is 830 nm. The zero time axis was arbitrarily chosen. The time-of-flight signal is due to the electron-hole pairs in the GaAs layer the "tail" is caused by the excitation of DX centers.

A time-of-flight current of sample I for an excitation wavelength of 820 nm is shown in Fig. 3.8. The experiment was performed at 77 K, at which the bandgap of GaAs lies at 830 nm. Because of the use of different delay lines, the time axis in Fig. 3.8 is a relative scale, in which the zero time axis was arbitrarily chosen at about 10 ns before the excitation of the laser pulse. We observe a time-of-flight current pulse with a width of 7 ns due to the electron hole pairs in the GaAs layer and a "tail" on a much longer time scale. In order to prove that this tail is caused by the excitation of *DX* centers we further investigate the wavelength dependence of this tail. In addition, when the tail is caused by excitation of *DX* centers, it should be possible to saturate it using a weak background illumination with white light.

The time-of-flight currents at 77 K for various excitation wavelengths are shown in Fig. 3.9, both with and without a continuous background illumination by the halogen lamp. We observe that the time-of-flight signal disappears when we excite with an energy smaller than the band gap, Fig. 3.9(c), whereas the tail is not affected by the increasing wavelength. That the tail at 830 nm is larger than at 820 nm is caused by the fact that the laser intensity was increased to maintain a constant excitation density in the GaAs layer. At 836 nm we used a laser intensity equal to the intensity at 820 nm, since a higher laser intensity could not be achieved at 836 nm. At all investigated wavelengths the tail almost disappears when a background illumination is used. These observations are in accordance with our suggestion that the tail is caused by excitation of *DX* centers. In order to investigate the transport properties of the excess carriers in the GaAs layer, a time-of-flight experiment should thus be performed with a continuous background illumination to saturate the excitation of *DX* centers.

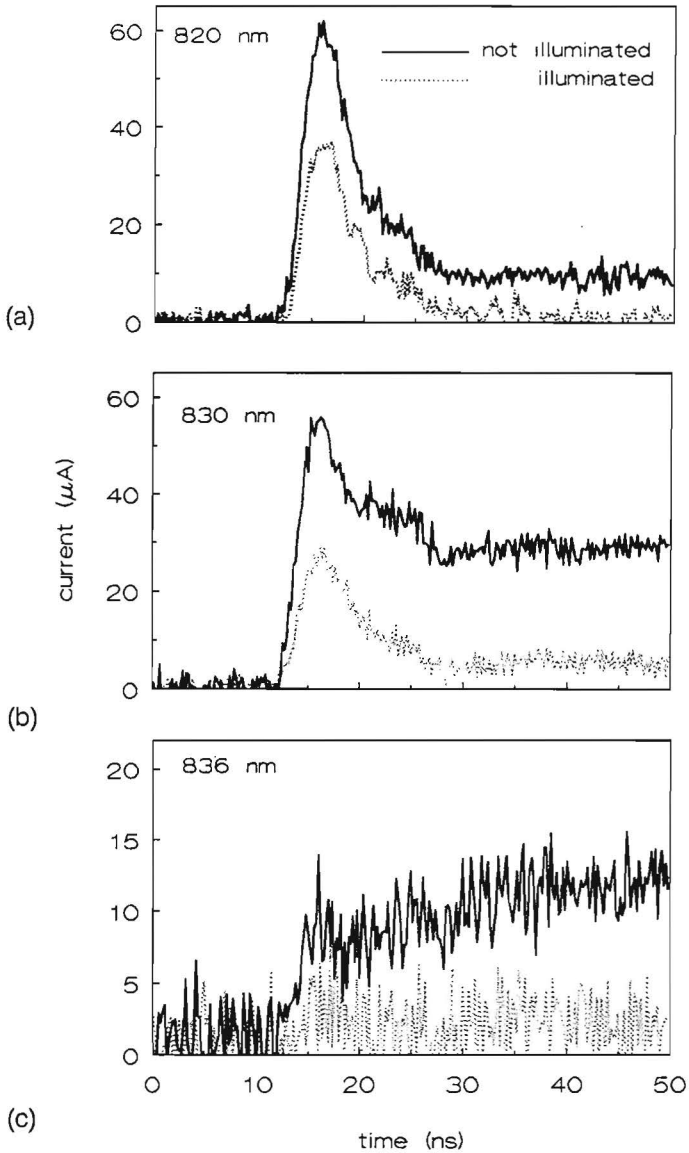


Fig. 3.9

The time-of-flight currents at 77 K for various excitation wavelengths near the GaAs band gap (830 nm) at an electric field of 1 kV/cm, with and without background illumination. Fig. (a) and (b) are measured using an excitation density of $2 \times 10^{11} \text{ cm}^{-2}$ and Fig. (c) with $0.5 \times 10^{11} \text{ cm}^{-2}$.

In order to investigate the contribution of the $\text{Al}_x\text{Ga}_{1-x}\text{As}$ layer to the time-of-flight signal, we performed time-of-flight experiments using various wavelengths above the GaAs band gap (885 nm at 300 K). We know that for an increasing excitation energy the possibility for real space transfer to the $\text{Al}_x\text{Ga}_{1-x}\text{As}$ layer increases. This is schematically indicated by Fig. 3.10, which was calculated by Ando *et al.*²⁶ for a GaAs/ $\text{Al}_x\text{Ga}_{1-x}\text{As}$ superlattice. Here, the width of the minibands is proportional to the transfer probability from the GaAs to the $\text{Al}_x\text{Ga}_{1-x}\text{As}$ layer.

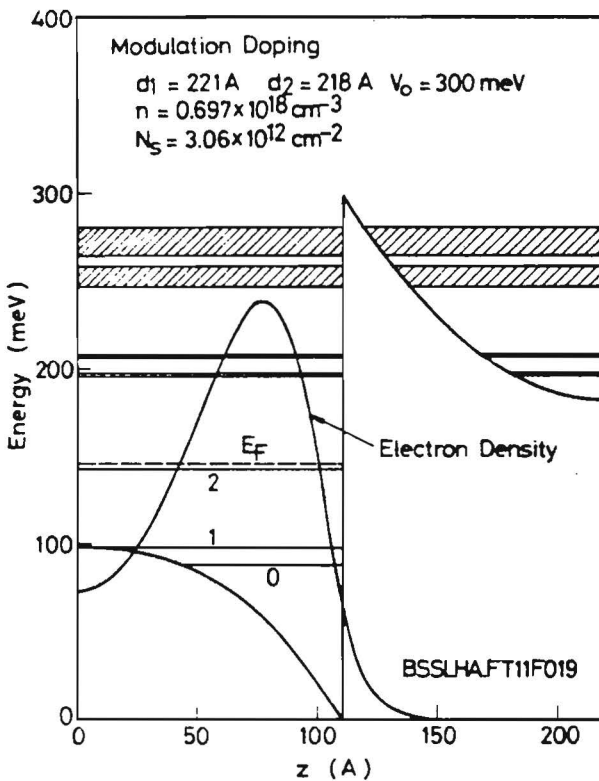


Fig. 3.10

Minibands in a GaAs/ $\text{Al}_x\text{Ga}_{1-x}\text{As}$ superlattice²⁶. The width of the minibands indicates the transfer probability from the GaAs to the $\text{Al}_x\text{Ga}_{1-x}\text{As}$ layer.

Although in a single GaAs/ $\text{Al}_x\text{Ga}_{1-x}\text{As}$ heterostructure no minibands are present, we show this Figure to illustrate the increasing tunnelling probability with increasing energy. We thus see that already at excitation energies smaller than the $\text{Al}_x\text{Ga}_{1-x}\text{As}$ band gap electrons can be transferred to the $\text{Al}_x\text{Ga}_{1-x}\text{As}$ layer. Since the height of the time-of-flight current is proportional to the drift velocity of the excited electrons, we expect a smaller time-of-flight current when an increasing fraction of the excess electrons is transferred to the $\text{Al}_x\text{Ga}_{1-x}\text{As}$ layer, because there the mobility is lower than in the 2DEG. In the experiments, which were performed at 300 K, we varied the wavelength from 885 nm, where only electron-hole pairs are excited in the GaAs layer, to 820 nm, where the electrons are able to tunnel to the $\text{Al}_x\text{Ga}_{1-x}\text{As}$ layer. Again, the laser intensity was adjusted to maintain a constant excitation density for all wavelengths. The results of the time-of-flight experiments are shown in Fig. 3.11.

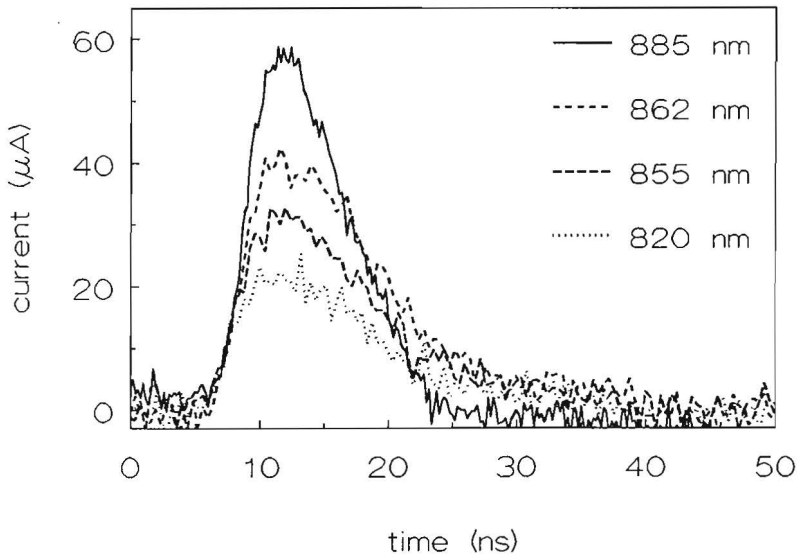


Fig. 3.11 Time-of-flight currents at 300 K for various excitation wavelengths above the GaAs band gap (885 nm). The electric field is 1 kV/cm and the excitation density is $2 \times 10^{11} \text{ cm}^{-2}$.

Here we observe that a shorter excitation wavelength leads to a smaller time-of-flight signal, as was predicted above. The duration of the time-of-flight current, however, is not affected by the varying wavelength, since it is determined by the mobility of the holes in the GaAs layer.

The experiments discussed above indicate that both excitation just above the GaAs band gap as well as a continuous background illumination are necessary prerequisites to determine the correct ambipolar mobility of the electron-hole pairs in the GaAs layer. We now discuss a series of time-of-flight experiments measured on sample II at various electric fields between 0.05 kV/cm and 1.0 kV/cm to measure the velocity-field characteristics of the holes in the GaAs layer. The experiments were performed at 10 K. An excitation wavelength of 810 nm just above the GaAs band gap was used, as well as a weak background illumination with white light. The time-of-flight currents for various electric fields are presented in Fig. 3.12.

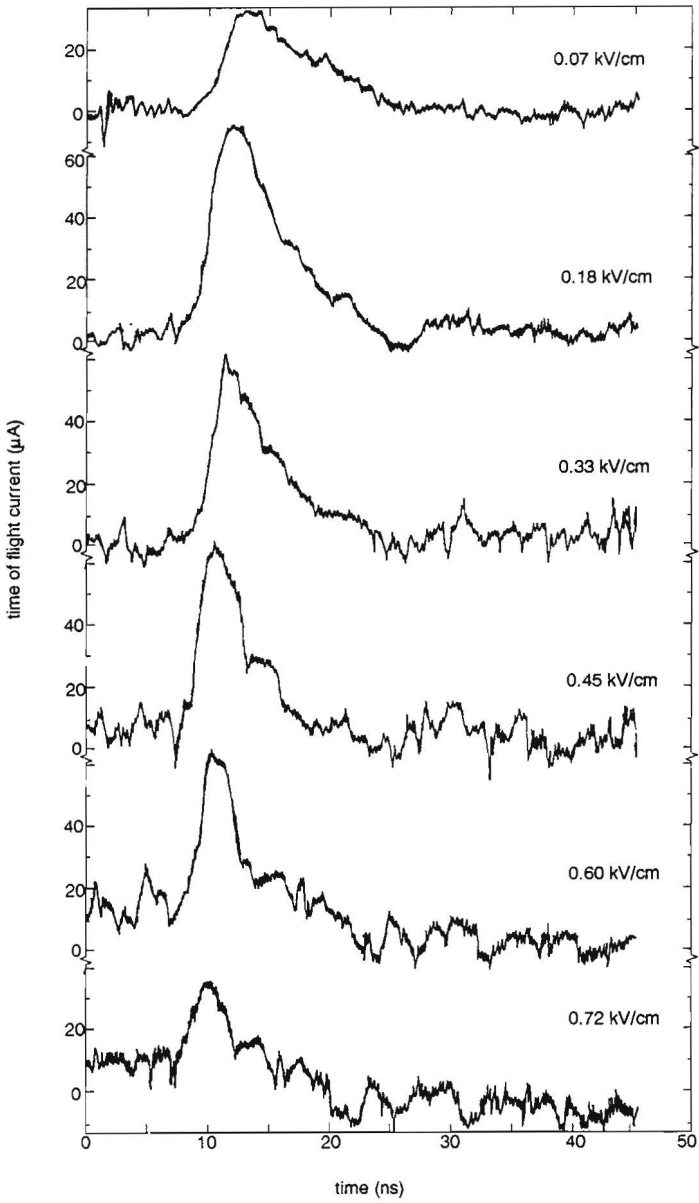


Fig. 3.12 Time-of-flight currents at 10 K for various electric fields between 0.05 and 1.0 kV/cm.

From the width (FWHM) of the time-of-flight currents and the flight distance, which was about 30 μm in these experiments, the ambipolar drift velocity was determined as a function of the electric field. The results are shown in Fig. 3.13. We observe that for electric fields higher than 0.2 kV/cm the drift velocity is proportional to the electric field according to a high-field mobility of 1700 cm^2/Vs . We compare this value to the low-field mobility known for holes in GaAs, which is about 4000 cm^2/Vs ²⁷. The reason that the value obtained by the time-of-flight experiments differs from the value known for holes in *p*-GaAs can be due to different reasons. First, the value from the literature is a low-field mobility, whereas the time-of-flight experiments determine a high-field drift mobility. Secondly, the value reported in the literature is a majority carrier mobility, whereas in the time-of-flight experiment the mobility of minority holes is determined.

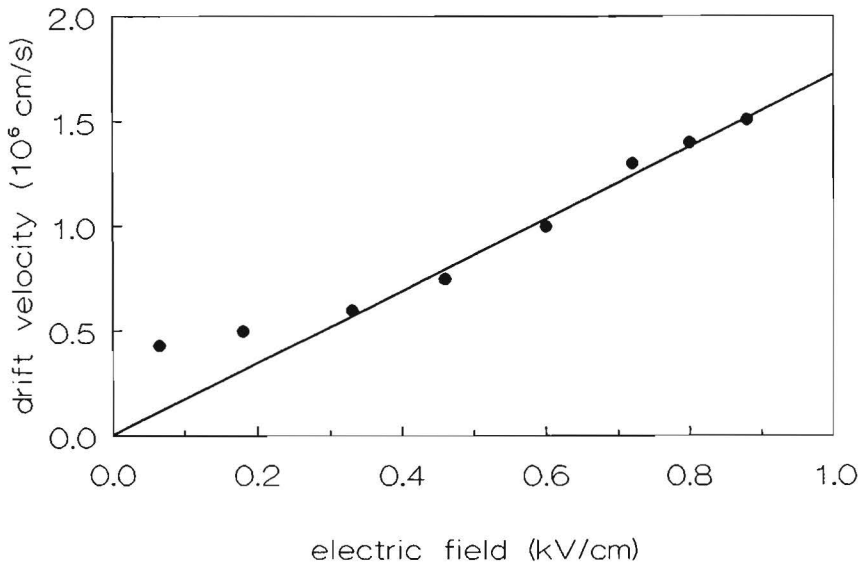


Fig. 3.13

Velocity-field characteristics of the minority holes in the GaAs layer of the GaAs/Al_{0.33}Ga_{0.67}As heterostructure at 10 K. The points correspond to the experimental data and the line corresponds to a fit of the data above a field of about 0.2 kV/cm.

Furthermore, in the heterostructure the holes are located close to the interface between GaAs and superlattice, which may result in an enhanced electron scattering by interface roughness. Note that in Fig. 3.13 at low electric fields the experimentally determined drift velocity deviates from the linear field dependence. This discrepancy is due to the fact that at these electric fields diffusion and recombination effects become dominant. Therefore at low electric fields the width of the time-of-flight current is not determined by drift but by diffusion and/or recombination. Hence, the experimentally determined drift velocity is too high.

We now discuss the results of the experiments at fields higher than 0.8 kV/cm. Time-of-flight currents at 0.80 kV/cm and 0.88 kV/cm are shown in Fig. 3.14. We observe that at the end of the time-of-flight signal a negative peak appears, followed by a current increase, which even results in a second positive current contribution at 0.88 kV/cm. These current contributions are observed on a time scale of several hundreds of ns. Under the same conditions also current instabilities appeared in the bias current of the heterostructure, corresponding to the instabilities induced by parallel conduction in the $\text{Al}_x\text{Ga}_{1-x}\text{As}$ layer, as described in chapter 2. From the time-of-flight currents in this regime we conclude that the excitation of excess carriers in this regime induces additional current instabilities in the heterostructure. Under these circumstances a correct determination of the time-of-flight is not possible. We will further investigate these current instabilities in chapters 4 and 5, and discuss their consequences for the time-of-flight experiments in chapter 6.

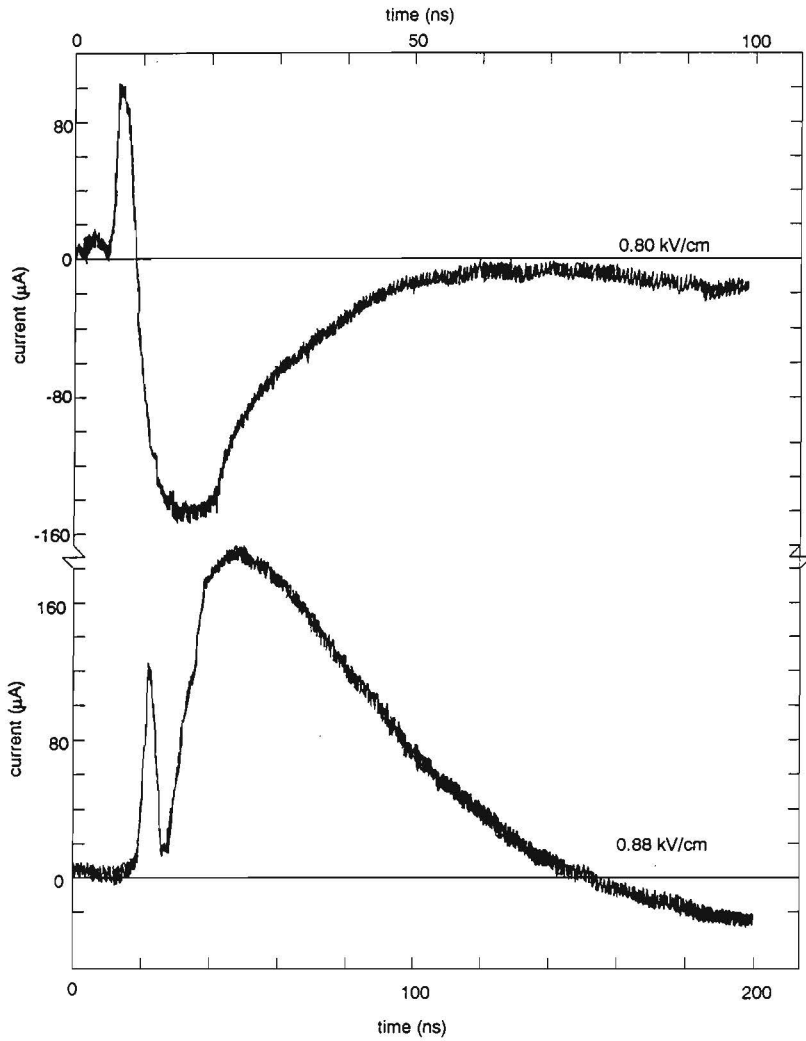


Fig. 3.14 Time-of-flight currents at 0.8 kV/cm and 0.9 kV/cm, showing an extra current signal on a longer time scale.

3.5 Conclusions

In this chapter we discussed a series of time-of-flight experiments on GaAs/Al_xGa_{1-x}As heterostructures. In the heterostructure, excess electron-hole pairs excited in the GaAs layer are separated in the growth direction due to the internal electric field. When an electric field is applied in the lateral direction, the excess electron-hole pairs move with an ambipolar group velocity which is equal to the drift velocity of the minority holes in the GaAs layer. At 10 K we determined an ambipolar drift mobility of 1700 cm²/Vs at electric fields up to 0.8 kV/cm. At higher electric fields the bias current shows a time dependent behavior and extra current peaks are observed in the time-of-flight signal. In this regime a correct determination of the ambipolar drift velocity by means of a time-of-flight experiment is not possible. The occurrence of current instabilities thus creates an upper limit for the electric field at which time-of-flight experiments can be performed. The lower limit is found at the electric field where the width of the time-of-flight signal is determined by the combined effect of recombination and diffusion rather than by the drift of the carriers.

In the next two chapters of this thesis we further examine the origin of the current instabilities observed in the GaAs/Al_xGa_{1-x}As heterostructure. In chapter 6 we comment on the applications of the time-of-flight technique for the research on two-dimensional semiconductor structures. Furthermore, we give some suggestions for future investigations on this subject.

References

1. A. Neukermans and G.S. Kino, Appl. Phys. Lett. 17, 102 (1970).
2. A. Neukermans and G.S. Kino, Phys. Rev. B 7, 2693 (1973).
3. W. van Roosbroeck, Phys. Rev. 91, 282 (1953).
4. G. Kino, IEEE Trans. Electron Devices ED-17, 178 (1970).
5. R. Haynes and W. Shockley, Phys. Rev. 81, 835 (1951).
6. W.E. Spear, Proc. Phys. Soc. 70, 669 (1957).
7. W.E. Spear, Proc. Phys. Soc. 78, 826 (1960).
8. J.G. Ruch and G.S. Kino, Phys. Rev. 174, 921 (1968).
9. C.B. Norris and J.F. Gibbons, IEEE Trans Electron Devices ED-14, 38 (1967).
10. L. Reggiani, in *Physics of Nonlinear Transport in Semiconductors*, ed. by D.K. Ferry, J.R. Barker and C. Jacoboni, (Plenum Press, New York, 1980), p. 243.
11. M. Morohashi, N. Sawaki, and I. Akasaki, Jpn. J. Appl. Phys. 24, 661 (1985).
12. M. Morohashi, N. Sawaki, and I. Akasaki, Jpn. J. Appl. Phys. 24, 732 (1985).
13. A. Neukermans and G.S. Kino, Phys. Rev. B 7, 2703 (1973).
14. J. Degani, R.F. Leheny, R.E. Nahory, and J.P. Heritage, Appl. Phys. Lett. 39, 569 (1981).
15. T. Furuta and M. Tomizawa, Appl. Phys. Lett. 56, 824 (1990).
16. W. Walukiewicz, J. Lagowski, L. Jastrzebski, and H.C. Gatos, J. Appl. Phys. 50, 5040 (1979).
17. T.P. McLean and E.G.S. Paige, J. Phys. Chem. Solids 16, 220 (1960).
18. M.B. Prince, Phys. Rev. 92, 681 (1955).
19. H. Ehrenreich, J. Phys. Chem. Solids 8, 130 (1959).
20. W. Walukiewicz, J. Lagowski, L. Jastrzebski, M. Lichtensteiger, and H.C. Gatos, J. Appl. Phys. 50, 899 (1979).
21. J.M. Ettenberg, H. Kressel, and S.L. Gilbert, J. Appl. Phys. 44, 827 (1973).

-
22. R.K. Ahrenkiel, D.J. Dunlavy, D. Greenberg, J. Schlupmann, H.C. Hamaker, and H.F. MacMillan, *Appl. Phys. Lett.* 51, 776 (1987).
 23. L.M. Weegels, J.E.M. Haverkort, M.R. Leys, and J.H. Wolter, *Superlat. Microstruct.* 7, 315 (1990).
 24. M.R. Leys, M.P.A. Vieggers, and G.W. 't Hooft, *Philips Techn. Rev.* 43, 144 (1986).
 25. G.E. Alberga, *J. Phys. E* 13, 1009 (1980).
 26. T. Ando and S. Mori, *J. Phys. Soc. Jpn.* 47, 1518 (1979).
 27. J.D. Wiley in *Semiconductors and Semimetals*, Vol. 10, ed. by R.K. Williardson and A.C. Beer (Academic Press, New York, San Fransisco, London, 1975) chapter 2.

Chapter 4

Current instabilities in GaAs/Al_xGa_{1-x}As heterostructures

4.1 Introduction

The aim of the research described in this thesis is to investigate the high-field transport properties of modulation-doped GaAs/Al_xGa_{1-x}As heterostructures. Generally, a GaAs/Al_xGa_{1-x}As heterostructure is considered to be a two-dimensional system in which all electrons are confined in a two-dimensional electron gas at the GaAs/Al_xGa_{1-x}As interface. As was explained in section 2.4, however, under high electric field conditions, hot electrons are not necessarily confined to the 2DEG but can be directly injected from the source contact into the Al_xGa_{1-x}As layer parallel to the 2DEG. This electron injection into the Al_xGa_{1-x}As layer is possible since the conduction band minimum is located only 50 meV above the Fermi level¹. Electron injection is usually observed as a collapse of the current, since the electrons in the Al_xGa_{1-x}As layer have a much lower mobility than in the 2DEG and are easily trapped by the deep Si-donors. Electron injection can also give rise to a more complicated time-dependent behavior, such as current oscillations or even a chaotic behavior of the current².

This chapter deals with another type of current instabilities related to electron injection. To explain these current instabilities we present a model in which we assume that at high enough electric fields, the electrons injected into the $\text{Al}_x\text{Ga}_{1-x}\text{As}$ layer cause avalanche ionization of occupied Si-donors. Avalanche ionization is a highly non-linear process, which gives rise to a sudden increase of the current as a function of time. In our experiments we observed that these current jumps show hysteresis effects as a function of the electric field. At even higher electric fields the current jumps become irregular and we observe a chaotic behavior of the current. The experiments described in this chapter are the first reported observation of avalanche ionization phenomena in a two-dimensional semiconductor structure.

In bulk semiconductors, current nonlinearities and instabilities induced by avalanche ionization of donors are well-known phenomena^{3,4,5,6,7}. Not only shallow^{3,4,5,6} but also deep impurities^{7,8} can be involved in the ionization process. During avalanche ionization, the current is a highly nonlinear function of the applied electric field: current jumps with hysteresis-effects are observed in the current-voltage characteristics, corresponding to an oscillatory or chaotic temporal behavior of the conductivity. The frequency range in which instabilities have been observed is from a few Hz up to several MHz under varying experimental conditions^{3,4,5,9,10}. The complex temporal behavior in the avalanche ionization regime is often related to the formation of highly conductive current filaments. Current filaments in bulk GaAs have first been visualized by Mayer *et al.* using a scanning electron microscope⁴. In these current filaments a very high mobility was reported, which was attributed to a reduced phonon scattering⁴. Optical phonons, emitted by the hot electrons in the filament, leave the filament and therefore do not contribute to the scattering. A second argument for high mobilities in current filaments is an enhanced screening of the ionized impurity scattering due to the high electron density in the filament.

Referring to the phenomena in bulk semiconductors we expect that avalanche ionization of Si-donors in the $\text{Al}_x\text{Ga}_{1-x}\text{As}$ layer of a GaAs/ $\text{Al}_x\text{Ga}_{1-x}\text{As}$ heterostructure also occurs by the formation of current filaments. Here we have to realize that due to

charge neutrality and Poisson's equation, these local variations of the carrier density in the $\text{Al}_x\text{Ga}_{1-x}\text{As}$ layer also induce fluctuations in the electron density of the 2DEG. Therefore the transport properties of a $\text{GaAs}/\text{Al}_x\text{Ga}_{1-x}\text{As}$ heterostructure are strongly affected by these injection and ionization processes in the $\text{Al}_x\text{Ga}_{1-x}\text{As}$ layer.

This chapter is organized as follows. In order to investigate the possibility for impact ionization of donors in the $\text{Al}_x\text{Ga}_{1-x}\text{As}$ layer of a $\text{GaAs}/\text{Al}_x\text{Ga}_{1-x}\text{As}$ heterostructure we performed Monte Carlo calculations on the energy distribution of the electrons in an $\text{Al}_x\text{Ga}_{1-x}\text{As}$ layer at various electric fields. The results of these calculations presented in section 4.2 indicate that at electric fields of about 1 kV/cm the high energy tail of the electron distribution extends to sufficiently high energies to cause impact ionization of deep donor levels in the $\text{Al}_x\text{Ga}_{1-x}\text{As}$ layer. In order to estimate the electron mobility in an $\text{Al}_x\text{Ga}_{1-x}\text{As}$ current filament we also studied the dependence of the high-field drift velocity on the carrier density in the $\text{Al}_x\text{Ga}_{1-x}\text{As}$ layer. In section 4.3 we present a rate equation model which describes the various processes in the $\text{Al}_x\text{Ga}_{1-x}\text{As}$ layer, such as trapping of electrons in deep donor levels and impact ionization of electrons out of these donors. In this way, we are able to describe the field dependence and the time dependence of the current instabilities observed in $\text{GaAs}/\text{Al}_x\text{Ga}_{1-x}\text{As}$ heterostructures. The results of the time-resolved current-voltage measurements on a $\text{GaAs}/\text{Al}_x\text{Ga}_{1-x}\text{As}$ heterostructure are presented in section 4.4. At room temperature as well as at low temperatures we observe a time-dependent behavior of the current at electric fields between 0.5 and 2.0 kV/cm. As a function of time we observe a collapse of the current followed by a rapid current increase. These current jumps show hysteresis effects as a function of the electric field, suggesting the formation of current filaments. We determined an electron mobility under avalanche conditions as high as 2×10^4 cm^2/Vs at 10 K, which is in accordance with a high mobility reported for bulk n -GaAs under avalanche conditions. Finally, in section 4.5 we summarize the results of this chapter.

4.2 Monte Carlo calculations

We now consider the transport properties of the electrons injected into the $\text{Al}_x\text{Ga}_{1-x}\text{As}$ layer of a $\text{GaAs}/\text{Al}_x\text{Ga}_{1-x}\text{As}$ heterostructure. In the $\text{Al}_{0.33}\text{Ga}_{0.67}\text{As}$ layer, deep donor levels (*DX* centers) are present at about 80 meV below the Γ minimum of the conduction band¹¹. Therefore the question arises whether the electrons injected into the $\text{Al}_x\text{Ga}_{1-x}\text{As}$ layer at high electric fields can achieve energies high enough to cause impact ionization of these occupied donors. Moreover, impact ionization in semiconductors often occurs in the form of so-called current filaments, where the electron density is high. One therefore also has to consider the influence of the carrier density on the drift velocity of the electrons. We carried out a number of Monte Carlo simulations. To investigate the possibility for impact ionization we calculated the electron distribution function at various values of the electric field. Furthermore, we calculated the electron drift velocity in an $\text{Al}_{0.33}\text{Ga}_{0.67}\text{As}$ current filament. The filament structure was modelled by taking a fixed ionized donor density and varying the carrier concentration. Before we present the results of these calculations in sections 4.2.2 to 4.2.4, we give a short overview of the Monte Carlo program and the theoretical formulae used.

4.2.1 The Monte Carlo program

As explained in section 2.5, the Monte Carlo method simulates carrier transport in semiconductors by choosing random numbers for the free time-of-flight between two collisions and for the probabilities and scattering angles of the various scattering mechanisms. In order to perform Monte Carlo simulations of the high-field transport properties of an $\text{Al}_x\text{Ga}_{1-x}\text{As}$ layer, we have developed a FORTRAN program for an IBM RS/6000 workstation. The program was designed to simulate transport in a three-dimensional semiconductor. The following mechanisms were taken into account: acoustic and optical phonon scattering, ionized impurity scattering, intervalley scattering, alloy scattering, and electron-electron scattering. For the dependence of the

squared matrix elements upon the momentum transfer q of these scattering mechanisms we used the expressions by Reggiani¹². Acoustic and optical phonon scattering were taken into account via an equilibrium phonon distribution of the appropriate temperature. Hot-phonon effects were not included. Since our main interest was concerned with the occurrence of impact ionization, we included this mechanism as well. However, the theoretical expressions for impact ionization as derived by Landsberg *et al.*¹³ contain an unknown overlap factor between the wave functions of the ionizing electron and the trapped electron. The impact ionization rate, defined as the number of impact ionizations per second per cm^3 , can therefore only be calculated relatively. In our calculations, we set this overlap factor arbitrarily equal to 1. The additional input parameters for the bandstructure and the coupling strengths used in the calculations are given in Table 4.1.

The major structure of the Monte Carlo program is shown by the flow chart representation given in Fig. 4.1. The simulation is started with a Fermi-Dirac distribution in which the initial state k_i of every particle is defined using random numbers. Then the actual simulation starts. For each particle in turn the time t after which it is scattered, is determined. The motion of the electron between two collisions is treated classically. Then, the scattering mechanism responsible for the end of the free flight is determined using the relative probability of all scattering mechanisms. After that step, the scattering angle is determined and the final wave vector k_f . As a last step, it was checked by a rejection technique¹⁴ whether the final state was already occupied. In that case, the transition is forbidden by the Pauli principle and the free flight is continued. If the transition is allowed, k_f is the start of the next flight. We continue with the same particle until the time t_0 , corresponding to a chosen time step, has elapsed. At the end of the first time step, when all particles have been considered, the obtained data are evaluated. In practice, each time step is divided in ministeps of 50 fs, after which an updating of the distribution function is made. This allows a more accurate treatment of the Pauli principle. The procedure described above is repeated for a number of time steps, such that the electron transport quantities, like the average

INPUT PARAMETERS for $\text{Al}_{0.33}\text{Ga}_{0.67}\text{As}$				
BAND STRUCTURE				
Lattice constant	Å	5.66		
Effective mass	m_e	0.09		
Non-parabolicity	1/eV	0.00		
ACOUSTIC PHONONS				
Deformation potential	eV	6.64		
Piezo electric constant	10^9 V/m	1.20		
Longitudinal elastic constant	10^{11} N/m ²	1.44		
Transverse elastic constant	10^{11} N/m ²	0.49		
OPTICAL PHONONS				
LO phonon energy	meV	38.53		
Static dielectric constant		12.15		
Optical dielectric constant		10.05		
ALLOY SCATTERING				
Al fraction		0.33		
Alloy potential	eV	1.00		
INTERVALLEY SCATTERING				
Energy L valley	meV	82.97		
Effective mass L valley	m_e	0.12		
Non-parabolicity	1/eV	0.50		
Energy L- Γ , L-L, L-X phonon	meV	27.80	29.00	29.30
Deformation potential L- Γ , L-L, L-X	10^{11} eV/m	1.00	1.00	0.50
Energy X valley	meV	92.89		
Effective mass X valley	m_e	0.30		
Non-parabolicity	1/eV	0.22		
Energy X- Γ , X-X, X-L phonon	meV	27.80	29.90	29.30
Deformation potential X- Γ , X-X, X-L	10^{11} eV/m	1.00	0.70	0.30

Table 4.1 Band structure and material parameters of $\text{Al}_{0.33}\text{Ga}_{0.67}\text{As}$, used in the Monte Carlo calculations.

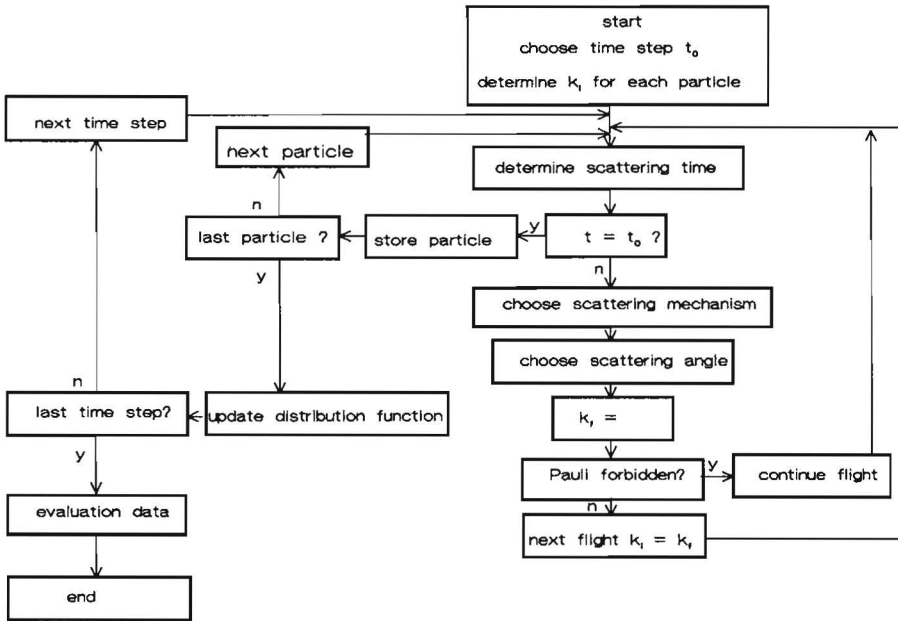


Fig. 4.1 A flow chart representation of the Monte Carlo program.

velocity and the energy of the carriers are obtained as a function of time. Since we start with a zero-field Fermi-Dirac distribution, it takes some time to reach a steady state. An example of the time-dependence of the drift velocity in $Al_{0.33}Ga_{0.67}As$ at 5 kV/cm is given in Fig. 4.2. In most simulations we followed 10.000 particles during 10 ps. To determine the steady-state properties, we averaged the derived quantities over the last 5 ps.

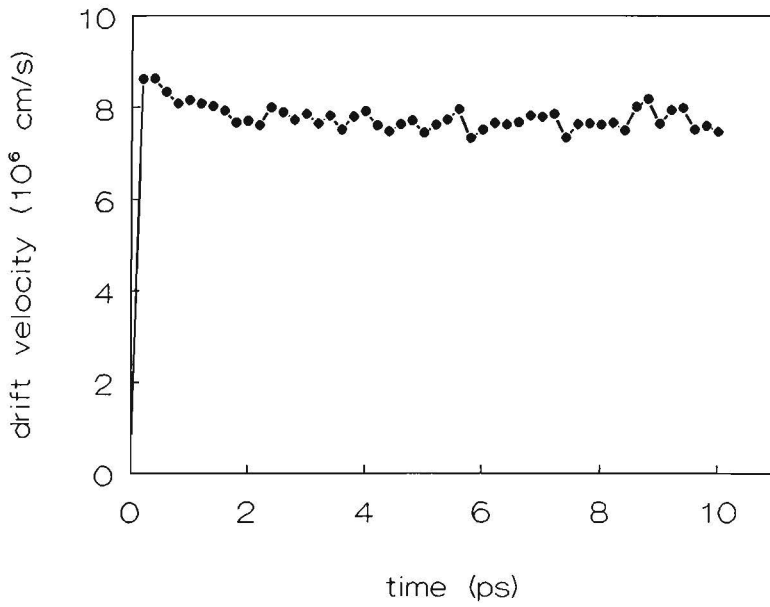


Fig. 4.2

The drift velocity in $\text{Al}_{0.33}\text{Ga}_{0.67}\text{As}$ at 10 K as a function of time, calculated for an electric field of 5 kV/cm. The electron density, ionized donor density, and occupied donor density are all equal to $1 \times 10^{18} \text{ cm}^{-3}$.

4.2.2 High-field drift velocities in n-Al_xGa_{1-x}As

We now discuss the results of the Monte Carlo calculations. Before we present the results on impact ionization, we first discuss the velocity-field characteristics calculated for Al_{0.33}Ga_{0.67}As as shown in Fig. 4.3(a). Here we show the drift velocities at 10 K, calculated for various donor concentrations and carrier densities. In bulk Al_xGa_{1-x}As these quantities are interrelated, but in the Al_xGa_{1-x}As layer of a GaAs/Al_xGa_{1-x}As heterostructure, these are independent quantities, which can be modified by temperature or the electric field. For comparison, the velocity-field curve of *n*-GaAs is also shown. Several features appear. First, the electron drift velocity in Al_{0.33}Ga_{0.67}As is lower than in GaAs. This is mainly due to the higher effective mass of the electrons in Al_{0.33}Ga_{0.67}As, which results in a lower mobility. Furthermore, since the scattering rates are proportional to the density of states, which in turn depends on the effective mass as $(m^*)^{3/2}$, a higher effective mass leads to a larger scattering rate and thus to a lower drift velocity. We also observe that the Al_{0.33}Ga_{0.67}As layer with the higher doping concentration shows a lower drift velocity, as was to be expected. On the other hand, the sample with the electron density of $2 \times 10^{18} \text{ cm}^{-3}$ shows a higher velocity than the sample with the lower electron density. We will further investigate this effect in section 4.2.4, where we calculate the drift velocity in high-density current filaments.

At electric fields higher than 5 kV/cm the drift velocity in GaAs saturates, and subsequently it shows a decrease at 8 kV/cm due to intervalley transfer. In Al_{0.33}Ga_{0.67}As the drift velocity saturates at a higher value of the electric field due to the higher effective mass. The relative contribution of intervalley scattering in Al_{0.33}Ga_{0.67}As is shown in Fig. 4.3(b), where the solid lines denote the occupation of Γ , L and X valley as a function of the electric field. If we include impact ionization of an occupied donor at 80 meV we obtain a relative occupation of the different valleys as shown by the dashed lines. We see that the contribution of intervalley transfer is decreased. Since impact ionization is an additional scattering mechanism, it is more difficult for the electrons to reach the energy thresholds for intervalley transfer, which at low

temperatures in $\text{Al}_{0.33}\text{Ga}_{0.67}\text{As}$ are about 111 meV and 121 meV for the L and X valley, respectively.

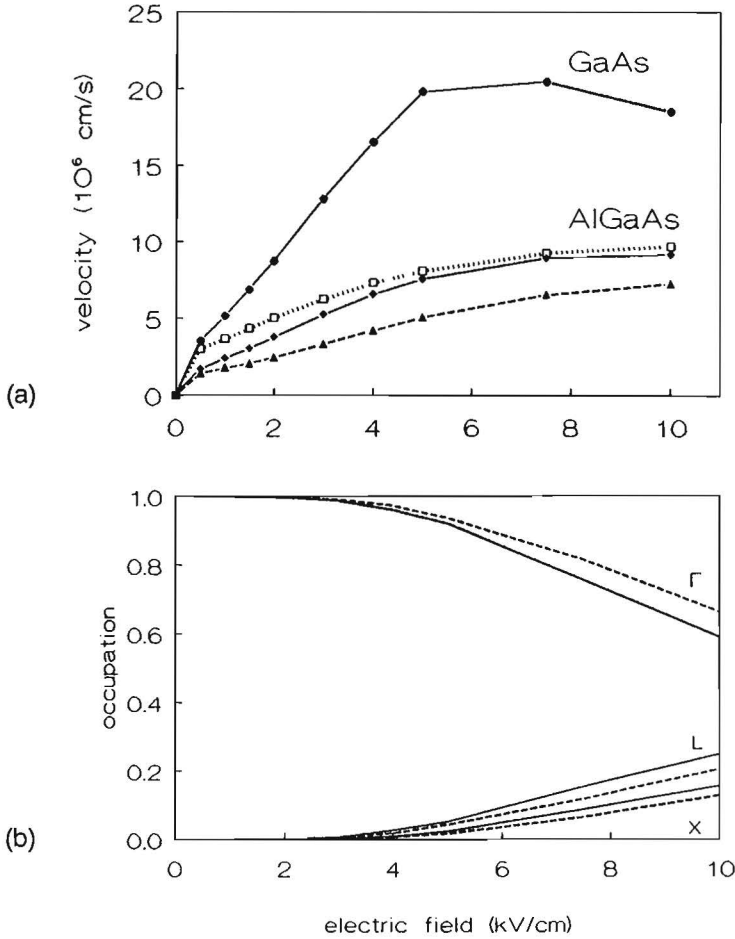


Fig. 4.3

(a) Average electron drift velocity at 10 K in n -GaAs and n - $\text{Al}_{0.33}\text{Ga}_{0.67}\text{As}$ as a function of the electric field for various values of the electron density n_e and the ionized donor density n_d^+ . (\bullet) $n_e = 1 \times 10^{18} \text{ cm}^{-3}$, $n_d^+ = 1 \times 10^{18} \text{ cm}^{-3}$, (\blacklozenge) $n_e = 1 \times 10^{18} \text{ cm}^{-3}$, $n_d^+ = 1 \times 10^{18} \text{ cm}^{-3}$, (\blacktriangle) $n_e = 1 \times 10^{18} \text{ cm}^{-3}$, $n_d^+ = 2 \times 10^{18} \text{ cm}^{-3}$, (\square) $n_e = 2 \times 10^{18} \text{ cm}^{-3}$, $n_d^+ = 1 \times 10^{18} \text{ cm}^{-3}$. (b) Relative occupation by electrons of the Γ , L and X conduction band minima in n - $\text{Al}_{0.33}\text{Ga}_{0.67}\text{As}$ at 10 K as a function of the electric field. The solid lines are calculated for an electron density and an ionized donor density both equal to $1 \times 10^{18} \text{ cm}^{-3}$. The dashed lines are calculated for the same densities of electrons and ionized donors, but also with an occupied donor density of $1 \times 10^{18} \text{ cm}^{-3}$, causing impact ionization.

4.2.3 Impact ionization in an n-Al_xGa_{1-x}As layer

Let us now turn to the impact ionization of occupied deep donors (*DX* centers) in the Al_xGa_{1-x}As layer. In order to investigate its possibility, we calculate the distribution function of the electrons in the Al_xGa_{1-x}As layer at various electric fields. The energy distributions of the electrons in the Γ band of Al_{0.33}Ga_{0.67}As at 10 K, calculated for several electric fields between 0.01 kV/cm and 5.0 kV/cm, are shown in Fig. 4.4. Here, we clearly see that already at electric fields of 1 to 2 kV/cm the tail of the electron distribution function extends to energies higher than 80 meV above the conduction band minimum, which corresponds to the threshold energy for impact ionization.

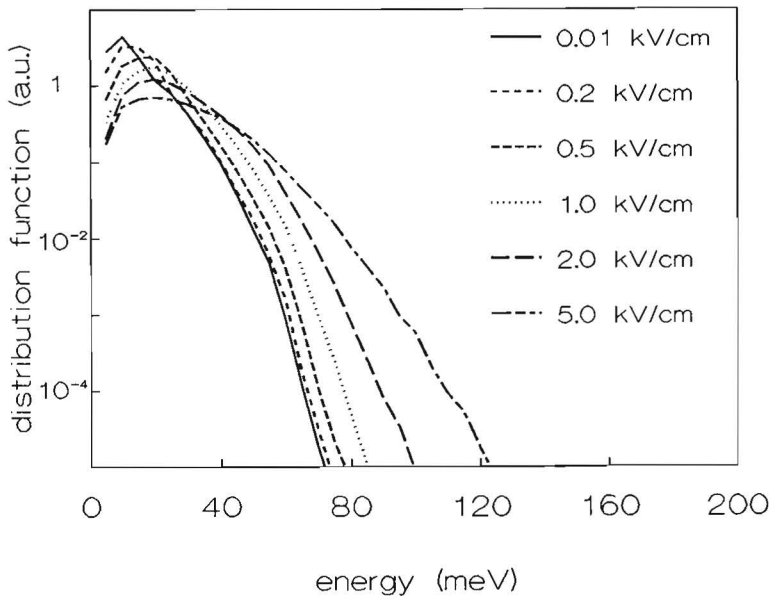


Fig. 4.4

The energy distribution of the electrons in Al_{0.33}Ga_{0.67}As at 10 K for various electric fields between 0.01 kV/cm and 5.0 kV/cm. The ionized donor density, the carrier density, and the density of occupied donors are all equal to $1 \times 10^{18} \text{ cm}^{-3}$.

We thus conclude that at these electric fields, a number of electrons in the $n\text{-Al}_{0.33}\text{Ga}_{0.67}\text{As}$ layer of a $\text{GaAs}/\text{Al}_x\text{Ga}_{1-x}\text{As}$ heterostructure achieve energies high enough to cause impact ionization of occupied Si-donors. Moreover, according to the Pauli principle, unoccupied states at the bottom of the conduction band are needed as final states for the ionizing electrons. In Fig. 4.4 we observe indeed that at higher electric fields the distribution function contains empty states at low energy.

By taking into account in the Monte Carlo program an occupied donor level, 80 meV below the Γ band, it is possible to determine a relative impact ionization rate as a function of the electric field. The impact ionization rate at 10 K, calculated for an occupied donor density of $1 \times 10^{18} \text{ cm}^{-3}$, is shown in Fig. 4.5 for three values of the electron density. From these results we conclude that the impact ionization rate increases with increasing electric field and increasing electron density. These observations are in accordance with our experiments reported in section 4.4.

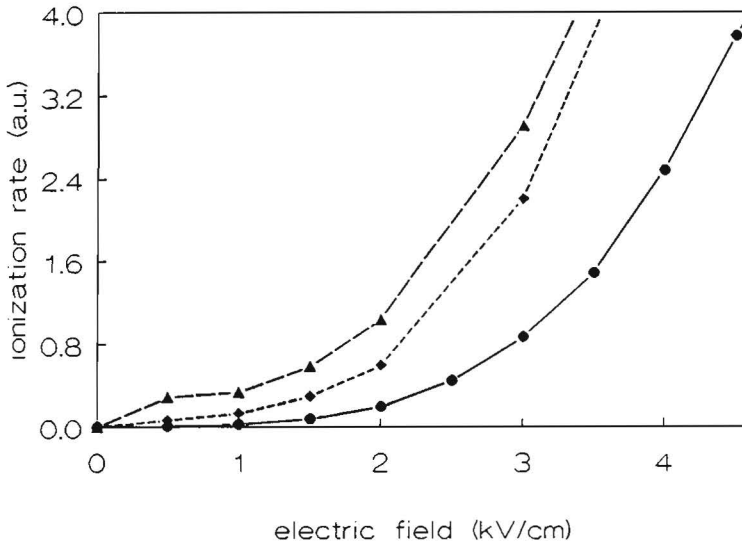


Fig. 4.5 The impact ionization rate at 10 K as a function of the electric field for a density of occupied donors of $1 \times 10^{18} \text{ cm}^{-3}$, and various electron densities. (●) $n_e = 1 \times 10^{18} \text{ cm}^{-3}$, (◆) $n_e = 2 \times 10^{18} \text{ cm}^{-3}$, and (▲) $n_e = 5 \times 10^{18} \text{ cm}^{-3}$.

4.2.4 Electron drift velocities in a current filament

Since in current filaments induced by avalanche ionization the electron density can be very high, we now investigate the influence of this high electron density on the drift velocity of the electrons in the filament. We calculated the electron drift velocity in an $n\text{-Al}_{0.33}\text{Ga}_{0.67}\text{As}$ layer as a function of the electron density for three values of the electric field and a fixed ionized donor density of $1 \times 10^{18} \text{ cm}^{-3}$. From the results presented in Fig. 4.6, we conclude that the electron drift velocity in $n\text{-Al}_x\text{Ga}_{1-x}\text{As}$ increases with increasing electron density and saturates at a value of about $5 \times 10^6 \text{ cm/s}$ at an electron density of $4 \times 10^{18} \text{ cm}^{-3}$. At an electric field of 1 kV/cm we determine from this a maximum high-field drift mobility of $0.5 \times 10^4 \text{ cm}^2/\text{Vs}$. This means that in avalanche ionization induced current filaments the electron drift velocities are higher than in bulk $n\text{-Al}_x\text{Ga}_{1-x}\text{As}$.

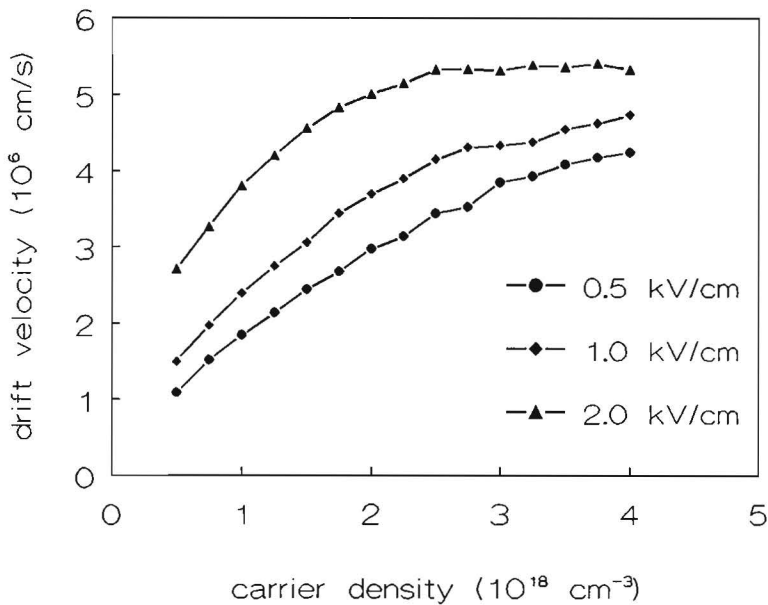


Fig. 4.6

The electron drift velocity in an $n\text{-Al}_x\text{Ga}_{1-x}\text{As}$ filament as a function of the electron density for three values of the electric field and a fixed ionized donor density of $1 \times 10^{18} \text{ cm}^{-3}$.

4.3 Impact ionization in a GaAs/Al_xGa_{1-x}As heterostructure

In order to describe the time dependence and the field dependence of the current instabilities observed in GaAs/Al_xGa_{1-x}As heterostructures at high electric fields, we now present a rate equation model of the various processes taking place in the Al_xGa_{1-x}As layer, such as trapping of electrons in deep donors and impact ionization of electrons out of these donors. The model described here will be used in section 4.4 to interpret the experimental results.

We assume an *n*-Al_xGa_{1-x}As layer of width W , with N_d donors per cm³, and describe this layer in terms of a surface depletion layer of width W_d and an "active" layer of width $W_a = W - W_d$. In the surface depletion region all donors are ionized to satisfy the surface potential. The surface depletion width is given by $W_d = n_i / N_d$, where n_i is the surface state density. The surface depletion layer is assumed to play no role in the time-dependent and field-dependent behavior of the conductivity. From now on we only consider the active layer. Only the active layer is meant when we speak of the Al_xGa_{1-x}As layer.

4.3.1 Time dependence of the injection and ionization process

We first consider the time dependence of the injection and ionization process in the Al_xGa_{1-x}As layer. At high electric fields, the generation-recombination processes in the Al_xGa_{1-x}As layer are governed by two major transitions: Trapping of electrons by *DX* centers with a trapping coefficient T and impact ionization of trapped electrons out of these *DX* centers with an impact ionization coefficient X , which is a function of the electric field^{15,16,17,18}. A diagram showing the processes involved, is shown in Fig. 4.7. In this diagram, I_{in} and I_{out} are the number of electrons per unit time flowing into and out of a segment of the Al_xGa_{1-x}As layer, respectively, $T n_e n_d^+$ is the trapping rate, and $X n_e n_t$ is the ionization rate. We take into account only the deep *DX* level of the Si-donor, since the shallow donor level lies above the Fermi level, and therefore

does not enter the generation-recombination statistics. The corresponding rate equation of the $\text{Al}_x\text{Ga}_{1-x}\text{As}$ conduction electrons is

$$\frac{dn_e}{dt} = I_{in} + X n_e n_t - T n_e n_d^+ - I_{out}, \quad (4.1)$$

where n_e is the sheet electron density in the $\text{Al}_x\text{Ga}_{1-x}\text{As}$ layer, and n_t and n_d^+ are the densities of occupied and ionized donors in the $\text{Al}_x\text{Ga}_{1-x}\text{As}$ layer, respectively. We now first derive an expression for the time dependence of the injection and trapping rate in the $\text{Al}_x\text{Ga}_{1-x}\text{As}$ layer. When an electrical pulse is applied, initially the number of ionized donors is large and thus the trapping rate is larger than the impact ionization rate. Therefore, all electrons injected into the $\text{Al}_x\text{Ga}_{1-x}\text{As}$ layer are trapped, and ionization is negligible. Then the rate equation for the ionized donor density becomes, according to Fig. 4.7,

$$\frac{dn_d^+}{dt} = -T n_e n_d^+. \quad (4.2)$$

Thus the time dependence of the ionized donor density during injection is given by

$$n_d^+(t) = n_d^+(0) \exp(-T n_e t), \quad (4.3)$$

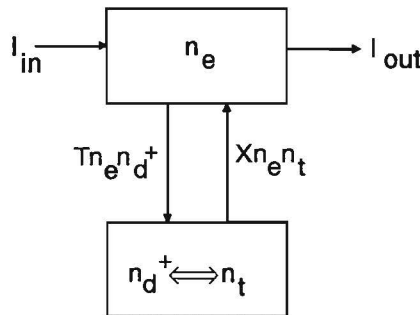


Fig. 4.7

Schematic representation showing the processes taking place in the $\text{Al}_x\text{Ga}_{1-x}\text{As}$ layer. I_{in} and I_{out} are the electron currents flowing into and out of a segment of the $\text{Al}_x\text{Ga}_{1-x}\text{As}$ layer, $T n_e n_d^+$ is the trapping rate, and $X n_e n_t$ is the ionization rate.

where $n_d^+(0)$ is the density of ionized donors at the beginning of the pulse. In the heterostructure, this decreasing donor density corresponds to a current decreasing in time with a time constant equal to $1/Tn_e$. This means that the time constant for current collapse is shorter when the electron concentration n_e is increased, for example by illumination.

During the injection and trapping process, the ratio between occupied and ionized donors increases. Therefore the impact ionization rate increases with respect to the trapping rate. When the electric field is high enough, the impact ionization rate exceeds the trapping rate at a critical time t_c during the pulse, and avalanche ionization is initiated. Due to the avalanche ionization, the carrier density n_e increases until a new steady state of higher conductivity has been reached. The time dependence of the density of ionized donors, the electron density in the $\text{Al}_x\text{Ga}_{1-x}\text{As}$ layer, and the electron density in the 2DEG are depicted schematically in Fig. 4.8. An expression for the critical time delay t_c can be found as follows. At t_c the ionization rate is equal to the trapping rate, thus

$$T n_e n_d^+ = X n_e n_t = X n_e (n_d - n_d^+), \quad (4.4)$$

where n_d is the total donor density in the active layer, equal to $n_d = N_d \times W_a$. By equating the ionized donor density n_d^+ at time t_c , obtained from equations (4.3) and (4.4), we find an expression for the critical time where avalanche starts

$$t_c = \frac{1}{Tn_e} \ln \frac{X+T}{X} \frac{n_d^+(0)}{n_d}. \quad (4.5)$$

In the expression for t_c the factors $1/Tn_e$ and $n_d^+(0)/n_d$ primarily depend on temperature and illumination, whereas $(X+T)/X$ is mainly determined by the electric field. Inspection of Eq. (4.5) tells us that increasing the electron density by illumination or heating, or increasing the impact ionization coefficient X through the electric field

shifts the ionization induced current jump to an earlier time in the pulse. We will use this expression for the interpretation of the temperature dependent measurements under avalanche conditions, discussed in section 4.4.3.

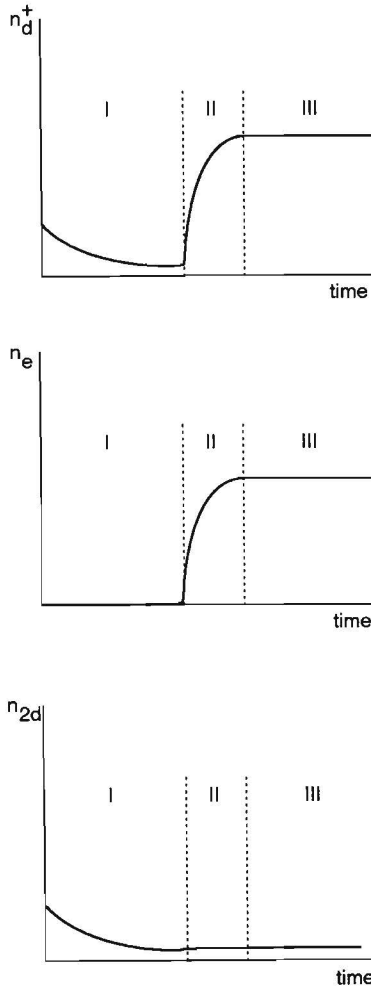


Fig 4.8 The density of ionized donors (n_d^+), the electron density in the $\text{Al}_x\text{Ga}_{1-x}\text{As}$ layer (n_e), and the electron density in the 2DEG (n_{2d}) as a function of time. I indicates the trapping regime, II the avalanche regime, and III the steady state.

From this semi-classical model describing hot-electron transport in an $n\text{-Al}_x\text{Ga}_{1-x}\text{As}$ layer, we conclude that trapping and impact ionization of Si-donors leads to a time-dependent behavior of the carrier density in a GaAs/ $\text{Al}_x\text{Ga}_{1-x}\text{As}$ heterostructure. The injection of electrons into the $\text{Al}_x\text{Ga}_{1-x}\text{As}$ is induced by the electric field, but the time dependence of the current collapse due to electron injection is determined by the trapping rate of the electrons into the DX centers. At a critical time during the pulse, the ionization rate exceeds the trapping rate and impact ionization initiates a rapid current increase during the pulse. After that, the current increases as a function of time until a new steady state of higher conductivity is reached.

4.3.2 Field dependence of the impact ionization

We now continue with the dependence of the avalanche ionization process on the electric field and derive an expression for the steady state current under avalanche conditions. This analysis is based on the theoretical work by Schöll¹⁶, who calculated the carrier concentration in bulk semiconductors under avalanche conditions. We adapted this theory to the case of avalanche ionization in the $\text{Al}_x\text{Ga}_{1-x}\text{As}$ layer of a two-dimensional $\text{GaAs}/\text{Al}_x\text{Ga}_{1-x}\text{As}$ heterostructure. When the steady state has been reached, the trapping rate is equal to the ionization rate.

$$X n_e n_t = T n_e n_d^+ \quad (4.6)$$

Substituting for the occupied donor density

$$n_t = n_d - n_{2d} - n_e, \quad (4.7)$$

n_{2d} being the electron density in the 2DEG, and for the ionized donor density

$$n_d^+ = n_d - n_t = n_{2d} + n_e \quad (4.8)$$

we find two stable steady state solutions:

$$n_e = 0 \quad \text{for } X < X_c,$$

and (4.9)

$$n_e = \frac{X(n_d - n_{2d}) - T(n_{2d})}{X + T}, \quad \text{for } X > X_c,$$

Here, X_c is the critical value of the avalanche ionization coefficient, corresponding to the threshold electric field for avalanche ionization. Using Eq.(4.8) and (4.9) X_c can be expressed as

$$X_c = \frac{T(n_{2d})}{n_e + n_t}, \quad (4.10)$$

showing that avalanche ionization occurs at lower electric fields when the trapping coefficient is smaller or when more electrons or occupied donors are available in the $\text{Al}_x\text{Ga}_{1-x}\text{As}$ layer. The calculated dependence of the carrier density on the impact ionization coefficient is depicted schematically in the Fig. 4.9 by the solid line¹⁶. Here we clearly observe that the carrier density shows a sharp rise at the critical value X_c . Until now, we assumed that optical and thermal ionization of the DX centers plays a negligible role compared to impact ionization. A non-zero value of the thermal and optical generation coefficient destroys the sharp phase transition by smoothing out the discontinuity of dn_e/dX at the critical field. This is shown by the dashed line¹⁶. For large X the carrier density saturates at a value $n_e = n_d - n_{2d}$, corresponding to a level where all donors in the $\text{Al}_x\text{Ga}_{1-x}\text{As}$ layer are ionized.

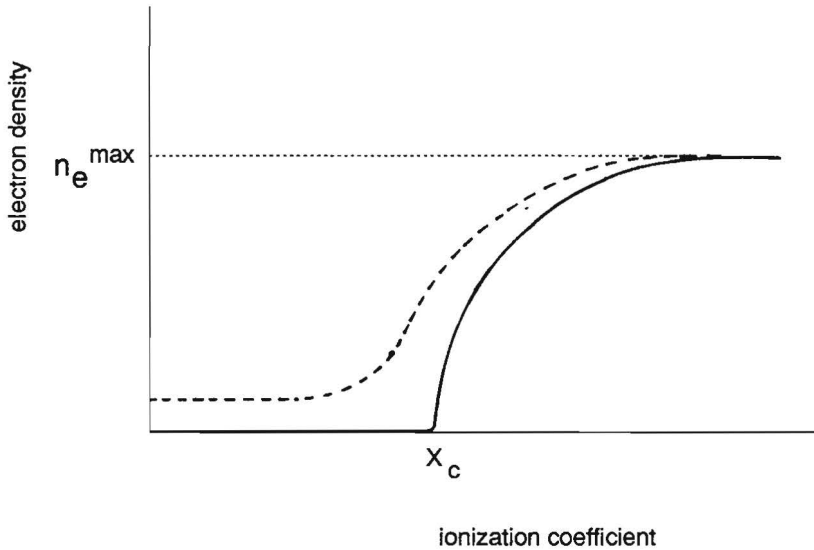


Fig. 4.9

Steady state carrier concentration as a function of the ionization coefficient X [Ref. 16]. The solid line represents the carrier concentration for the case that thermal and optical ionization is neglected; the dashed line includes a weak thermal and optical ionization, in addition to impact ionization.

4.4 Experiments

In this section we present the results of the experiments on the high-field current instabilities in GaAs/ $\text{Al}_x\text{Ga}_{1-x}\text{As}$ heterostructures. We performed time-resolved current-voltage measurements at room temperature and at low temperatures. In these experiments a time-dependent behavior of the current was observed. We describe these current instabilities at high electric fields in terms of electron injection and avalanche ionization processes in the $\text{Al}_x\text{Ga}_{1-x}\text{As}$ layer of the heterostructure, according to the model presented in sections 4.2 and 4.3. Whereas avalanche ionization in bulk semiconductors is a well-known phenomenon, the experiments reported in this section are the first reported observation of avalanche ionization in a two-dimensional semiconductor structure.

4.4.1 Experimental details

The modulation doped GaAs/ $\text{Al}_{0.33}\text{Ga}_{0.67}\text{As}$ heterostructure was grown by Molecular Beam Epitaxy. It consists of a 35 nm Si-doped $\text{Al}_{0.33}\text{Ga}_{0.67}\text{As}$ layer on top of a 55 nm GaAs layer and a 10 nm undoped $\text{Al}_{0.33}\text{Ga}_{0.67}\text{As}$ spacer layer. The heterostructure was grown on top of a semi-insulating substrate and a 25 period 5 nm/5 nm GaAs/AlAs superlattice. Finally, a 17 nm undoped GaAs cap layer was grown. At 4 K, the electron density in the 2DEG is $8 \times 10^{11} \text{ cm}^{-2}$ after illumination with a mobility of $4 \times 10^5 \text{ cm}^2/\text{Vs}$. At room temperature an electron density of $6 \times 10^{10} \text{ cm}^{-2}$ is measured in the dark with a mobility of $5 \times 10^3 \text{ cm}^2/\text{Vs}$. Ohmic contacts were made by evaporating and alloying AuGe/Ni. A rectangular structure, with a width of 200 μm and a contact spacing of 60 μm , was photolithographically defined. The contact resistances are about 0.6 Ωmm at 10 K and 10 Ωmm at room temperature, and were determined using a transmission line geometry. The low-field resistivity of the structure is 20 Ω at 4 K (illuminated) and about 2-20 k Ω at 300 K, dependent on illumination.

Pulsed current-voltage measurements at electric fields up to 2 kV/cm are performed at room temperature and at low temperatures. To avoid lattice heating the 3 μ s electric pulses are applied at a low repetition rate of 1000 Hz, using a 50 Ω pulse generator. Both applied voltage and current are measured by means of a LeCroy 9400 digital sampling oscilloscope in a 50 Ω circuit. To study the influence of illumination, the sample can be illuminated homogeneously using a quartz halogen lamp. In order to allow experiments at various temperatures, the sample is mounted in an optical flow cryostat.

4.4.2 Room temperature experiments

We now present the results of the time resolved current-voltage measurements on a GaAs/Al_xGa_{1-x}As heterostructure. An example of the current instabilities observed at room temperature, is given in Fig. 4.10. Here we show the time resolved conductivities for electric fields up to 2 kV/cm when the sample is not illuminated.

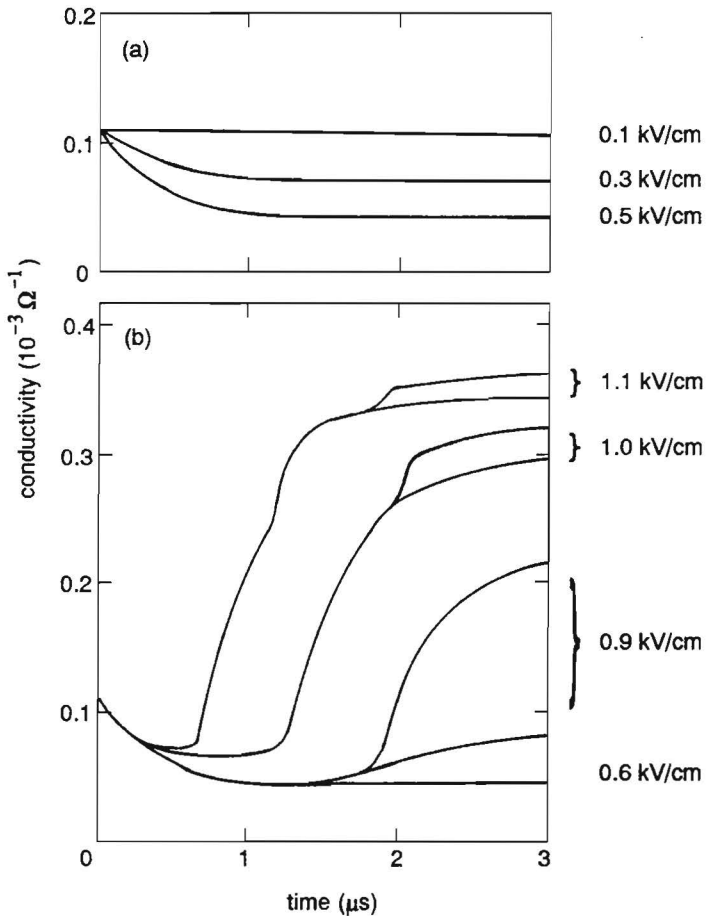


Fig. 4.10

Room temperature conductivity in the dark as a function of time at various electric fields (a) between 0.1 kV/cm and 0.5 kV/cm and (b) between 0.6 kV/cm and 1.1 kV/cm.

We see that at an electric field of 0.1 kV/cm the current is independent of time. Here, the sample conductivity corresponds to the low-field ohmic conductivity. At 0.3 kV/cm and 0.5 kV/cm we observe a current collapse as a result of carrier injection into the $\text{Al}_x\text{Ga}_{1-x}\text{As}$ layer. At electric fields between 0.6 and 1.1 kV/cm, we observe the development of several current jumps at some well-defined values of the electric fields. We ascribe these current jumps to the occurrence of avalanche ionization in the $\text{Al}_x\text{Ga}_{1-x}\text{As}$ layer. After the electrons are injected into the $\text{Al}_x\text{Ga}_{1-x}\text{As}$ conduction band, they are accelerated by the electric field and avalanche ionization of donors in the $\text{Al}_x\text{Ga}_{1-x}\text{As}$ layer takes place.

In Fig. 4.11 we present the steady state conductivities as a function of the electric field obtained from the results of Fig. 4.10 at a time 2.5 μs after the beginning of the voltage pulse. Note that the experimental curve above 0.5 kV/cm roughly shows the same

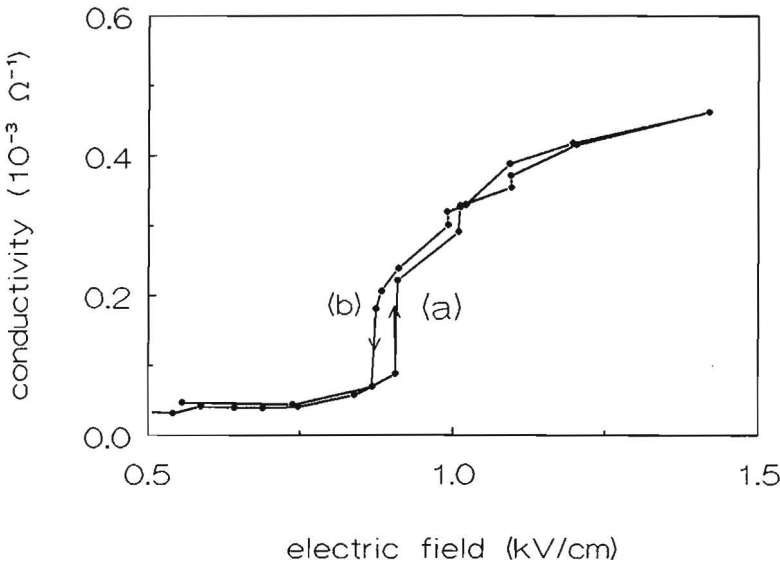


Fig. 4.11

Steady state conductivity (2.5 μs after the beginning of the voltage pulse) at room temperature as a function of the applied electric field. Curve (a), measured as a function of an increasing electric field, was derived from the data of Fig. 4.10. Curve (b) is measured as a function of a decreasing electric field.

features as the theoretical curve calculated by Schöll, presented in Fig. 4.9. The data represented by curve (a) were measured as a function of an increasing electric field. If we measure the conductivity-field characteristics as a function of a decreasing electric field, as is shown in curve (b), we observe hysteresis effects in the current jumps. Such hysteresis effects are an indication that the current jumps are created through a highly nonlinear mechanism. We suggest that the impact ionization in the $\text{Al}_x\text{Ga}_{1-x}\text{As}$ layer occurs in the form of current filaments. If a high electric field induces injection and impact ionization in a distinct region of the sample, a high conductivity current filament is created. If we lower the voltage, the filament does not disappear immediately but remains stable for a while. This explains the observed hysteresis effects.

To study the influence of illumination on the injection and avalanche process, we measured the conductivity as a function of the electric field for various illumination intensities. The results are presented in Fig. 4.12. Here we distinguish two different regimes: first, a conductivity decrease due to carrier injection at electric fields below 0.7 kV/cm, and secondly, a conductivity increase due to avalanche at higher electric fields. Note that an increasing illumination enhances the current collapse. This is to be expected, since illumination decreases the $\text{Al}_x\text{Ga}_{1-x}\text{As}$ contact barrier and hence enhances the electron injection and thus the current collapse. Furthermore, illumination smoothes out the onset of avalanche, since there is a larger offset current and a smaller number of occupied donors which can be ionized by impact ionization. Also the abrupt current jumps and the hysteresis effects observed in the dark are smoothed out by illumination.

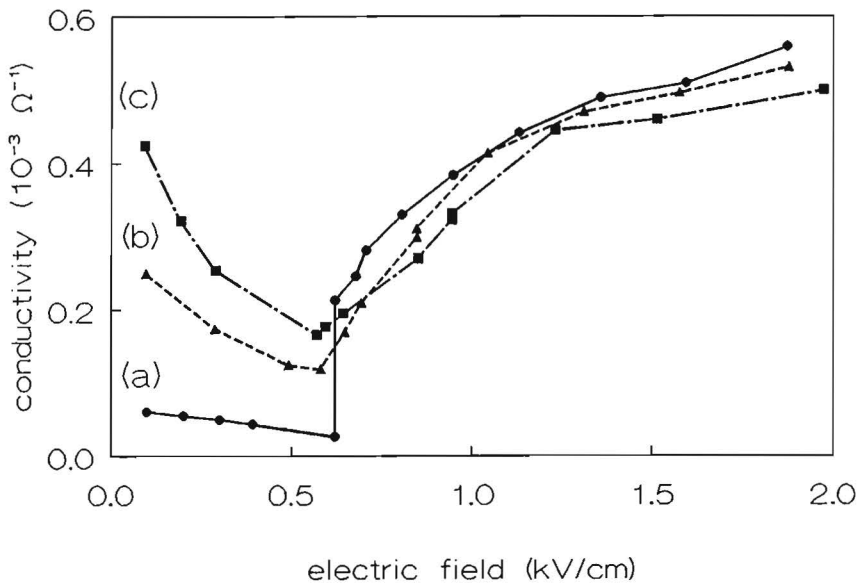


Fig. 4.12 Steady state conductivity as a function of the electric field for various illumination intensities. (a) is measured with ambient light, (b) with a weak illumination of the halogen lamp, and (c) with a bright illumination.

In order to estimate the electron mobility in the current filaments we studied the saturation behavior. At high electric fields the conductivity saturates as predicted by the theory. This conductivity saturation corresponds to the situation that all donors in the $\text{Al}_x\text{Ga}_{1-x}\text{As}$ layer are ionized. Experiments indicate¹⁹ that the maximum electron concentration in 2DEG and $\text{Al}_x\text{Ga}_{1-x}\text{As}$ layer together equals $8 \times 10^{11} \text{ cm}^{-2}$. If we assume that n_{2d} does not change with the applied electric field and is equal to $1 \times 10^{11} \text{ cm}^{-2}$, then the excess carrier concentration generated in the $\text{Al}_x\text{Ga}_{1-x}\text{As}$ layer is of the order of $7 \times 10^{11} \text{ cm}^{-2}$. From Fig. 4.11 we determine the difference between the saturation conductivity at high electric fields and the low field conductivity to be about $4.5 \times 10^{-4} \Omega^{-1}$. From these data we deduce that the electron mobility in the current filaments is about $4 \times 10^3 \text{ cm}^2/\text{Vs}$. This value is in accordance with the mobility limit

for optical phonon scattering in $\text{Al}_{0.3}\text{Ga}_{0.7}\text{As}$ at 300 K²⁰. In $n\text{-Al}_x\text{Ga}_{1-x}\text{As}$ ($n = 10^{18} \text{ cm}^{-3}$) values of 250 and 500 cm^2/Vs are reported^{21,23}. As was discussed in the introduction of this chapter, we observe that the electron mobility in the filaments under avalanche conditions is higher than the bulk mobility. At low temperatures, where ionized impurity scattering is the dominant scattering mechanism, this mobility enhancement in current filaments is even higher. The experimental observation of such a high mobility at low temperatures will be presented in section 4.4.4.

4.4.3 Determination of the activation energy

The experiments performed at room temperature do not provide an absolute proof that the processes causing current instabilities take place in the $\text{Al}_x\text{Ga}_{1-x}\text{As}$ layer. For this reason we now investigate this process more quantitatively. In section 4.3, where we described the model for avalanche ionization in the $\text{Al}_x\text{Ga}_{1-x}\text{As}$ layer, we derived an expression for the critical time t_c , at which avalanche ionization occurs. According to this expression t_c is inversely proportional to the carrier density n_e . Hence, if our model is correct, the temperature dependence of the critical time should correspond to the temperature dependence of the carrier density in the $\text{Al}_x\text{Ga}_{1-x}\text{As}$ layer, which for temperatures above 100 K shows an activation energy equal to the donor energy of Si in $\text{Al}_x\text{Ga}_{1-x}\text{As}$. At temperatures below 100 K no thermal equilibrium is established because of the energy barrier between *DX* center and ionized state. In order to check our model, we performed pulsed current-voltage measurements in the avalanche regime at various temperatures between 100 K and 200 K and determined the temperature dependence of t_c for two different values of the electric field.

Arrhenius plots for the temperature dependence of the critical time t_c for an electric field of 0.4 and 0.5 kV/cm are shown in Fig. 4.13. For both values of the electric field we observe the same temperature dependence corresponding to an activation energy of 81 ± 2 meV. This value is in accordance with experimental and theoretical values reported for the activation energy of the *DX* center in $\text{Al}_{0.33}\text{Ga}_{0.67}\text{As}$ ¹². We thus conclude that at high electric fields the avalanche ionization process takes place in the $\text{Al}_x\text{Ga}_{1-x}\text{As}$ layer.

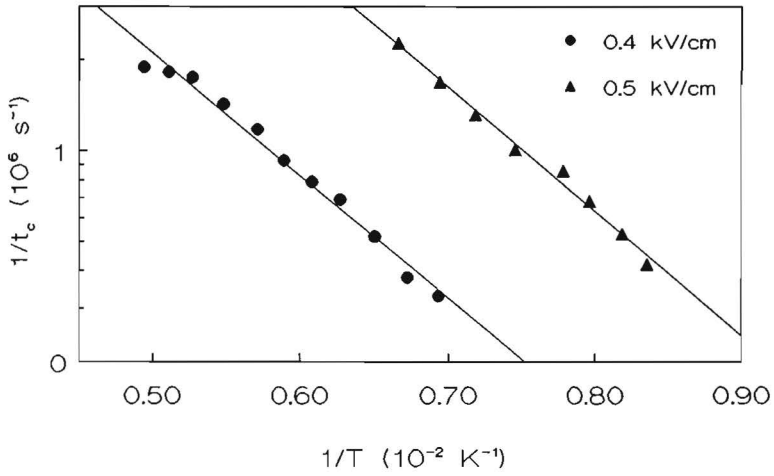


Fig. 4.13

Arrhenius plot of the inverse critical time versus the inverse temperature, for electric fields of 0.4 and 0.5 kV/cm. The slope of the lines yields an activation energy of 81 meV.

4.4.4 Low temperature experiments

At low temperatures the mobility of the 2DEG is strongly enhanced, resulting in a saturation of the current, whereas the mobility in the $\text{Al}_x\text{Ga}_{1-x}\text{As}$ is low. Therefore, it is much easier to separate the current in the $\text{Al}_x\text{Ga}_{1-x}\text{As}$ layer from the current through the 2DEG than at room temperature, where the electron mobilities in the 2DEG and in the $\text{Al}_x\text{Ga}_{1-x}\text{As}$ layer are of the same order of magnitude. We now present the results of our experiments at low temperatures, where we use this difference in mobility to determine the low-temperature mobility in an $\text{Al}_x\text{Ga}_{1-x}\text{As}$ filament under avalanche conditions.

What do we expect from the conductivity of the heterostructure at low temperatures? First, due to the large difference in mobility between 2DEG and $\text{Al}_x\text{Ga}_{1-x}\text{As}$ layer, the injection of electrons into the $\text{Al}_x\text{Ga}_{1-x}\text{As}$ should give rise to a more pronounced current collapse. On the other hand, at low temperatures there are less electrons with sufficient energy for injection into the $\text{Al}_x\text{Ga}_{1-x}\text{As}$ layer, which reduces the effect of current collapse for decreasing temperatures. With respect to avalanche ionization, the difference in mobility between 2DEG and $\text{Al}_x\text{Ga}_{1-x}\text{As}$ results in a relatively small avalanche contribution to the current compared to the large bias current in the 2DEG. Furthermore, the effects of avalanche ionization are expected to be more abrupt, since thermal ionization is reduced.

The trapping coefficient of the DX centers increases if we decrease the temperature from 300 K to 100 K. Since the threshold electric field for avalanche ionization is proportional to the trapping coefficient T , it will shift to higher electric fields with decreasing temperature. At temperatures below 100 K the persistent photo conductivity effect plays a role. Due to the potential barrier between ionized and bound state of the DX center, ionized electrons are not recaptured by the deep state, unless their energy is sufficient to overcome the potential barrier. Therefore, at low temperatures only hot electrons can be trapped in the DX center.

The contribution of avalanche ionization to the conductivity of the heterostructure is illustrated by Fig. 4.14, where the steady state values of the conductivity are shown for various temperatures. All data were taken with a weak illumination.

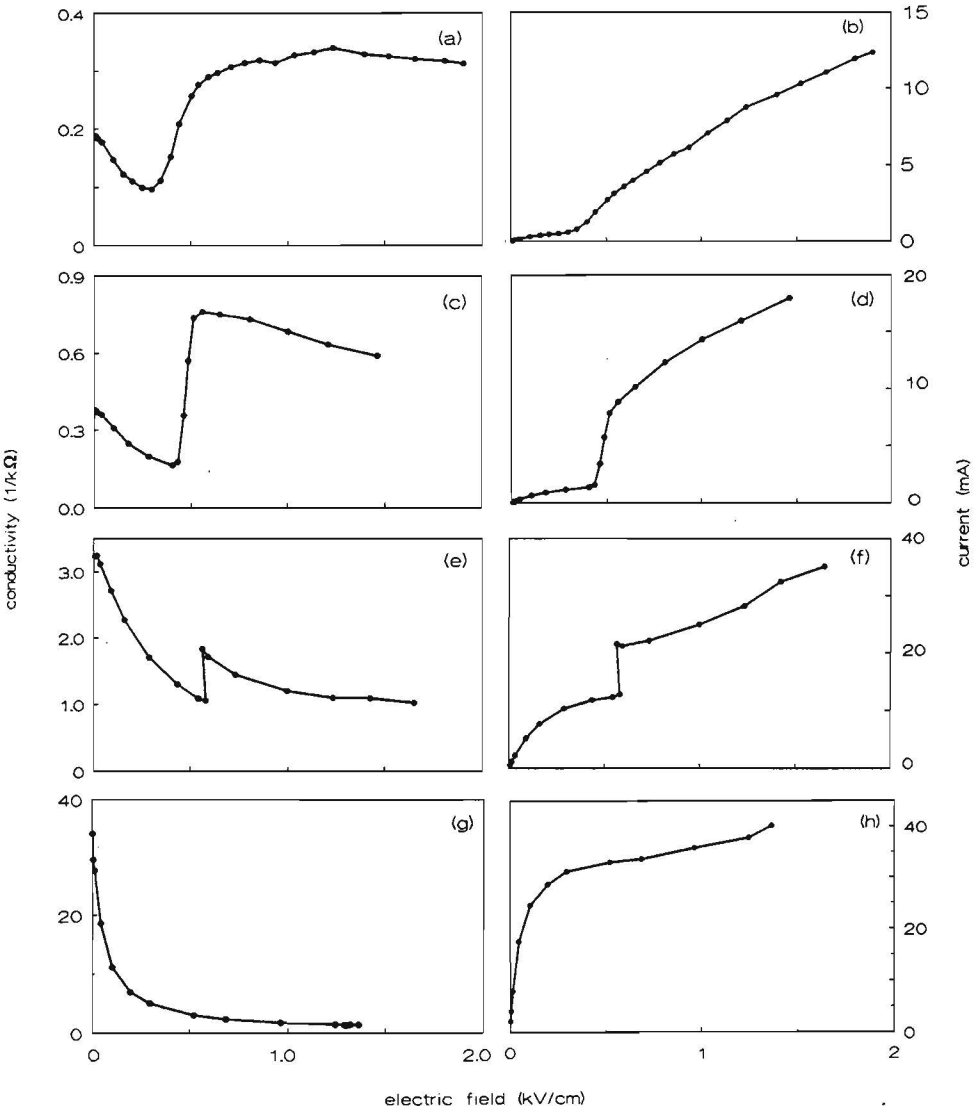


Fig. 4.14 Conductivity and current as a function of the electric field at 300 K (a,b), 200 K (c,d), 130 K (e,f), and 40 K (g,h).

At room temperature, a conductivity increase is measured at an electric field of about 0.5 kV/cm as a result of impact ionization. All current pulses at electric fields higher than this threshold value showed a current jump during the pulse. The threshold electric field for avalanche ionization shifts to 0.6 kV/cm when we decrease the temperature to 100 K. Furthermore, the conductivity increase at the threshold field is more abrupt at lower temperatures, as was predicted above.

The current collapse, not shown here, was observed to get less pronounced for decreasing temperatures. At 40 K it completely disappeared and all current pulses were independent of time. Accordingly, we observe a purely two-dimensional behavior at fields up to 2 kV/cm, such as a saturation of the current and a mobility which is inversely proportional to the electric field. From this we conclude that at 40 K the electrons do not have enough energy to overcome the $\text{Al}_x\text{Ga}_{1-x}\text{As}$ contact barrier through thermionic emission.

Since the largest effects of the filament structure on the electron mobility are expected at low temperatures, we measured the current-voltage characteristics at 10 K and used illumination to lower the contact barrier for electron injection. The results are shown in Fig. 4.15. For comparison, the I - V curve without illumination is also shown. Here we see that when the sample is illuminated, the I - V curve is not symmetrical anymore, which implies that the barriers to the $\text{Al}_x\text{Ga}_{1-x}\text{As}$ are not equal for both contacts. In fact it shows that the barrier between contact and $\text{Al}_x\text{Ga}_{1-x}\text{As}$ is lower at the contact where the voltage is applied than at the ground contact, resulting in electron injection when a negative voltage is applied. The positive branch of the curve shows a 2DEG behavior with a saturation current higher than the one observed in the dark, due to an increased electron density resulting from the persistent photo conductivity (PPC) effect²². All current pulses observed in this regime are independent of time, thus indicating that no electron injection into the $\text{Al}_x\text{Ga}_{1-x}\text{As}$ takes place. In the negative branch, however, at electric fields between 0.3 and 1.0 kV/cm, we observed a current collapse during the pulse, which leads to a smaller steady state current. At higher

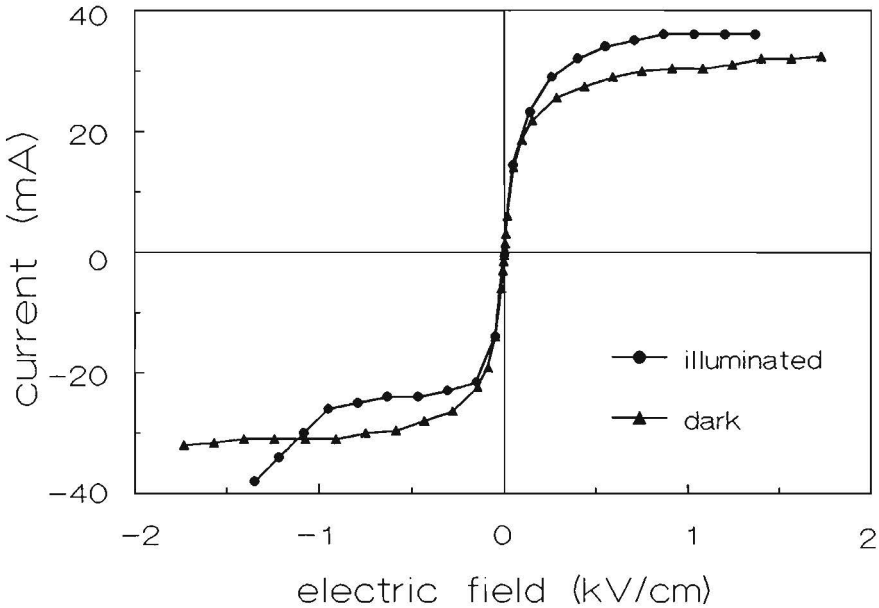


Fig. 4.15 Current-field characteristics at 10 K in the dark and with illumination.

electric fields avalanche shaped current pulses are observed and the steady state current in the $\text{Al}_x\text{Ga}_{1-x}\text{As}$ layer increases with increasing electric field.

We now estimate the electron mobility in the $\text{Al}_x\text{Ga}_{1-x}\text{As}$ layer in the avalanche regime. From the 2D saturation current in the injection regime between 0.3 and 1.0 kV/cm, a 2D electron density of $4 \times 10^{11} \text{ cm}^{-2}$ can be determined assuming a saturation velocity of $2 \times 10^7 \text{ cm/s}$. If at high electric fields all donors are ionized²⁰, resulting in a total electron concentration of roughly $8 \times 10^{11} \text{ cm}^{-2}$, then the $\text{Al}_x\text{Ga}_{1-x}\text{As}$ electron density is about $4 \times 10^{11} \text{ cm}^{-2}$. Since we determine an $\text{Al}_x\text{Ga}_{1-x}\text{As}$ conductivity of $1.4 \times 10^{-3} \Omega^{-1}$ from Fig. 4.15, this results in an $\text{Al}_x\text{Ga}_{1-x}\text{As}$ mobility of $2 \times 10^4 \text{ cm}^2/\text{Vs}$ in the filament. The mobility in the current filament is exceptionally high as compared to the low-field mobility in bulk $n\text{-Al}_x\text{Ga}_{1-x}\text{As}$ at low temperatures, which is lower than $100 \text{ cm}^2/\text{Vs}$ for

comparable donor densities²³. Comparably high mobilities under avalanche conditions at low temperatures, however, have also been reported for bulk n -GaAs⁴. Since our Monte Carlo calculations presented in section 4.2 indicate that the electron drift mobility in $\text{Al}_x\text{Ga}_{1-x}\text{As}$ increases with an increasing electron density we suggest that the high mobility in the filaments might be caused by an enhanced screening of the ionized impurity scattering due to this high electron density. However, the experimentally observed mobility in the filament presented here is even higher than our calculated maximum value of $0.5 \times 10^4 \text{ cm}^2/\text{Vs}$ at an electric field of 1 kV/cm. We assume that our calculations still underestimate the high mobility. Maybe this is caused by the fact that in our calculations we assumed a three-dimensional $\text{Al}_x\text{Ga}_{1-x}\text{As}$ layer, whereas in the $\text{Al}_x\text{Ga}_{1-x}\text{As}$ layer of the heterostructure only a thin sheet of the $\text{Al}_x\text{Ga}_{1-x}\text{As}$ layer is populated by electrons, i.e. where the conduction band shows a minimum. Probably this gives rise to a quasi two-dimensional behavior with even higher electron mobilities.

4.5 Conclusions

In this chapter, we investigated high-field current instabilities in GaAs/ $\text{Al}_x\text{Ga}_{1-x}\text{As}$ heterostructures, both theoretically and experimentally. In the time-resolved current-voltage measurements we observed a current collapse during the pulse, followed by one or more current jumps. To explain these current instabilities, we assume that at high electric fields electrons are injected into the $\text{Al}_x\text{Ga}_{1-x}\text{As}$ layer, thus giving rise to a current collapse. In the $\text{Al}_x\text{Ga}_{1-x}\text{As}$ layer the electrons are accelerated and cause impact ionization of occupied donors, resulting in a conductivity increase at high electric fields. The experiments reported in this chapter are the first reported observation of avalanche phenomena in a two-dimensional semiconductor heterostructure.

Let us now shortly summarize the arguments which led us to the model described above. The hypothesis that impact ionization of occupied donors is the mechanism which is responsible for the current instabilities is based on the following observations.

- The instabilities only occur above a certain threshold electric field.
- The dependence of the conductivity on the electric field shows a qualitative agreement with the theoretical calculations by Schöll.
- They are observed as a rapid current increase at a critical time during the pulse, suggesting an increasing carrier density.
- The current jumps show hysteresis effects as a function of the applied electric field, indicating that they are induced by a highly nonlinear mechanism.
- Monte Carlo calculations indicate that at electric fields of about 1 kV/cm the electrons in the $\text{Al}_x\text{Ga}_{1-x}\text{As}$ layer achieve sufficiently high energies to cause impact ionization of occupied donors.

The conclusion that the injection and avalanche process takes place in the $\text{Al}_x\text{Ga}_{1-x}\text{As}$

layer is based on the following arguments.

- The critical time at which the current jump is observed shows a thermal activation energy of 80 meV, which is in accordance with the model in which the current jump is ascribed to avalanche ionization in the $\text{Al}_x\text{Ga}_{1-x}\text{As}$ layer.
- At low temperatures, the current induced by avalanche ionization increases with an increasing electric field, whereas the current through the 2DEG saturates at high electric fields.

Our experiments indicate that the carriers generated by avalanche ionization show exceptionally high mobilities at low temperatures. This indicates that impact ionization occurs in the form of current filaments. In these filaments the carrier density is much higher than in the bulk of the sample, which results in an enhanced screening of the ionized impurity scattering. Moreover, in a current filament hot phonon effects are reduced, since optical phonons emitted by the hot electrons leave the filament and therefore do not contribute to the scattering.

References

1. P. Hendriks, E.A.E. Zwaal, J.G.A. Dubois, F.A.P. Blom, and J.H. Wolter, *J. Appl. Phys.* 69, 302 (1991).
2. P. Hendriks, A.A.M. Staring, R.G. van Welzenis, J.H. Wolter, W. Prost, K. Heime, W. Schlapp, and G. Weimann, *Appl. Phys. Lett.* 54, 2688 (1989).
3. A. Brandl, W. Kröninger, W. Prettl, and G. Obermaier, *Phys. Rev. Lett.* 64, 212 (1990).
4. K.M. Mayer, J. Parisi, and R.P. Huebener, *Z. Phys. B-Cond. Matt.* 71, 171 (1988).
5. R. Obermaier, W. Böhm, W. Prettl, and P. Dirnhofer, *Phys. Lett.* 105A, 149 (1984).
6. K. Aoki, T. Kobayashi, and K. Yamamoto, *J. de Physique C7*, 51 (1981).
7. K. Piragas, Yu. Pozhela, A. Tamashyavichyus, and Yu. Ul'bikas, *Sov. Phys. Semicond.* 21, 335 (1987).
8. G.A. Maracas, D.A. Johnson, and H. Goronkin, *Appl. Phys. Lett.* 46, 305 (1985).
9. G.N. Maracas, W. Porod, D.A. Johnson, D.K. Ferry, and H. Goronkin, *Physica* 134B, 276 (1985).
10. R.P. Huebener, J. Peinke, and J. Parisi, *Appl. Phys. A* 48, 107 (1989).
11. N. Chand, T. Henderson, J. Klem, W.T. Masselink, Y.C. Chand, H. Morkoç, and R. Fischer, *Phys. Rev. B* 30, 4481 (1984).
12. L. Reggiani, in *Hot electron transport in semiconductors*, Topics in applied physics, Vol. 58, ed. by L. Reggiani (Springer Verlag, Berlin, Heidelberg, New York, Tokyo, 1985), p. 66.
13. P.T. Landsberg, C. Rhys-Roberts, and P. Lal, *Proc. Phys. Soc.* 84, 915 (1964).
14. C. Jacoboni and P. Lugli, *The Monte Carlo method for semiconductor device simulation* (Springer Verlag, Wien, New York, 1989), p. 341.
15. E. Schöll, *Nonequilibrium Phase Transitions in Semiconductors* (Springer Verlag, Berlin, 1987), p. 40-48.
16. V.A. Kuz'min, N.N. Kryukova, and A.S. Kyuregyan, *Sov. Phys. Semicond.* 9, 1136 (1976).

-
17. D.J. Robbins, Phys. Stat. Sol. (b) 98, 11 (1980).
 18. R.G. van Welzenis, Ph.D. Thesis, Eindhoven (1972).
 19. Experiments at 4 K show a 2D electron concentration of $8 \times 10^{11} \text{ cm}^{-2}$ after illumination. If a low front gate voltage is applied the 2D electron density decreases immediately, thus indicating that the $\text{Al}_x\text{Ga}_{1-x}\text{As}$ layer is completely depleted. Referring to Eq. (4.7) we thus conclude that in this sample n_d is equal to $8 \times 10^{11} \text{ cm}^{-2}$. Then, the maximum electron concentration at high electric fields, $n_e^{\text{max}} + n_{2d}$, is also equal to $8 \times 10^{11} \text{ cm}^{-2}$.
 20. S. Adachi, J. Appl. Phys. 58, R1 (1985).
 21. L.G. Salmon, I.J. D'Haenens, J. Vac. Sci. Technol. B2, 197 (1984).
 22. S.T. Pantelides, *Deep Centers in Semiconductors* (Gordon and Beach Science Publishers, London, 1986).
 23. D.M. Collins, D.E. Mars, B. Fischer, and C. Kocot, J. Appl. Phys. 54, 857 (1983).

Chapter 5

Imaging of current instabilities in GaAs/Al_xGa_{1-x}As heterostructures

5.1 Introduction

In this chapter, we further investigate the current instabilities occurring in two-dimensional GaAs/Al_xGa_{1-x}As heterostructures at high electric fields^{1,2,3,4,5,11,16}. We already discussed that these current instabilities can be explained by the injection of electrons into the Al_xGa_{1-x}As layer and subsequent avalanche ionization of occupied Si-donors at high electric fields^{6,7}.

In bulk semiconductors, current instabilities caused by avalanche ionization are a well-known phenomenon^{8,9,10,11,12,13}. Above the threshold electric field for impact ionization, current jumps with hysteresis-effects are observed in the current-voltage characteristics². At higher electric fields even an oscillatory or chaotic temporal behavior of the conductivity has been observed^{1,2,3,14}. This complex temporal behavior during avalanche breakdown is often related to the formation of one or more current filaments in the sample. Current filaments in a bulk semiconductor have first

been visualized by Mayer *et al.* using a scanning electron microscope^{6,15} and by Brandl *et al.* using a scanning laser microscope^{16,17}.

From the observed similarity between current instabilities in GaAs/ $\text{Al}_x\text{Ga}_{1-x}\text{As}$ heterostructures and in bulk semiconductors we suggested that also in the $\text{Al}_x\text{Ga}_{1-x}\text{As}$ layer of a heterostructure, current filaments might be formed during avalanche ionization¹⁷. Since the barrier between source contact and $\text{Al}_x\text{Ga}_{1-x}\text{As}$ layer shows small variations in height along the contact, there are certain positions along the contact where electron injection can take place more easily. Therefore, distinct "channels" exist in the sample, where current filaments can develop more easily. The actual proof of the model described above can only be given by the experimental observation of the avalanche ionization induced current filaments.

In this chapter we discuss experiments which image the current patterns related to the injection and ionization process in the $\text{Al}_x\text{Ga}_{1-x}\text{As}$ layer. We developed a technique to image the current distribution in the heterostructure under high electric field conditions. This technique enables us to study the high electric field induced current patterns in the $\text{Al}_x\text{Ga}_{1-x}\text{As}$ layer of a GaAs/ $\text{Al}_x\text{Ga}_{1-x}\text{As}$ heterostructure as a function of time. The experimental details of the imaging technique are discussed in section 5.2. In section 5.3 the current images in the injection and avalanche regime are discussed. In these current images, current patterns are observed, which we attribute to the formation of current filaments in the $\text{Al}_x\text{Ga}_{1-x}\text{As}$ layer, parallel to the 2DEG. Even in samples where the two-dimensional electron gas and the contacts to the 2DEG are perfectly ohmic and homogeneous, current filaments can still develop in high electric fields. Finally, in section 5.4 we summarize the conclusions of this chapter.

5.2 The TROBIC technique

The modulation doped GaAs/Al_{0.33}Ga_{0.67}As heterostructure was grown by Molecular Beam Epitaxy. It consists of a 35 nm Si-doped Al_{0.33}Ga_{0.67}As layer on top of a 55 nm GaAs layer and a 10 nm undoped Al_{0.33}Ga_{0.67}As spacer layer. The heterostructure was grown on top of a 25 period 5 nm/5 nm GaAs/AlAs superlattice deposited on a semi-insulating substrate. Finally, a 17 nm undoped GaAs cap layer was grown. At 4 K, the electron density after illumination is $8 \times 10^{11} \text{ cm}^{-2}$ with a mobility of $4 \times 10^5 \text{ cm}^2/\text{Vs}$. Ohmic contacts were made by evaporating and alloying AuGe/Ni. A rectangular structure was photolithographically defined with dimensions of $200 \mu\text{m} \times 200 \mu\text{m}$. The contact resistances to the 2DEG are about $1.5 \Omega\text{mm}$ at 15 K, and were determined in a transmission line geometry. Conventional optical beam induced current (OBIC) images, which reveal the homogeneity of the sample through the lateral photo effect¹⁸, show that the 2DEG is perfectly homogeneous when no electric field is applied and that the contacts to the 2DEG are homogeneous as well.

The time-resolved optical beam induced current (TROBIC) images under high electric field conditions were obtained as follows. We performed pulsed current-voltage measurements in a 50Ω coaxial circuit. Both the applied voltage and the current were measured by means of a 12 GHz sampling oscilloscope. The $3 \mu\text{s}$ electric pulses were applied at a low repetition rate of 1000 Hz to avoid lattice heating. Using the sample-and-hold mode of the oscilloscope, we measured the current at a selected time in the pulse and applied this signal to the analog input of the Zeiss scanning laser microscope. The sample was scanned by the focused He-Ne laser beam of the laser microscope. The optical beam induced changes of the sample current were measured as a function of the position of illumination, and were stored in the 512×512 frame store memory of the scanning laser microscope. A large value of the optical beam induced current signal is obtained at those positions, where the optically excited carriers induce the largest conductivity increase in the sample. This corresponds to a bright region in the current image. The sample was illuminated with a laser power of about 3 nW, using a Zeiss long working-distance objective with a spot size of $2 \mu\text{m}$.

To obtain a maximum spatial resolution, we scanned the laser beam very slowly at a rate of 800 $\mu\text{m}/\text{sec}$, resulting in a digitizing error of less than 1 μm . The sample was mounted in an optical flow cryostat to allow measurements at low temperatures. All TROBIC images were measured at 15 K.

5.3 Experimental results

The current patterns observed in the modulation-doped GaAs/Al_xGa_{1-x}As heterostructure at 15 K were found to be closely related to the time-dependent current behavior. When the sample is not illuminated, three different regimes in the time-dependent behavior of the current can be distinguished. Current pulses, corresponding to these three regimes, are shown in Fig. 5.1. (i) At electric fields lower than 1 kV/cm we observe a current which is constant during the pulse, corresponding to a purely two-dimensional behavior. (ii) At electric fields between 1.0 and 1.7 kV/cm we observe current collapse in the heterostructure. This is explained by the injection of electrons into the Al_xGa_{1-x}As layer. (iii) At electric fields higher than 1.7 kV/cm an abrupt current increase is observed during the pulse. In this avalanche regime, electrons are injected into the Al_xGa_{1-x}As and induce there impact ionization of Si-donors.

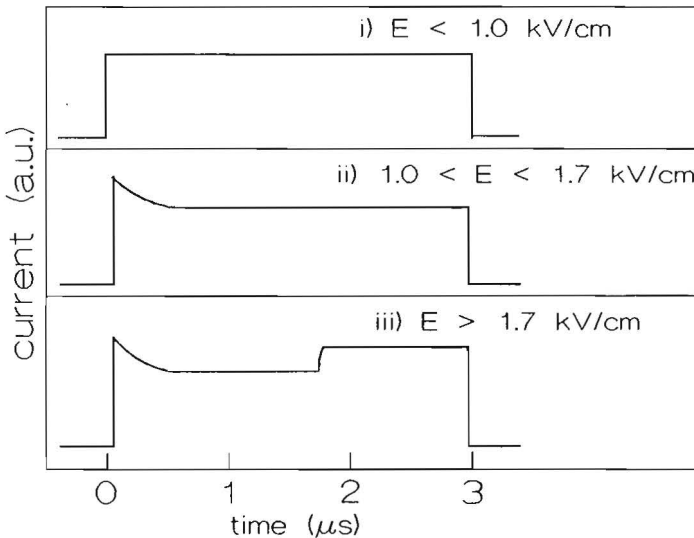


Fig. 5.1

Current pulses at 15 K, observed in the three different regimes of the electric field. (i) At electric fields lower than 1.0 kV/cm the current is independent of time. (ii) Current collapse at fields between 1.0 and 1.7 kV/cm. (iii) At electric fields higher than 1.7 kV/cm impact ionization of Si-donors in the Al_xGa_{1-x}As layer gives rise to a current jump during the pulse.

The mechanism of avalanche ionization can be understood as follows. In the beginning of the pulse, electrons are injected into the $\text{Al}_x\text{Ga}_{1-x}\text{As}$ layer. Here, they are trapped in the deep level of the Si-donors (*DX* centers). With increasing time, the ratio between occupied and ionized donors increases. Since the probability for impact ionization is proportional to the density of occupied donors, the ionization probability thus also increases. At a critical ratio of occupied and ionized donors, corresponding to a critical time during the pulse, the impact ionization rate exceeds the electron capture rate, initiating avalanche ionization in the $\text{Al}_x\text{Ga}_{1-x}\text{As}$ layer and yielding a rapid current increase during the pulse. In section 4.3.1 we derived that the critical time t_c , at which avalanche ionization begins, is given by

$$t_c = \frac{1}{Tn_e} \ln \frac{X+T}{X} \frac{n_d^+(0)}{n_d}, \quad (5.1)$$

where n_e is the electron density in the $\text{Al}_x\text{Ga}_{1-x}\text{As}$ layer, T is the trapping coefficient of electrons into the *DX* centers, X is the impact ionization coefficient of the *DX* centers, n_d is the donor concentration, and $n_d^+(0)/n_d$ is the fraction of ionized donors at the beginning of the pulse.

At electric fields below 1.0 kV/cm (regime (i)) the TROBIC images are homogeneous. An example is given in Fig. 5.2. In this image a relatively high laser power of 4 μW was used. We see that the sample is brighter than the background, since illumination increases the current through the sample. If we take a current image in regime (i), using a laser power of 4 nW, no beam induced current is detected. In the image experiments at higher electric fields, where we observe inhomogeneous behavior, we only used the low laser power of about 4 nW. The fact that a homogeneous image is obtained at low electric fields shows that the inhomogeneities measured at higher electric fields are caused by the high electric field and not by the non-uniformity of the sample itself.

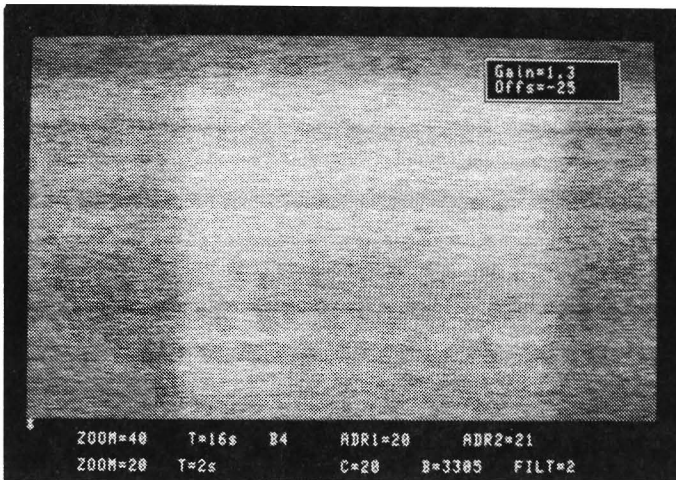


Fig. 5.2 TROBIC image at an electric field lower than 1.0 kV/cm. The electric field is applied in vertical direction. The bottom side of the picture is the negative contact.

At electric fields higher than 1.7 kV/cm (regime (iii)), where we measure a sudden increase of the current as a result of avalanche ionization, all donors in the channel are ionized by impact ionization. If we take a current image in this regime, no beam induced current is detected and again a homogeneous current image is obtained. The TROBIC images presented hereafter all correspond to electric fields in regime (ii).

Let us now consider the TROBIC images which we get in regime (ii). We first show an image at an electric field of 1.4 kV/cm. When the sample is not illuminated, the time-dependence of the current is as shown by the solid line in Fig. 5.3(a). In Fig. 5.3(b) we show the corresponding TROBIC image. In all TROBIC images the electric field is applied in vertical direction and the bottom side of the picture is the injecting source contact. The image is taken at the time t as indicated in Fig. 5.3(a). We observe that the TROBIC image is strongly inhomogeneous and shows a bright channel, which corresponds to a large value of the optical beam induced current signal. Illumination

in the bright channel of Fig. 5.3(b) corresponds to a current pulse shown by the dashed line in Fig. 5.3(a), whereas illumination of the sample outside the channel induces no detectable current increase (solid line). We ascribe this local increase of the TROBIC signal inside the channel to the formation of an optical beam induced filament. At an electric field below the threshold for spontaneous avalanche breakdown, a light-induced increase of the free carrier density locally enhances the impact ionization rate and thus initiates the formation of a current filament. This is most likely to occur in a region where a high density of injected and trapped electrons is present. We therefore suggest that the bright region in our image corresponds to a channel where the electrons are injected out of the source contact into the $\text{Al}_x\text{Ga}_{1-x}\text{As}$ layer.

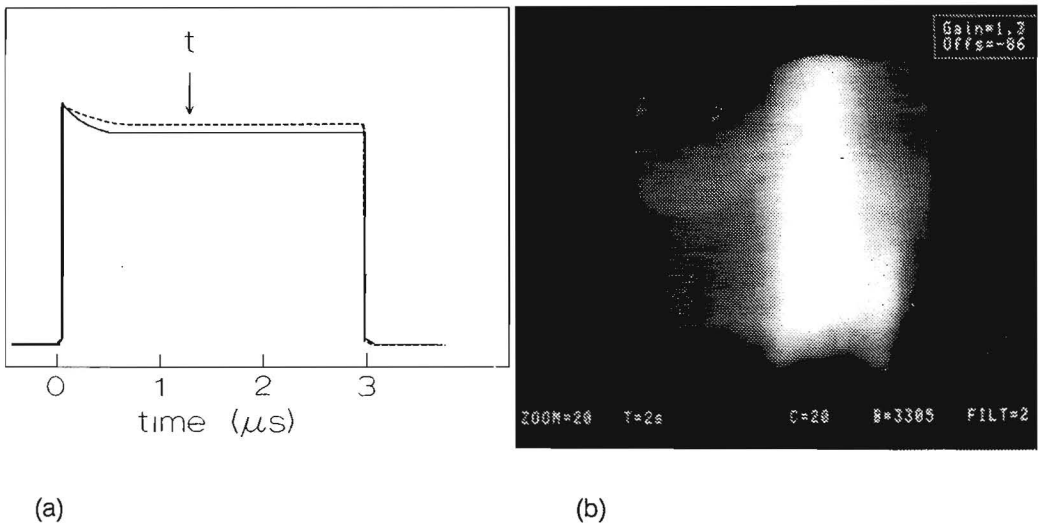


Fig. 5.3 (a) Current pulses at 15 K, when the sample is not illuminated (solid line). The dashed line corresponds to the current pulse when the sample is illuminated in the bright region of Fig. 3(b). (b) Current image of the heterostructure at 15 K and an electric field of 1.4 kV/cm, taken at the time t indicated in Fig. 3(a) by the arrow. The bottom side of the picture is the negative contact.

When we increase the electric field to 1.5 kV/cm, we observe two channels, and at 1.6 kV/cm three channels are created, as is shown in the current images in Fig. 5.4. This behavior can be explained by assuming that the contact barrier to the $\text{Al}_x\text{Ga}_{1-x}\text{As}$ shows small variations in height along the contact. Current injection into the $\text{Al}_x\text{Ga}_{1-x}\text{As}$ thus starts at the position where the barrier height is lowest¹⁷. At higher electric fields, current injection can also occur at other positions, leading to the formation of one or more than one filament. When the polarity is reversed, we measure the same phenomena, but at other positions along the contact. In general, all complex spatial TROBIC patterns are well reproducible, even after several days.

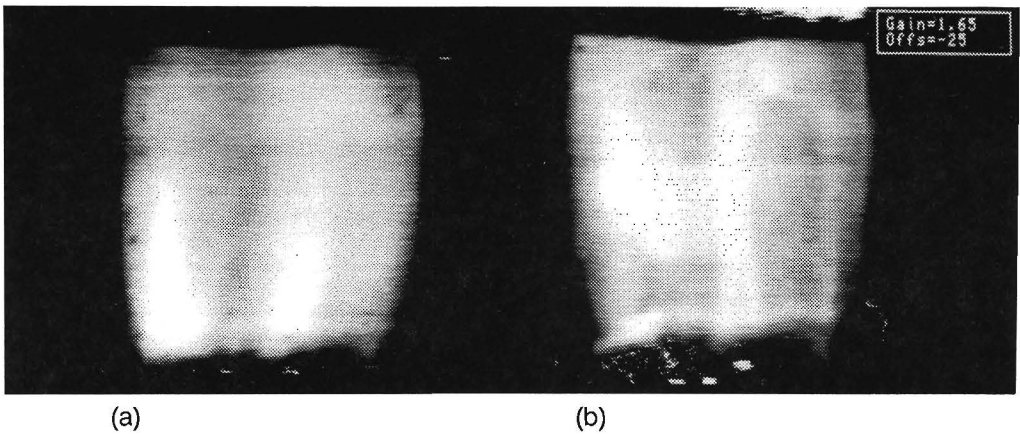


Fig. 5.4 (a) Current image at 1.5 kV/cm, showing two optical beam induced filaments. (b) Current image at 1.6 kV/cm, showing three filaments. Both images were taken at $t = 1.3 \mu\text{s}$.

We now discuss the time-dependence of the current images. The time dependence of the current pattern at 1.5 kV/cm is shown by the TROBIC images in Fig. 5.5. The images in Figs. 5.5(a), (b), and (c) are measured at different times during the pulse. We see that during the pulse the bright regions where optical beam induced avalanche occurs, are gradually extending in the direction of the positive contact as a function of time. This means that during the pulse the electrons injected out of the source

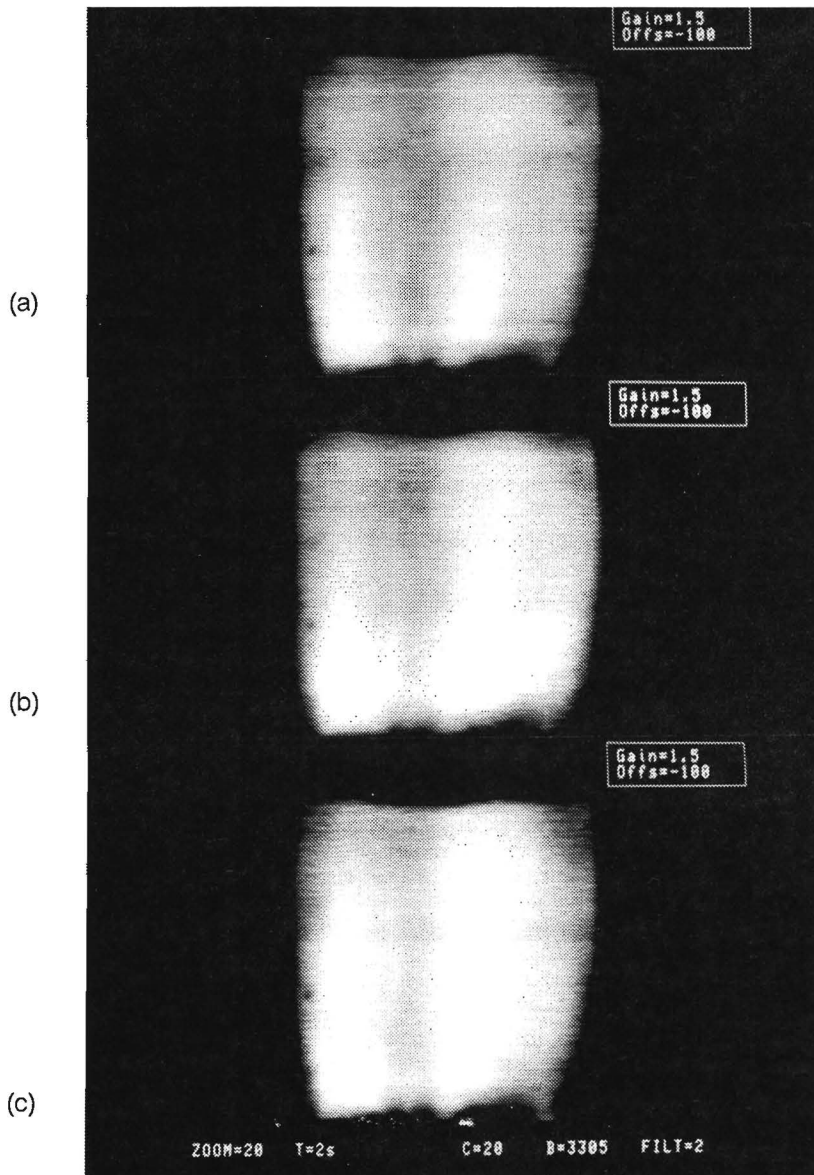


Fig. 5.5 Current images at 1.5 kV/cm, taken at three different times t during the pulse. (a) $t = 1.3 \mu\text{s}$, (b) $t = 1.7 \mu\text{s}$, and (c) $t = 2.5 \mu\text{s}$.

contact are moving in the direction of the positive contact, being trapped and detrapped by the DX centers in the $Al_xGa_{1-x}As$. This process takes place on a μs time scale¹⁷.

Until now, we only presented TROBIC images corresponding to experimental conditions where we did not find a current jump during the pulse. In the images presented below we will see that the threshold electric field where the current jump is observed can be lowered from 1.7 to 1.6 kV/cm as a result of the laser illumination. In Fig. 5.6 we show the time dependence of the current filaments at 1.6 kV/cm. In the images (b) and (c), a bright spot appears close to the positive contact. This bright spot corresponds to the switching of the sample current from pulse I to pulse III (see Fig. 6(d)), which means that spontaneous avalanche ionization is initiated, ionizing all donors in the sample. We thus conclude that illumination in the positive contact region lowers the threshold voltage for avalanche ionization from 1.7 kV/cm to 1.6 kV/cm.

The reason for this sensitivity of the positive contact region is not exactly clear at present. A possible explanation is the presence of a Schottky barrier between the $Al_xGa_{1-x}As$ layer and the ohmic contact. The electrons injected out of the source contact are trapped and detrapped while moving in the direction of the positive contact. When the field is higher than the threshold field, the electrons arriving at the positive contact cross the barrier and avalanche ionization takes place. At a lower value of the electric field the electrons do not have enough energy to cross the barrier and accumulate in traps near the positive contact. Illumination in this positive contact region can lower the Schottky barrier and thus decrease the threshold field for spontaneous avalanche breakdown. However, a complete model of this process is not available at present and additional experiments have to be performed to investigate this phenomenon.

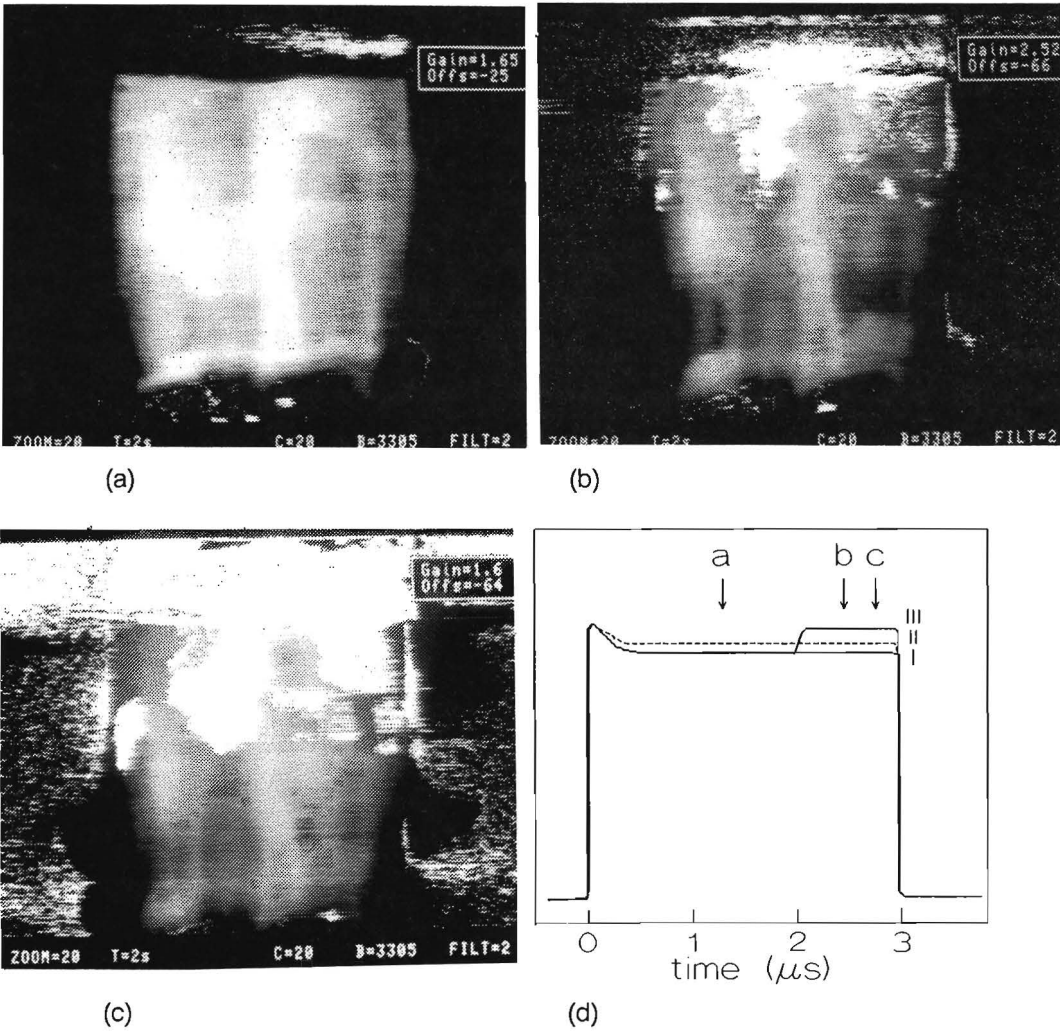


Fig. 5.6

Current images at 1.6 kV/cm at different times during the pulse. The times at which the images are taken, are indicated by the arrows. Pulse I is measured when the laser spot is positioned outside the channels, pulse II corresponds to illumination in the channels, and pulse III corresponds to the bright spot close to the positive contact.

5.4 Conclusions

In this chapter we discussed a novel time-resolved optical beam induced current (TROBIC) technique, and discussed several time-resolved current imaging experiments on a GaAs/ $\text{Al}_x\text{Ga}_{1-x}\text{As}$ heterostructure under high electric field conditions. In the images we observed the development of time-dependent current patterns, related to current instabilities in the heterostructure. Imaging of these current patterns in the regime of current collapse and avalanche ionization in GaAs/ $\text{Al}_x\text{Ga}_{1-x}\text{As}$ heterostructures is a useful tool to understand the complex high-field current instabilities observed in these structures. When high electric fields are applied to the heterostructure, electrons are injected from the source contact into the $\text{Al}_x\text{Ga}_{1-x}\text{As}$ layer. After being injected, the electrons are trapped and detrapped and move in the direction of the positive contact. The development of these injection channels has been visualized using the TROBIC technique. We observed a progressive extension of the injection channels in the direction of the positive contact as a function of time, as well as an increasing number of injection channels as a function of an increasing electric field. When the electric field is high enough, impact ionization of occupied donors in the $\text{Al}_x\text{Ga}_{1-x}\text{As}$ layer creates a highly conducting current filament in the $\text{Al}_x\text{Ga}_{1-x}\text{As}$. The threshold field for avalanche breakdown can be decreased by illumination in the positive contact region, corresponding to the development of a bright spot in the TROBIC image. The origin of this bright spot near the positive contact might be caused by an accumulation of trapped electrons close to the positive contact due to the presence of a Schottky barrier.

References

1. P. Hendriks, A.A.M. Staring, R.G. van Welzenis, J.H. Wolter, W. Prost, K. Heime, W. Schlapp, and G. Weimann, *Appl. Phys. Lett.* 54, 2668 (1989).
2. R.G. van Welzenis, H. Wijshoff, and K. Ploog, *Physica* 134 B, 347 (1985).
3. K. Hirakawa and H. Sakaki, *J. Appl. Phys.* 63, 803 (1988).
4. N. Balkan and B.K. Ridley, *Semicond. Sci. Technol.* 3, 507 (1988).
5. N. Balkan, B.K. Ridley, and J.S. Roberts, *Superlat. Microstruct.* 5, 539 (1989).
6. P. Hendriks, E.A.E. Zwaal, J.G.A. Dubois, F.A.P. Blom, and J.H. Wolter, *J. Appl. Phys.* 69, 302 (1991).
7. E.A.E. Zwaal, P. Hendriks, P.T.J. van Helmond, J.E.M. Haverkort, and J.H. Wolter, submitted to *J. Appl. Phys.* (1991).
8. K. Aoki, T. Kobayashi, and K. Yamamoto, *J. Physique C7*, 51 (1981).
9. K. Aoki, *Proceedings 20th Int. Conf. on the Physics of Semiconductors, Tesseloniki, 1990.*
10. A. Brandl, W. Kröninger, W. Prettl, and G. Obermair, *Phys. Rev. Lett.* 64, 212 (1990).
11. R.P. Huebener, J. Peinke, and J. Parisi, *Appl. Phys. A* 48, 107 (1989).
12. R. Symanczyk, E. Pieper, and D. Jäger, *Phys. Lett. A* 143, 337 (1990).
13. K.M. Mayer, R. Gross, J. Parisi, J. Peinke, and R.P. Huebener, *Solid State Commun.* 63, 55 (1987).
14. J. Spangler, A. Brandl, and W. Prettl, *Appl. Phys. A* 48, 143 (1989).
15. K.M. Mayer, J. Parisi, and R.P. Huebener, *Z. Phys. B* 71, 171 (1988).
16. A. Brandl, M. Völcker, and W. Prettl, *Appl. Phys. Lett.* 55, 238 (1989).
17. A. Brandl, M. Völcker, and W. Prettl, *Solid State Commun.* 72, 847 (1989).
18. P.F. Fontein, P. Hendriks, J.H. Wolter, R. Peat, D.E. Williams, and J.P. André, *J. Appl. Phys.* 64, 3085 (1988).

Chapter 6

Time-of-flight experiments on two-dimensional semiconductors

In the introduction of this thesis we formulated the question whether the time-of-flight technique is suitable to study the high-field transport properties of two-dimensional semiconductor structures. In this chapter we examine to what extent the preceding chapters have provided an answer to this question. After we have analyzed the possibilities and limitations of time-of-flight experiments on GaAs/ $\text{Al}_x\text{Ga}_{1-x}\text{As}$ heterostructures, we discuss the possibilities of other, more complicated two-dimensional semiconductor structures. In particular, we present a semiconductor structure enabling to measure the drift velocity of two-dimensional minority carriers in an undoped quantum well. Finally, we summarize the main conclusions of this thesis.

The question whether it is possible to perform time-of-flight experiments on two-dimensional semiconductor structures was resolved by the experiments described in chapter 3. We concluded that the time-of-flight technique is a very direct way to measure high-field drift velocities which cannot be measured by other techniques. However, the drift velocity determined by a time-of-flight experiment is equal to the drift velocity of the minority carriers in the structure. Contrary to bulk semiconductors,

where the mobility is mainly determined by impurity and phonon scattering, the minority carrier velocities in two-dimensional semiconductors cannot be interpreted in terms of majority carrier velocities to predict device properties. In modulation doped heterostructures, due to the spatial separation between ionized donors in the $\text{Al}_x\text{Ga}_{1-x}\text{As}$ layer and the electrons in the 2DEG, the impurity scattering is reduced and carrier-carrier interactions plays a major role. For that reason, minority electrons in a p -doped heterostructure show a much lower mobility than two-dimensional majority electrons in a 2DEG, leading to lower peak drift velocities and a different behavior with respect to transfer effects under hot electron conditions.

In order to obtain an indication of the device properties of two-dimensional semiconductor structures at high electric fields, one should measure directly the two-dimensional majority carrier drift velocity using the time-of-flight technique. The only attempt to measure the drift velocity of two-dimensional majority electrons was reported by Höpfel *et al.*¹. Since in principle the time-of-flight technique only allows to measure the drift velocity of minority carriers, they tried to circumvent this problem by using a specially designed two-dimensional heterostructure, as depicted in Fig. 6.1. The structure consists of a GaAs/ $\text{Al}_x\text{Ga}_{1-x}\text{As}$ heterojunction, grown on a heavily doped p -type GaAs layer, such that the two-dimensional well at the GaAs/ $\text{Al}_x\text{Ga}_{1-x}\text{As}$ interface lies above the Fermi level. When this structure is illuminated locally, at the position of excitation the electrons and holes are separated in the growth direction: the two-dimensional well is filled with electrons and the holes flow into the parallel p -doped GaAs layer. Here, the time-of-flight current due to the photo-excited carriers is determined by the drift velocity of the electrons in the two-dimensional well. The authors claim that in this structure the drift mobility of two-dimensional "majority" electrons is measured. In our opinion, this statement is not correct. First, the electrons studied in this structure still are not really majority electrons, since the two-dimensional well is empty except at the position of excitation. Thus, there is no laterally homogeneous two-dimensional electron gas. Furthermore, since the electron density is very low, the carrier-carrier interaction in this structure is completely different compared to the case of majority electrons in a 2DEG. It is therefore quite dubious

to interpret their results in terms of the drift velocity of a two-dimensional electron gas. In our opinion, the application of the time-of-flight technique should be limited to the investigation of minority carriers, which in fact can be very useful, as will be discussed below.

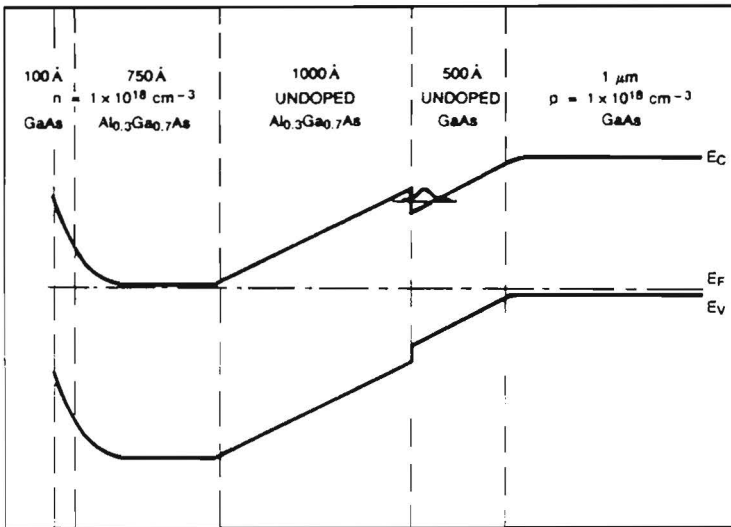


Fig. 6.1

The structure used by Höpfel¹ consists of a GaAs/ $\text{Al}_x\text{Ga}_{1-x}\text{As}$ heterojunction, grown on a heavily doped p -type GaAs layer, such that the two-dimensional well at the GaAs/ $\text{Al}_x\text{Ga}_{1-x}\text{As}$ interface lies above the Fermi level. When this structure is illuminated locally, at the position of excitation the electrons and holes are separated in the growth direction: the two-dimensional well is filled with electrons and the holes flow into the parallel p -doped GaAs layer.

In an n -type modulation doped GaAs/ $\text{Al}_x\text{Ga}_{1-x}\text{As}$ heterostructure, the drift velocity determined by a time-of-flight experiment is equal to the drift velocity of the minority holes in the GaAs layer. These holes are not confined to a two-dimensional layer but show quasi three-dimensional behavior. Let us now consider for what purposes this minority hole velocity can be relevant with respect to the high-field transport properties

of the heterostructure. It is an interesting feature of the drift velocity of the holes in the GaAs layer that it reveals information on the quality of the GaAs layer under high electric field conditions. This is an important quantity since it directly correlates with the quality of the 2DEG. A time-of-flight experiment thus reveals additional information on the properties the heterostructure, not obtained by the common characterization measurements performed at low electric fields. More important, however, the time-of-flight technique can also be used to measure the drift velocities of two-dimensional minority holes. Such a two-dimensional minority hole drift velocity can be obtained when a two-dimensional well is included in the GaAs layer of the modulation doped heterostructure in such a way that the minority holes are captured in the two-dimensional quantum well. This structure will be discussed furtheron.

We first discuss the limitations of the time-of-flight experiments on GaAs/ $\text{Al}_x\text{Ga}_{1-x}\text{As}$ heterostructures. The lower limit of the electric field range where time-of-flight experiments are possible is found at the electric field where the width of the time-of-flight signal is determined by recombination and diffusion effects rather than by the drift of the carriers. The upper limit for the electric field is determined by the threshold electric field where current instabilities are observed, caused by electron injection and avalanche ionization in the $\text{Al}_x\text{Ga}_{1-x}\text{As}$ layer of the heterostructure. At these high electric fields, many two-dimensional structures show a combination of two-dimensional and three-dimensional behavior. The transport properties of the system become highly nonlinear and unstable and also spatial inhomogeneities are observed. When a time-of-flight experiment is performed in the regime where the injection and avalanche phenomena are observed, the excess carriers induce additional current instabilities in the heterostructure. This situation becomes too complex to obtain any quantitative information from a time-of-flight experiment.

We now discuss the possibilities of other two-dimensional structures, in which these problems can be circumvented. Before discussing these other structures, we shortly recapitulate the conditions which must be satisfied with respect to the material. In the first place, the lifetime of the excited carriers must be longer than the time-of-flight

under experimental conditions, which is about several ns. Secondly, in order to screen the space charge of the excited minority carriers, the structure must contain a highly extrinsic conducting layer. This conducting channel is also used to detect the excess current induced by the ambipolar drift of the excess carriers. Finally, the structure has to be designed in such a way that current instabilities or other conductivity features on the same time scale as the time-of-flight signal are avoided.

Let us first consider the last restriction. The threshold electric field at which current instabilities are observed depends on the composition, the doping concentration, and the layer thickness of the $\text{Al}_x\text{Ga}_{1-x}\text{As}$ layer as well as on the composition and the injection properties of the ohmic contacts. We thus have to examine how these factors could be changed in order to reduce the possibility of electron injection. Only very little is known about the properties of the contact barrier between the alloyed contact and the $\text{Al}_x\text{Ga}_{1-x}\text{As}$ layer. This subject is very difficult to access by experimental methods. Consequently, a tractable route is missing for improving the semiconductor-metal contact in such a way that injection into the $\text{Al}_x\text{Ga}_{1-x}\text{As}$ layer is prevented.

A possible way to reduce the probability for electron injection into the $\text{Al}_x\text{Ga}_{1-x}\text{As}$ layer is to use a p -doped $\text{GaAs}/\text{Al}_x\text{Ga}_{1-x}\text{As}$ heterostructure. A p -doped heterostructure is expected to show less injection problems than an n -doped structure since the majority holes are heated less easily because of their higher effective mass. Time-of-flight experiments on p -type $\text{GaAs}/\text{Al}_x\text{Ga}_{1-x}\text{As}$ heterostructures were performed by Furuta *et al.*² They studied the interaction between minority electrons and majority holes at room temperature, using various structures with a different separation between electrons and holes. They observed a decreasing mobility in structures with a smaller electron-hole separation, which they ascribed to an enhanced electron-hole scattering. It would be interesting to investigate the effect of carrier-carrier scattering also at lower temperatures. From the experiments by Höpfel *et al.*^{3,4} we know that at low temperatures and low electric fields even negative mobilities of the minority carriers in quantum wells are possible due to carrier drag by the majority carriers.

An alternative way of avoiding electron injection into the $n\text{-Al}_x\text{Ga}_{1-x}\text{As}$ layer is to increase the aluminium fraction of the $\text{Al}_x\text{Ga}_{1-x}\text{As}$ layer, maybe even to 100%. The energy difference between the $\text{Al}_x\text{Ga}_{1-x}\text{As}$ conduction band minimum and the Fermi level is thus increased and the ionization of DX centers plays no role, since all donors are already ionized. In this way we have thus modified the modulation doped $\text{GaAs}/\text{Al}_x\text{Ga}_{1-x}\text{As}$ heterostructure to a GaAs/AlAs heterostructure with optimized two-dimensional behavior at high electric fields.

The resulting two-dimensional structure for time-of-flight experiments at high electric fields is presented in Fig. 6.2. It consists of a GaAs/AlAs heterostructure, in which a thin $\text{In}_{0.5}\text{Ga}_{0.5}\text{As}$ quantum well is included in the GaAs layer to capture the minority holes. In this case, real two-dimensional minority holes are measured, contrary to the ordinary $\text{GaAs}/\text{Al}_x\text{Ga}_{1-x}\text{As}$ heterostructure described previously. Since GaAs and InAs differ 6% in lattice constant, whereas GaAs and AlAs differ less than 1%, the thickness of the $\text{In}_{0.5}\text{Ga}_{0.5}\text{As}$ quantum well has to be less than 2 nm^5 . For layers thicker than this

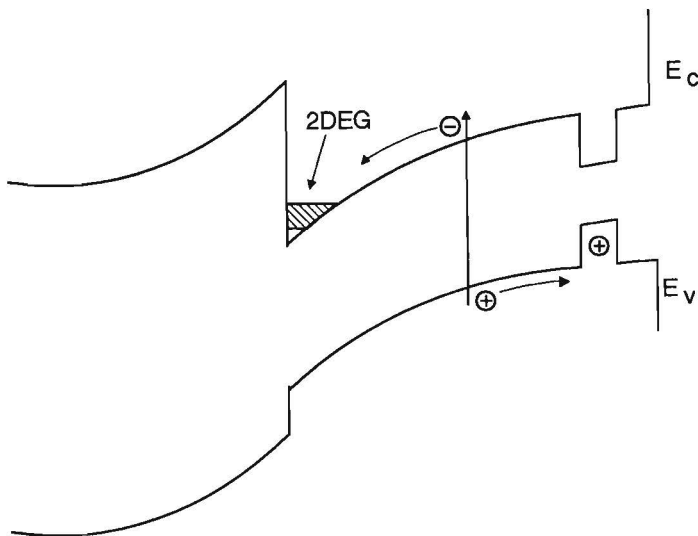


Fig. 6.2

A GaAs/AlAs heterostructure containing a thin $\text{In}_{0.5}\text{Ga}_{0.5}\text{As}$ quantum well to capture the minority holes.

critical layer thickness, the quantum well shows strain relaxation by forming misfit dislocations⁶. For an $\text{In}_{0.3}\text{Ga}_{0.7}\text{As}$ quantum well the critical layer thickness is 3 to 4 nm. Of course, it is also possible to use a p -doped $\text{GaAs}/\text{Al}_x\text{Ga}_{1-x}\text{As}$ heterostructure with an $\text{In}_x\text{Ga}_{1-x}\text{As}$ quantum well enabling to measure electron mobilities in the $\text{In}_x\text{Ga}_{1-x}\text{As}$ quantum well. A possible drawback of this structure is that the minority electrons are more easily accelerated out of the $\text{In}_x\text{Ga}_{1-x}\text{As}$ quantum well.

Another interesting two-dimensional structure is a p -doped GaAs/AlAs type II superlattice, consisting of p -doped GaAs wells separated by undoped AlAs barriers, as indicated in Fig. 6.3. When excess electron-hole pairs are created in the GaAs wells, the holes remain in the 2D hole gas in the GaAs layer, but the electrons are transferred to the X minimum of the conduction band in the AlAs layer, which lies

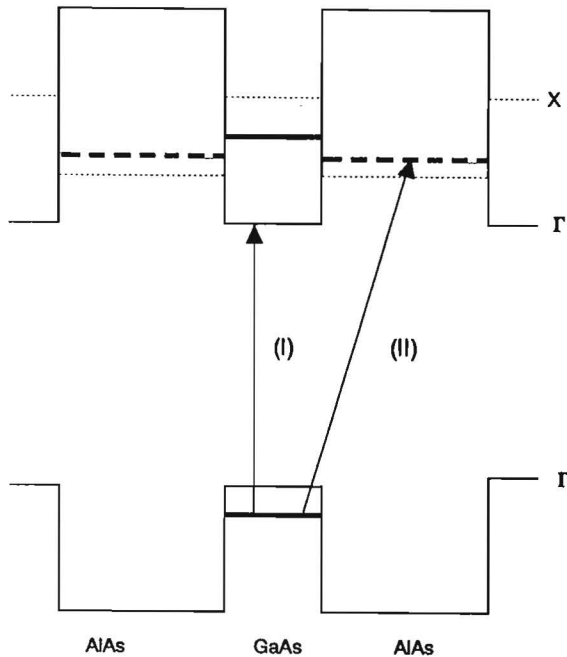


Fig. 6.3

A p -doped GaAs/AlAs type II superlattice, consisting of p -doped GaAs wells separated by undoped AlAs barriers.

energetically lower than the Γ minimum in the GaAs layer. By performing a time-of-flight experiment on this structure the mobility of minority electrons in the X minimum of the AlAs barriers can be measured. It would be interesting to vary the thickness of the wells and the barriers or to vary the majority hole concentration in the well in order to study the interaction between the majority holes in the wells and the minority electrons in the barriers.

We end this chapter by summarizing the conclusions of the work described in this thesis. We conclude that the time-of-flight technique is a valuable tool to investigate the high-field properties of two-dimensional semiconductor structures. The time-of-flight technique can not be used to measure majority carrier drift velocities in e.g. a two-dimensional electron gas, but it is a very direct way to measure minority drift velocities under high electric field conditions. These minority carrier properties obtained by the time-of-flight technique can be used to model the properties of electro-optic devices or transistors in which excess carriers are present. Furthermore, the time-of-flight technique enables the investigation of intrinsic semiconductor layers which cannot be investigated by the conventional characterization techniques. Whereas in the experiments on n -type modulation doped GaAs/Al_xGa_{1-x}As heterostructures the drift velocity of three-dimensional holes is measured, the time-of-flight technique can be extended to obtain high-field transport properties of two-dimensional minority carriers, in the case of a GaAs/AlAs heterostructure containing an In_xGa_{1-x}As quantum well. The time-of-flight technique thus reveals additional information on the material properties, which cannot be obtained by other, more conventional experimental methods.

For a time-of-flight experiment, a structure has to be designed in such a way that it retains its two-dimensional character even under high electric field conditions. The occurrence of current instabilities as described in chapters 4 and 5 disturbing the two-dimensional character of the structure must be avoided. Before performing a time-of-flight experiment on a two-dimensional semiconductor structure, the high-field properties of the majority carriers should be investigated by performing high-field current-voltage measurements in order to determine the limiting experimental

conditions for a time-of-flight experiment. Chapter 4 and 5 provide the guidelines for judging whether the two-dimensional character is still maintained. Finally, the threshold electric field for the injection and avalanche phenomena can be suppressed to much higher values by using a GaAs/AlAs heterostructure in which the injection barrier is approximately 0.7 eV and where the *DX* centers are all ionized in equilibrium, thus preventing avalanche ionization.

References

1. R.A. Höpfel, J. Shah, T.Y. Chang, and N.J. Sauer, Appl. Phys. Lett. 51, 1815 (1987).
2. T. Furuta, N. Shigekawa, T. Mizutani, and A. Yoshii, Appl. Phys. Lett. 55, 2310 (1989).
3. R.A. Höpfel, J. Shah, P.A. Wolff, and A.C. Gossard, Phys. Rev. Lett. 56, 2736 (1986).
4. R.A. Höpfel, J. Shah, P.A. Wolff, and A.C. Gossard, Appl. Phys. Lett. 49, 572 (1986).
5. M.R. Leys, NATO Conf. Ser. of Sci., Plenum Press. Proc. of NATO summerschool "Low dimensional structures in semiconductors" Erice 1-14 July 1990.
6. J.W. Matthews, in *Epitaxial growth* (Academic Press, New York, 1975), p. 559.

Summary

This thesis deals with the transport properties of GaAs/Al_xGa_{1-x}As heterostructures at high electric fields. A very direct method to measure high-field drift velocities in bulk semiconductors is the time-of-flight technique. The major aim of this work was to study the possibilities and limitations of time-of-flight experiments on two-dimensional semiconductor structures.

After shortly discussing the scope of this thesis in chapter 1, the basic concepts of the GaAs/Al_xGa_{1-x}As heterostructure are introduced in chapter 2, where we also discuss its transport properties at high electric fields.

In chapter 3 we present the results of our time-of-flight experiments on a GaAs/Al_xGa_{1-x}As heterostructure, resulting in the determination of the high-field drift velocity of the minority holes in this structure. At an electric field of about 1 kV/cm we measured an anomalous behavior of the time-of-flight current. In this regime also current instabilities in the bias current were observed. In order to investigate these current instabilities, we performed pulsed current-voltage measurements at high electric fields. These are discussed in chapter 4. A complicated time-dependent behavior of the current was measured, as well as hysteresis effects in the current-voltage characteristics. These observations suggest that at high electric fields the current is distributed inhomogeneously in the sample. We therefore developed a technique to image the current distribution in the heterostructure under high electric field conditions. These imaging experiments are presented in chapter 5.

Using the results of the time-resolved and spatially resolved experiments, we developed a phenomenological model describing the behavior of GaAs/Al_xGa_{1-x}As heterostructures at high electric fields. This model describes the high-field current instabilities in a heterostructure in terms of electron injection from the source contact into the Al_xGa_{1-x}As, followed by avalanche processes in the Al_xGa_{1-x}As layer. This model was supported by the results of our Monte Carlo calculations, in which we

calculated the velocities and energy distribution of the electrons in the $\text{Al}_x\text{Ga}_{1-x}\text{As}$ layer at high electric fields.

We conclude that the high-field properties of $\text{GaAs}/\text{Al}_x\text{Ga}_{1-x}\text{As}$ heterostructures cannot be described by only taking into account the two-dimensional conducting channel. Instead, a full three-dimensional model of hot electron transport in these structures must be developed, including the high-field properties of the $\text{Al}_x\text{Ga}_{1-x}\text{As}$ layer and the contacts.

In chapter 6 we summarize the main conclusions of this thesis and consider the possibilities and limitations of time-of-flight experiments on two-dimensional semiconductor structures.

Samenvatting

Dit proefschrift is gewijd aan een onderzoek naar de eigenschappen van gelaagde GaAs/ $\text{Al}_x\text{Ga}_{1-x}\text{As}$ heterostructuren in hoge elektrische velden. In een GaAs/ $\text{Al}_x\text{Ga}_{1-x}\text{As}$ heterostructuur zijn de elektronen opgesloten in een tweedimensionale laag aan het grensvlak tussen GaAs en $\text{Al}_x\text{Ga}_{1-x}\text{As}$ laag. Omdat dit tweedimensionale elektronengas (2DEG) ruimtelijk gescheiden is van de geïoniseerde donoratomen in de $\text{Al}_x\text{Ga}_{1-x}\text{As}$ laag kunnen in dit soort structuren zeer hoge elektronen-beweeglijkheden worden bereikt. Hierdoor is dit materiaal geschikt voor de fabricage van snelle elektronische schakelingen. Omdat deze transistoren in de praktijk moeten werken bij hoge elektrische velden, is het van belang om inzicht te verkrijgen in de hoog-veld eigenschappen van GaAs/ $\text{Al}_x\text{Ga}_{1-x}\text{As}$ heterostructuren. Een belangrijke parameter hierbij is de driftsnelheid van de elektronen onder hoog-veld condities.

In bulk halfgeleiders kunnen deze driftsnelheden worden gemeten d.m.v. vliegtijdexperimenten. Doel van het werk beschreven in dit proefschrift was om te onderzoeken in hoeverre deze vliegtijdexperimenten geschikt zijn om driftsnelheden in gelaagde halfgeleiderstructuren te meten. De vliegtijdexperimenten aan de GaAs/ $\text{Al}_x\text{Ga}_{1-x}\text{As}$ heterostructuren zijn als volgt uitgevoerd. Met behulp van een korte laserpuls worden extra ladingsdragers vrijgemaakt in het materiaal. De drift van deze ladingsdragers o.i.v het aangelegde elektrische veld veroorzaakt een fotostroom in het uitwendige circuit. De tijdsduur van deze fotostroom geeft informatie over de driftsnelheid van de extra ladingsdragers. Op deze manier kon door ons de driftsnelheid van de minderheidsladingsdragers in de heterostructuur worden gemeten.

Bij een elektrisch veld van ongeveer 1 kV/cm constateerden we een afwijkend gedrag in de vliegtijdmetingen en werden instabiliteiten in de stroom waargenomen. Om deze instabiliteiten verder te onderzoeken, werden stroom-spanningsmetingen bij hoge elektrische velden uitgevoerd. Omdat het vermoeden bestond dat onder deze omstandigheden de stroom niet homogeen verdeeld was in het materiaal, werd een

methode ontwikkeld waarmee het mogelijk is de stroomverdeling in het materiaal zichtbaar te maken.

Om de stroom-instabiliteiten in GaAs/ $\text{Al}_x\text{Ga}_{1-x}\text{As}$ heterostructuren bij hoge elektrische velden te verklaren hebben we een model opgesteld, waarin we aannemen dat bij hoge elektrische velden elektronen vanuit het negatieve contact worden geïnjecteerd in de $\text{Al}_x\text{Ga}_{1-x}\text{As}$ laag, waar ze botsings-ionisatie van gevulde donoren veroorzaken. We concluderen dat de rol van het $\text{Al}_x\text{Ga}_{1-x}\text{As}$ bij het modelleren van GaAs/ $\text{Al}_x\text{Ga}_{1-x}\text{As}$ heterostructuren vaak ten onrechte wordt verwaarloosd.

We besluiten dit proefschrift met een overzicht van de mogelijkheden en beperkingen van vliegtijdexperimenten aan tweedimensionale halfgeleiderstructuren.

List of publications

1. E.A.E. Zwaal, W.T. Gorissen, J.E.M. Haverkort, P.J. van Hall, and J.H. Wolter, Time-of-flight experiments on 2D electron gases, *Sol. Stat. Electr.* 32, 1109 (1989).
2. P. Hendriks, E.A.E. Zwaal, J.G.A. Dubois, F.A.P. Blom, and J.H. Wolter, Hot electron transport in GaAs/AlGaAs heterostructures, *Proceedings of the 20th Int. conf. on the physics of semiconductors*, ed. by E.M. Anastassakis and J.D. Joannopoulos (World Scientific, Singapore 1990), p. 1605.
3. P. Hendriks, E.A.E. Zwaal, J.G.A. Dubois, F.A.P. Blom, and J.H. Wolter, Electric field induced parallel conduction in GaAs/AlGaAs heterostructures, *J. Appl. Phys.* 69, 302 (1991).
4. P. Hendriks, E.A.E. Zwaal, J.E.M. Haverkort, and J.H. Wolter, Modulation doping and delta doping of III-V compound semiconductors, to be published in the *Proceedings of the Conf. of the Society of Photo-optical Instrumentation Engineers*, Aachen 1990.
5. E.A.E. Zwaal, P. Hendriks, P.T.J. van Helmond, M.J.M. Vermeulen, J.E.M. Haverkort, and J.H. Wolter, Origin of current instabilities in GaAs/Al_xGa_{1-x}As heterostructures: Avalanche ionization in the Al_xGa_{1-x}As layer, submitted to *J. Appl. Phys.* 1991.
6. E.A.E. Zwaal, M.J.M. Vermeulen, P. Hendriks, J.E.M. Haverkort, and J.H. Wolter, Observation of current filaments in GaAs/Al_xGa_{1-x}As heterostructures using a time-resolved imaging technique, submitted to *J. Appl. Phys.* 1991.

Curriculum Vitae

geboren: 26 januari 1964 te Winterswijk

middelbaar onderwijs: VWO, Chr. Scholengemeenschap Aalten
1976 - 1982

doctoraal examen: Rijksuniversiteit Groningen
1982 - 1987
Subfaculteit Scheikunde
hoofdvak: Vaste Stof Chemie
bijvak: Technische Fysica

promotie: Technische Universiteit Eindhoven
1987 - 1991
Faculteit Technische Natuurkunde
Groep Halfgeleiderfysica
in dienst van de Stichting voor
Fundamenteel Onderzoek der Materie (FOM)



Stellingen

behorende bij het proefschrift

Time-of-flight experiments on GaAs/Al_xGa_{1-x}As heterostructures

1. In tegenstelling tot de bewering van Morohashi *et al.* dient in de uitdrukking voor de time-of-flight stroom de som van de elektronen- en gatenmobiliteit te worden meegenomen in plaats van de ambipolaire mobiliteit.
 - M. Morohashi, N. Sawaki, and I. Akasaki, Jpn. J. Appl. Phys. 24, 661 (1985).
2. De time-of-flight techniek is niet geschikt om de driftsnelheid van elektronen in een tweedimensionaal elektronengas te bepalen.
 - Dit proefschrift, hoofdstuk 3.
3. Vanwege het feit dat Walukiewicz *et al.* in hun mobiliteitsberekeningen alleen verstrooiing van de elektronen aan het Fermi-niveau meenemen, is de door hen berekende temperatuurafhankelijkheid van de mobiliteit ten gevolge van verstrooiing aan onzuiverheden onjuist.
 - W. Walukiewicz, H.E. Ruda, J. Lagowski, and H.C. Gatos, Phys. Rev. B 29, 4818 (1984).
4. Bij het modelleren van GaAs/Al_xGa_{1-x}As heterostructuren wordt de rol van de Al_xGa_{1-x}As laag vaak ten onrechte verwaarloosd.
 - Dit proefschrift, hoofdstuk 4 en 5.

5. De blauwverschuiving in het fotoluminescentiespectrum van een GaAs/Al_xGa_{1-x}As heterostructuur wordt door Bergman *et al.* ten onrechte toegeschreven aan de neutralisatie van acceptoren in de GaAs laag.
 - J.P. Bergman, Q.X. Zhao, P.O. Holtz, B. Monemar, M. Sundaran, J.L. Merz, and A.C. Gossard, Phys. Rev. B 43, 4771 (1991).

6. Monte Carlo berekeningen dienen niet beschouwd te worden als een alternatief voor fenomenologische modellen, maar dienen gebruikt te worden voor de ondersteuning ervan.
 - C. Jacoboni and L. Reggiani, Rev. Mod. Phys. 55, 645 (1983).

7. Hoewel de Algemene Nabestaandenwet wordt gepresenteerd als een herziening van de Algemene Weduwen- en Wezenwet, is deze in feite gebaseerd op een totaal ander principe.

8. Het voorontwerp inzake de herziening van het afstammingsrecht vertoont de tekenen van een januskop.

9. Zowel in een halfgeleider als in de samenleving is de invloed van minderheden op de meerderheid soms groter dan andersom.